



Search for long-lived charginos and τ -sleptons using final states with a disappearing track in pp collisions at $\sqrt{s} = 13$ TeV with the ATLAS detector

The ATLAS Collaboration

This paper reports a search for decays of long-lived charginos or τ -sleptons to final states containing a short disappearing track, a single high-energy jet, and missing transverse momentum. The search uses 137 fb^{-1} of data from 13 TeV proton–proton collisions recorded by the ATLAS detector during Run 2 of the LHC. Multiple search regions are defined, all requiring the presence of a track reconstructed from either three or four measurements in the innermost layers of the ATLAS detector. Regions with tracks having only three measurements are further characterised by the absence or presence of a low-energy charged pion reconstructed using a dedicated algorithm, leveraging machine learning. Data-driven methods are used to estimate the background contributions in the search regions. No significant excesses are found and 95% CL lower limits are placed on the masses of charginos and τ -sleptons in the lifetime range 0.01–10 ns. Observed (expected) mass limits of up to 225 GeV (250 GeV) are set for pure-higgsino charginos in scenarios with lifetimes below 0.03 ns, where the electroweakino mass splitting is entirely due to loop corrections involving the Standard Model bosons, and up to 720 GeV (840 GeV) for charginos with a lifetime of around 1 ns. For wino production, charginos with masses up to 880 GeV (1020 GeV) are excluded for lifetimes of around 1 ns. For τ -sleptons with lifetimes of around 1 ns, masses are excluded up to 320 GeV (390 GeV) in Constrained Minimal Supersymmetric Standard Model scenarios and 300 GeV (380 GeV) in Gauge-Mediated Supersymmetry-Breaking scenarios.

Contents

| | | |
|----------|---|-----------|
| 1 | Introduction | 2 |
| 2 | ATLAS detector | 5 |
| 3 | Data and simulated event samples | 6 |
| 4 | Event reconstruction | 8 |
| 5 | Analysis strategy | 10 |
| 6 | Background estimation | 12 |
| 7 | Systematic uncertainties | 19 |
| 8 | Results | 20 |
| 9 | Conclusion | 28 |

1 Introduction

Supersymmetry (SUSY) [1–6] is a theoretical framework based on a space-time symmetry that predicts the existence of a partner for each Standard Model (SM) particle. These partner particles have the same quantum numbers as their SM counterparts, but differ by one half unit of spin. SUSY offers a solution to the hierarchy problem [7–10] if some of the partner particles have masses around the electroweak scale. The supersymmetric partners are named to reflect their SM counterparts: for example, the τ -slepton is the SUSY partner of the τ -lepton. The supersymmetric partners of the electroweak gauge bosons and the Higgs bosons, collectively referred to as electroweakinos, consist of the bino and winos and the higgsinos, respectively. These states mix to form the mass eigenstates: the bino, neutral wino, and neutral higgsinos mix to form the neutralinos ($\tilde{\chi}_{1,2,3,4}^0$), while the charged wino and charged higgsinos mix to form charginos ($\tilde{\chi}_{1,2}^\pm$), where the subscripts denote increasing mass. The superpartners of the third-generation charged leptons (τ_L, τ_R) are referred to as τ -sleptons ($\tilde{\tau}_L, \tilde{\tau}_R$) and mix to form two mass eigenstates $\tilde{\tau}_1$ and $\tilde{\tau}_2$, where $\tilde{\tau}_1$ is the lighter of the two and is henceforth referred to as the τ -slepton ($\tilde{\tau}$). R -parity-conserving supersymmetry [11] addresses several limitations of the SM, providing a natural candidate for dark matter (DM) in the form of the lightest supersymmetric particle (LSP) [12, 13]. In SUSY scenarios with very heavy, strongly interacting superpartners, the direct production cross-section of electroweakinos and sleptons in high-energy proton-proton (pp) collisions at the Large Hadron Collider (LHC) can significantly exceed that of strongly interacting superpartners.

In scenarios where the $\tilde{\chi}_1^0$ and $\tilde{\chi}_1^\pm$ are wino-like and all other SUSY particles are decoupled, the mass difference, $\Delta m(\tilde{\chi}_1^\pm, \tilde{\chi}_1^0)$, is small (~ 100 MeV) and arises from SM radiative corrections [14, 15]. Anomaly-mediated supersymmetry-breaking (AMSB) models [16, 17] naturally predict such mass splittings and give rise to a wino-like LSP. In these scenarios, the mass-splitting between the charged wino and neutral wino is suppressed at tree level by the approximate custodial symmetry, and has been calculated at the two-loop level to be approximately 160 MeV [14], corresponding to a chargino lifetime of $\tau(\tilde{\chi}_1^\pm) \sim 0.2$ ns and a decay length of $c\tau(\tilde{\chi}_1^\pm) \sim 60$ mm. Furthermore, a number of ‘natural’ SUSY models [18–20],

where the $\tilde{\chi}_2^0$ is no longer decoupled, predict a light higgsino LSP with a mass near the electroweak scale. In these scenarios, the higgsino mass parameter $|\mu|$ is small compared to the other electroweakino mass parameters, which could mean higgsinos are discoverable at the LHC. While the charged and neutral higgsino states are mass degenerate at tree level, higher-order SM loop corrections generate a mass splitting of approximately 300 MeV. For chargino masses between 91 GeV and 1000 GeV, the mass splitting ranges approximately from 280 MeV to 350 MeV [21], corresponding to chargino lifetimes of $\tau(\tilde{\chi}_1^\pm) \sim 0.026\text{--}0.048$ ns ($c\tau(\tilde{\chi}_1^\pm) \sim 7\text{--}14$ mm) [15]. Due to the small mass splitting, the $\tilde{\chi}_1^\pm$ is assumed to decay via $\tilde{\chi}_1^\pm \rightarrow \pi^\pm \tilde{\chi}_1^0$ with a branching fraction of 100% in the wino scenarios and 95% in the higgsino scenarios [22]. The neutralino masses are set such that $m(\tilde{\chi}_2^0) = m(\tilde{\chi}_1^0)$, hence the $\tilde{\chi}_2^0$ cannot decay to the $\tilde{\chi}_1^\pm$ or $\tilde{\chi}_1^0$ and is treated as a stable particle that escapes the detector, similarly to the $\tilde{\chi}_1^0$.

Models featuring light τ -sleptons can yield a dark-matter relic density consistent with cosmological observations [23] and, more generally, light sleptons can participate in the co-annihilation of neutralinos [24, 25]. Long-lived τ -sleptons arise naturally in co-annihilation dark-matter models [26–28] and in gauge-mediated supersymmetry-breaking (GMSB) models [29–31]. Two simplified SUSY models are considered for τ -sleptons in this paper. The first is inspired by the Constrained Minimal Supersymmetric Standard Model (CMSSM) [32–34], where a long-lived τ -slepton can arise from a small (~ 2 GeV) mass-splitting between the τ -slepton and the $\tilde{\chi}_1^0$ LSP, CP-violating phases, and the mixing angle between the left- and right-handed τ -slepton states. The CMSSM-inspired scenarios are parameterised by the τ -slepton mass and lifetime, and the τ -slepton decays with 100% branching fraction as $\tilde{\tau} \rightarrow \tau \tilde{\chi}_1^0$. The second scenario is inspired by GMSB models, where a long-lived τ -slepton can arise from small couplings to its decay products. The LSP is the almost massless gravitino (\tilde{G}), the superpartner of a proposed graviton. This model is parameterised by the τ -slepton mass and lifetime, and assumes a 100% branching fraction for $\tilde{\tau} \rightarrow \tau \tilde{G}$.

In all considered scenarios, the charged SUSY particle (wino, higgsino or τ -slepton) can be produced with large momentum and live long enough to traverse multiple layers of the ATLAS pixel detector before decaying. In models containing charginos, the chargino deposits energy in the innermost tracking layers before it decays and can be reconstructed as a short track if at least three layers of the tracking detector are hit. The weakly interacting LSP will escape detection and lead to missing transverse momentum (\vec{p}_T^{miss}) and the charged pion from the chargino decay has a very low momentum and is not reconstructed as a track by existing algorithms, this gives rise to the characteristic ‘disappearing track’ signature where the track from the chargino stops a short distance into the detector. The algorithms used to reconstruct the short tracks, referred to as tracklets, need energy deposits (hits) in at least three pixel layers. Therefore successful reconstruction requires charginos to have transverse path lengths that at least exceed the radius of the third pixel layer at ~ 88.5 mm. This makes the higgsino-like scenarios considerably more challenging than the wino-like models from an experimental perspective because of the extremely short chargino lifetime predicted in the higgsino models. A similar scenario occurs in the case of τ -slepton production, where a long-lived τ -slepton particle will traverse the inner layers of the pixel detector before decaying into a τ -lepton and the LSP. The LSP escapes the detector unobserved, resulting in missing transverse momentum, and the τ -leptons evade standard reconstruction techniques, again resulting in a signature containing a disappearing track and missing transverse momentum.

In addition to the SUSY-specific wino and higgsino models studied in this paper, the disappearing-track signature is typical of a large class of DM models that predict a DM thermal relic from a massive particle with only electroweak gauge interactions [35]. The wino and higgsino models probed in this search are part of a more generic class of models containing spin-1/2 particles transforming under SU(2) symmetry,

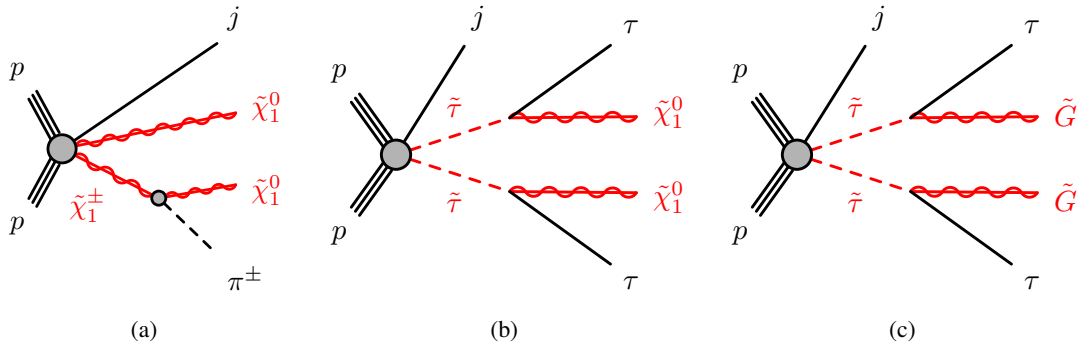


Figure 1: Representative signal diagrams for (a) the electroweak production of $\tilde{\chi}_1^\pm \tilde{\chi}_1^0$, and τ -slepton pair production in (b) CMSSM-inspired or (c) GMSB-inspired SUSY models. The signal signature consists of a long-lived $\tilde{\chi}_1^\pm$ or τ -slepton, missing transverse momentum, and quarks or gluons, which are observed as jets (j). When considering the electroweakino scenarios, the production of $\tilde{\chi}_1^+ \tilde{\chi}_1^-$ is also considered, as is $\tilde{\chi}_1^\pm \tilde{\chi}_2^0$ specifically in the higgsino scenario.

which give rise to nearly mass-degenerate doublets $(\tilde{\chi}_1^\pm, \tilde{\chi}_1^0)$ and triplets $(\tilde{\chi}_1^\pm, \tilde{\chi}_2^0, \tilde{\chi}_1^0)$ of new particles, respectively. In both cases, the $\tilde{\chi}_1^0$ is a DM candidate, while the $\tilde{\chi}_1^\pm$ gives rise to the disappearing-track signature. These DM models have gained interest in the wider community as an important area of study at future colliders [36–39].

This paper targets two electroweak production processes, the production of charginos and neutralinos, and the production of τ -slepton pairs in CMSSM- and GMSB-inspired scenarios, as shown in Figure 1, in the context of simplified SUSY models [40–42]. In all scenarios, the charged SUSY partner is long-lived and can be reconstructed from hits in the ATLAS pixel detector. A high-momentum jet from initial-state radiation (ISR) is required in order to ensure that significant missing transverse momentum is available for event triggering.

Previous ATLAS searches for long-lived supersymmetric charged particles searched for events with a disappearing track with at least four pixel hits [43–45]. Their results benefited from the addition of a new innermost pixel tracking layer installed during the LHC long shutdown between Run 1 and Run 2. The extra layer of pixels enabled the reconstruction of tracks shorter than those in the previous Run-1 analysis [46] and enhanced the sensitivity to shorter charged-particle lifetimes. The Run-2 ATLAS search excluded wino-like charginos with lifetimes of 0.2 ns for masses up to 460 GeV, and higgsino-like charginos with masses up to 152 GeV [43]. Searches performed by the CMS Collaboration excluded wino-like charginos with masses below 474 GeV and a lifetime of 0.2 ns [47]. Both the ATLAS and CMS collaborations have performed searches for stable charginos and τ -sleptons using ionisation-loss or time-of-flight techniques, excluding charginos with masses smaller than 1.3 TeV for lifetimes exceeding 100 ns, and τ -sleptons with masses 200–560 GeV for lifetimes of 10 ns [48, 49].

In order to improve on these results, significant developments were made in the tracking techniques necessary for shorter lifetime scenarios. This search employs a dedicated tracking algorithm to reconstruct tracklets with as few as three pixel hits. Furthermore, to enhance sensitivity to the electroweakino production scenario, the charged pion from the decay of the $\tilde{\chi}_1^\pm$ is targeted with a specially optimised reconstruction algorithm. Due to the small mass-splitting between the $\tilde{\chi}_1^\pm$ and $\tilde{\chi}_1^0$, the charged pion has extremely low momentum, ranging from 250 to 350 MeV for the $\tilde{\chi}_1^\pm$ lifetimes considered, and typically has large impact parameters measured relative to the interaction region. In this paper, the sensitivity to charginos with wino and higgsino lifetimes motivated by SM loop corrections is significantly improved

due to new analysis methods including updated signal region selection criteria, the previously mentioned reconstruction algorithms, and improved track-quality requirements. The new track-quality criteria requires the disappearing track not to be associated with any energy deposits in the calorimeter. This significantly enhances the rejection of dominant backgrounds and accounts for two-thirds of the total improvement in the mass reach of the search in the electroweak wino-like production channel.

The paper is structured as follows: Section 2 introduces the ATLAS detector apparatus; Section 3 describes the dataset and the Monte Carlo simulation samples used; Section 4 discusses the object-level event reconstruction, while Section 5 describes the signal selection optimisation and Section 6 describes the background estimation techniques; Section 7 provides an overview of the systematic uncertainties considered, with Section 8 presenting the results and interpretation thereof; and finally, Section 9 summarises the conclusions.

2 ATLAS detector

The ATLAS detector [50] at the LHC covers nearly the entire solid angle around the collision point.¹ It consists of an inner tracking detector surrounded by a thin superconducting solenoid, electromagnetic and hadronic calorimeters, and a muon spectrometer incorporating three large superconducting air-core toroidal magnets.

The inner-detector system (ID) is immersed in a 2 T axial magnetic field and provides charged-particle tracking in the range $|\eta| < 2.5$. The high-granularity silicon pixel detector covers the vertex region and typically provides four measurements per track, the first hit generally being in the insertable B-layer (IBL) installed before Run 2 [51, 52]. It is followed by a silicon microstrip detector called the SemiConductor Tracker (SCT), which usually provides eight measurements per track, two per double-sided detector layer. The barrel region, $|\eta| < 1.7$, is of special interest to this analysis. Here the pixel detector comprises four layers at radii of 33.25 mm (IBL), 50.5 mm, 88.5 mm, and 122.5 mm. This is followed by the four SCT barrel layers, located at radii of 299 mm, 371 mm, 443 mm, and 514 mm. These silicon detectors are complemented by the transition radiation tracker (TRT), which enables radially extended track reconstruction up to $|\eta| = 2.0$. The TRT also provides electron identification information based on the fraction of hits (typically 30 in total) above a higher energy-deposit threshold corresponding to transition radiation.

The calorimeter system covers the pseudorapidity range $|\eta| < 4.9$. Within the region $|\eta| < 3.2$, electromagnetic calorimetry is provided by barrel and endcap high-granularity lead/liquid-argon (LAr) calorimeters, with an additional thin LAr presampler covering $|\eta| < 1.8$ to correct for energy loss in material upstream of the calorimeters. Hadronic calorimetry is provided by the steel/scintillator-tile calorimeter, segmented into three barrel structures within $|\eta| < 1.7$, and two copper/LAr hadronic endcap calorimeters. The solid angle coverage is completed with forward copper/LAr and tungsten/LAr calorimeter modules optimised for electromagnetic and hadronic energy measurements, respectively.

¹ ATLAS uses a right-handed coordinate system with its origin at the nominal interaction point (IP) in the centre of the detector and the z -axis along the beam pipe. The x -axis points from the IP to the centre of the LHC ring, and the y -axis points upwards. Polar coordinates (r, ϕ) are used in the transverse plane, ϕ being the azimuthal angle around the z -axis. The pseudorapidity is defined in terms of the polar angle θ as $\eta = -\ln \tan(\theta/2)$ and is equal to the rapidity $y = (1/2) \ln[(E + p_z)/(E - p_z)]$ in the relativistic limit. Angular distance is measured in units of $\Delta R \equiv \sqrt{(\Delta y)^2 + (\Delta \phi)^2}$.

The muon spectrometer (MS) comprises separate trigger and high-precision tracking chambers measuring the deflection of muons in a magnetic field generated by the superconducting air-core toroidal magnets. The field integral of the toroids ranges between 2.0 and 6.0 T m across most of the detector. Three layers of precision chambers, each consisting of layers of monitored drift tubes, cover the region $|\eta| < 2.7$, complemented by cathode-strip chambers in the forward region, where the background is highest. The muon trigger system covers the range $|\eta| < 2.4$ with resistive-plate chambers in the barrel, and thin-gap chambers in the endcap regions.

The luminosity is measured mainly by the LUCID-2 detector [53], which records Cherenkov light produced in the quartz windows of photomultipliers located close to the beam pipe.

Events were selected by the first-level trigger system implemented in custom hardware, followed by selections made by algorithms implemented in software in the high-level trigger [54]. The first-level trigger accepted events from the 40 MHz bunch crossings at a rate close to 100 kHz, which the high-level trigger reduced in order to record complete events to disk at about 1.25 kHz.

A software suite [55] is used in data simulation, in the reconstruction and analysis of real and simulated data, in detector operations, and in the trigger and data acquisition systems of the experiment.

3 Data and simulated event samples

This search uses data from an integrated luminosity of 137 fb^{-1} of pp collisions at a centre-of-mass energy $\sqrt{s} = 13 \text{ TeV}$ recorded by the ATLAS experiment during Run 2 of the LHC (2015–2018). In this data-taking period, the number of interactions per bunch crossing ranged from about 8 to 70, with an average of 34 [56]. The uncertainty in the integrated luminosity is 0.83% [57], obtained using the LUCID-2 detector for the primary luminosity measurements, complemented by measurements using the ID and calorimeters. Only events recorded under stable beam conditions are used in the analysis, and general data-quality requirements ensure that all detector subsystems were operational [56]. In about 2% of Run 2 data taking the SCT experienced a significant increase in readout errors compared to standard operation. These data periods are removed as it increases the number of spuriously reconstructed pixel-only tracks which can mimic a disappearing-track signature.

The data were collected primarily with a missing transverse momentum trigger [58, 59], to target events where the sparticle system recoils against a high- p_T ISR jet and the undetected neutral particles lead to a large amount of missing transverse momentum. The trigger threshold was raised as the luminosity increased during Run 2, but each threshold value provided an efficiency of $>90\%$ when requiring online a reconstructed missing transverse momentum of at least 230 GeV. Additional single-lepton ($\ell = e, \mu$) triggers are used to select regions to constrain background estimates, and these triggers operate on an efficiency plateau when applying an offline lepton transverse momentum requirement of $p_T(\ell) > 27 \text{ GeV}$ [60, 61].

Monte Carlo (MC) simulated samples are used to model SM processes and estimate the expected signal yields. All samples were produced using the ATLAS simulation infrastructure [62] and either GEANT4 [63] or a faster simulation based on a parameterisation of the calorimeter response and GEANT4 for the other detector systems. The effect of multiple interactions in the same and neighbouring bunch crossings (pile-up) was modelled by overlaying each simulated hard-scattering event with inelastic pp events generated with PYTHIA 8.186 [64] using the NNPDF2.3LO set of parton distribution functions (PDFs) [65] and the A3 set of tuned parameters [66]. The MC simulated samples were reweighted to match the actual distribution of the mean number of interactions per bunch crossing observed in data in 2015–2018.

The electroweakino signal samples were generated with MADGRAPH5_AMC@NLO 2.9.9 [67] at leading order (LO) and interfaced to PYTHIA 8.306 [68] for the modelling of the parton showering (PS), hadronisation and underlying event. In the wino scenarios, $\Delta m(\tilde{\chi}_1^\pm, \tilde{\chi}_1^0)$ is dependent upon $m(\tilde{\chi}_1^\pm)$ and follows from the calculations in Refs. [16, 17]. In the higgsino scenarios, the mass splitting is dependent upon $m(\tilde{\chi}_1^\pm)$ and is set according to the calculations in Ref. [22]. The CMSSM τ -slepton signals were generated with MADGRAPH5_AMC@NLO 2.9.5 at LO and interfaced to PYTHIA 8.306, while the GMSB τ -slepton signals used MADGRAPH5_AMC@NLO 2.6.1 at LO and PYTHIA 8.230.

For all signal scenarios the underlying event was modelled with the A14 [69] set of tuned parameters. The matrix element (ME) calculation was performed at tree level and includes the emission of up to two additional partons. The ME–PS merging was done using the CKKW-L [70] prescription. The NNPDF3.0_{LO} set of PDFs was used throughout [71]. To ensure efficient sample generation, a lifetime reweighting procedure was used, where a single signal-mass scenario and lifetime has a set of event weights allowing the signal to be reweighted to different proper lifetimes of the long-lived particle. The charginos and τ -sleptons are propagated through the detector to their decay point using the standard simulation, including magnetic field effects and electromagnetic interactions with detector material.

Signal cross-sections are calculated to next-to-leading order (NLO) in the strong coupling constant, adding the resummation of soft gluon emission at next-to-leading-logarithm (NLL) accuracy [72–80] using RESUMMINO 2.0.1. The nominal cross-section and its uncertainty are taken from an envelope of cross-section predictions using different PDF sets and factorisation and renormalisation scales, as described in Ref. [81]. For the wino and higgsino signal samples, only processes involving the direct production of a $\tilde{\chi}_1^\pm$ are considered in order to produce the disappearing-track signature. Therefore, the wino samples include $\tilde{\chi}_1^+ \tilde{\chi}_1^-$ and $\tilde{\chi}_1^\pm \tilde{\chi}_1^0$ production, while the higgsino signal samples include $\tilde{\chi}_1^+ \tilde{\chi}_1^-$, $\tilde{\chi}_1^\pm \tilde{\chi}_1^0$, and $\tilde{\chi}_1^\pm \tilde{\chi}_2^0$. Taking an example for higgsino production with $m(\tilde{\chi}_1^\pm) = 300$ GeV and $m(\tilde{\chi}_2^0) = m(\tilde{\chi}_1^0) = 299$ GeV, the cross-section value for each of the $\tilde{\chi}_1^\pm \tilde{\chi}_2^0$ and $\tilde{\chi}_1^\pm \tilde{\chi}_1^0$ processes is 90.8 fb, while the cross-section is 53 fb for $\tilde{\chi}_1^+ \tilde{\chi}_1^-$ production. For wino production with $m(\tilde{\chi}_1^\pm) = 300$ GeV and $m(\tilde{\chi}_1^0) = 299$ GeV, the cross-section values are 387 fb and 190 fb for $\tilde{\chi}_1^0 \tilde{\chi}_1^\pm$ and $\tilde{\chi}_1^+ \tilde{\chi}_1^-$ production, respectively. Finally, the cross-section for τ -slepton pair production of $m(\tilde{\tau}) = 300$ GeV is 6.3 fb in both the CMSSM and GMSB models.

MC simulation of V +jets events was used to study the fake-tracklet background. They were simulated with the SHERPA 2.2.1 [82] generator using NLO matrix elements for up to two partons, and LO matrix elements for up to four partons, calculated with the Comix [83] and OPENLOOPS [84–86] libraries. The matrix elements were matched with the SHERPA parton shower [87] using the MEPS@NLO prescription [88–91] and the set of tuned parameters developed by the SHERPA authors. The NNPDF3.0_{NNLO} set of PDFs [71] was used and the samples were normalised to a NNLO prediction [92].

To evaluate the detector response when reconstructing short tracks and to calculate the associated reconstruction efficiencies, a set of so-called ‘particle gun’ samples are used. These samples do not represent a specific physical event or process; instead, for each generated event the particle of interest is placed at the centre of the detector with a certain momentum and direction and can be used to investigate detector reconstruction capabilities. These samples do not include pile-up. The analysis uses three ‘particle gun’ samples, corresponding to electrons, muons and charged pions, generated uniformly across a transverse momentum range of 10–100 GeV; they are used to estimate the reconstruction efficiencies as needed for the data-driven background estimation methods employed.

4 Event reconstruction

The analysis uses standard ATLAS reconstruction techniques to reconstruct leptons and jets, and to calculate the missing transverse momentum, enabling the identification of potential events of interest before employing a dedicated tracklet algorithm to specifically identify events containing disappearing tracks.

Standard tracks are reconstructed in the ID within $|\eta| < 2.5$ [93] and subsequently combined to create primary vertex candidates formed from at least two tracks with $p_T > 500$ MeV [94]. Among these, the primary vertex is identified as the vertex with the largest $\sum p_T^2$, where the sum runs over tracks associated with the vertex. All events considered in the analysis are required to have a primary vertex. The transverse and longitudinal impact parameters of all tracks, denoted by d_0 and z_0 respectively, are calculated relative to the beamline. The z -position of the primary vertex is used to calculate the point of closest approach, which is used as the reference point to calculate z_0 .

Electron candidates are reconstructed from clustered energy deposits in the electromagnetic calorimeter matched to tracks re-fitted to account for bremsstrahlung losses [95]. They are required to have $p_T > 10$ GeV and $|\eta| < 2.47$, and must satisfy the ‘LooseAndBLayer’ quality criteria [96]. In order to ensure that the trajectories of the electrons are consistent with originating from the primary vertex, the longitudinal impact parameter must satisfy $|z_0 \sin \theta| < 0.5$ mm, while the significance of the transverse impact parameter, $|d_0|/\sigma(d_0)$, must be less than 5. Electrons are required to be isolated from other objects by assessing a combination of track- and calorimeter-based information at the ‘FCLoose’ working point [97].

Muon candidates are reconstructed by combining ID tracks with matching MS tracks. They are required to have $p_T > 10$ GeV and $|\eta| < 2.7$, and must satisfy the ‘Medium’ quality criteria [98]. Muons originating from the primary vertex are selected by requiring $|z_0 \sin \theta| < 0.5$ mm and $|d_0|/\sigma(d_0) < 3$. The muons must satisfy isolation requirements similar to those applied to electrons, but using the ‘Loose_FixedRad’ working point [99]. Muons reconstructed purely from MS information are used to estimate muon backgrounds, and are referred to as stand-alone muons.

Hadronic jets are reconstructed using the anti- k_t algorithm [100] as implemented in FastJet [101] with a jet radius parameter $R = 0.4$. The input to this algorithm consists of particle flow (PFlow) objects [102], which combine measurements from the ID and calorimeters [103] to improve the jet energy resolution and increase the jet reconstruction efficiency, especially at low jet p_T . Calibrations are applied to the jet energy scale and resolution, and these include components derived from both simulation and in situ measurements [104]. The analysis uses jets within $|\eta| < 2.8$ with a calibrated $p_T > 20$ GeV. In order to reduce contributions from jets produced in pile-up interactions, all jets with $|\eta| < 2.5$ and $p_T < 60$ GeV are required to satisfy the jet-to-vertex tagger (JVT) [105] ‘Tight’ working point requirements. The tagger is configured to identify jets from the hard-scatter vertex with 92% efficiency.

An overlap removal procedure is applied to avoid double counting of energy from different types of objects. If an electron and a jet are reconstructed within $\Delta R < 0.2$, the jet is rejected, while the electron candidate is kept. Subsequently, if an electron or muon is separated from a jet by $\Delta R < 0.4$, the electron or muon is discarded and the jet is kept.

The missing transverse momentum, with magnitude E_T^{miss} , is calculated as the negative vector sum of the transverse momenta of all identified hard physics objects (electrons, muons, jets), plus a contribution from an additional ‘soft term’. Forward jets within $2.8 < |\eta| < 4.5$ are also included in the E_T^{miss} calculation. The soft term is calculated from tracks matched to the primary vertex and not assigned to any of the hard

objects [106] but does not contain the reconstructed tracklets or charged pions described in the following paragraphs.

To reconstruct the disappearing track due to a charged particle decaying after passing through the pixel detector, a dedicated tracklet reconstruction algorithm is applied after the standard reconstruction techniques described above are performed [107]. The tracking-detector hits already associated with reconstructed standard tracks are excluded from this tracklet-finding iteration. The algorithm attempts to identify tracklets having three or four hits in the pixel detector. The procedure attempts to extend the tracks into the SCT and TRT detectors and vetoes the tracklet if it can be associated with additional hits. Compared to the previous ATLAS analysis using the disappearing-track signature [43], the veto does not consider an association if more SCT hits are only found multiple layers away from the tracklet. This reduces cases where tracklets would have been vetoed due to spurious SCT hits [107] further into the detector. To improve the momentum resolution of the tracklets, they are re-fitted, adding the primary vertex as an additional constraint, and the tracklet is required to have $|d_0|/\sigma(d_0) < 1.5$ and $|z_0 \sin \theta| < 0.2$ mm. An overlap removal procedure discards tracklets within $\Delta R = 0.4$ of a jet, a lepton, or a track in the MS. Isolation requirements are also applied to the tracklets: the scalar sum of the p_T of all tracks within a cone of radius $\Delta R = 0.4$ around the tracklet, p_T^{cone40} , must satisfy $p_T^{\text{cone40}}/p_T^{\text{tracklet}} < 0.04$ and the total transverse energy of all topological clusters within the $\Delta R = 0.4$ cone, $E_T^{\text{topoclus40}}$, must be less than 5 GeV. Tracklets are required to have $|\eta| > 0.1$, vetoing the central region where MS coverage is reduced. Figure 2(a) shows that the reconstruction efficiency for three- and four-layer tracklets can reach 80% depending upon the distance travelled by the chargino before decaying.

To identify low-energy charged pions, indicative of the electroweakino signal scenario, a boosted decision tree (BDT) machine-learning algorithm is used. After performing the tracklet reconstruction described above, a set of low-momentum tracks (‘soft tracks’) are reconstructed from the remaining hits. These low-momentum tracks are seeded from at least three SCT hits that are within $\Delta R = 0.8$ of a tracklet and are then extended using further SCT or TRT hits. A minimum of six hits, and at most two holes² [107], are required to reconstruct a soft track and a requirement of $p_T > 200$ MeV is applied. As only a limited number of four-layer tracklet events have a matching soft-track that satisfies the soft-track reconstruction requirements, only events containing tracklets produced with three pixel hits are used when performing the pion reconstruction. The BDT is used to select viable charged pion candidates and to reject events with coincidental hits forming a soft track. The algorithm is trained with MC signal simulation, using soft tracks that have been ‘truth-matched’ at generator level to charged pions from long-lived chargino decays using a ΔR -matching criterion.

The background is taken from data, selecting tracklets that have large impact parameter values with respect to the primary vertex. From MC studies this is expected to be dominated by accidental crossings, referred to as the ‘fake track’ background. The algorithm uses eight input variables related to the properties of the soft tracks, including the kinematic properties p_T and η , the number of hits/holes associated with the track in the SCT, the number of hits associated with the track in the TRT, the distance in ΔR between the soft track and the tracklet, the distance in z between the soft track and the tracklet, and the χ^2 value of the soft track when fitted to the tracklet’s endpoint. The TMVA architecture [108] is used with gradient boost, and a hyperparameter optimisation is performed to prevent overtraining. Figure 2(b) displays the BDT output score. A low-energy charged pion is identified if the score for a soft track is >0.8 and, to reduce the misidentification rate, a transverse impact parameter requirement of $|d_0|/\sigma(d_0) < 40$ is satisfied. The latter rejects an additional 4% of the tracklet background with minimal impact on the signal, according to

² A hole is a missing hit on a reconstructed track trajectory, possibly due to a non-functioning strip which was not masked.

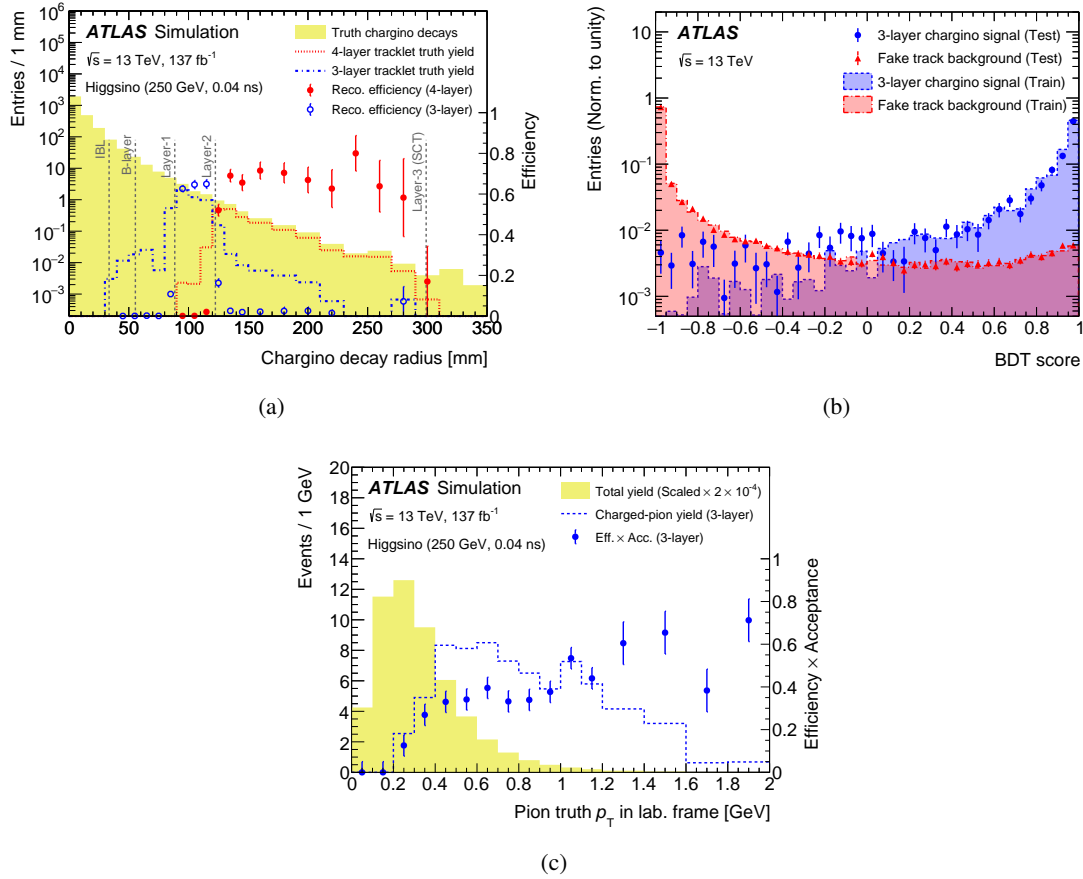


Figure 2: Representative distributions related to the reconstruction of tracklets and charged pions: (a) event yields and reconstruction efficiencies for three- and four-layer tracklet reconstruction as a function of $\tilde{\chi}_1^\pm$ decay radius; (b) BDT output score used to judge if an event contains a low-energy pion, showing the training dataset (solid histogram) and the test dataset (points); (c) event yields and reconstruction efficiency for charged pions as a function of the true pion transverse momentum as measured in the lab-frame, where the acceptance includes all charged-pion reconstruction effects but not geometric acceptance from tracklet reconstruction (which is assumed to already have been reconstructed). The true transverse momentum is defined as $p_T = \sqrt{p_x^2 + p_y^2}$ in the global detector coordinate system with the z -axis along the beam pipe. For (a) and (c) the filled histogram displays the total yield without applying a selection, while the dashed lines present the yield after applying the tracklet selection or tracklet+pion selection. The points denote the reconstruction efficiency. A representative higgsino signal scenario with $m(\tilde{\chi}_1^\pm) = 250 \text{ GeV}$ and $\tau(\tilde{\chi}_1^\pm) = 0.04 \text{ ns}$ is shown.

MC simulation. Figure 2(c) shows that the pion reconstruction efficiency, measured as a function of the true pion p_T in the lab-frame, is as high as 70% for p_T near 2 GeV.

5 Analysis strategy

The signal scenarios investigated contain a tracklet, E_T^{miss} , and in the case of the chargino production scenarios a low-energy charged pion. In all considered signal scenarios, the E_T^{miss} is however too small to satisfy the E_T^{miss} trigger requirements. Therefore, events are required to contain a high- p_T initial-state

Table 1: Summary of the signal region selection requirements.

| Variable | SR ^{4High} | SR ^{4Mid} | SR ^{3High1π} | SR ^{3High0π} |
|--|---------------------|--------------------|--------------------------------------|--------------------------------------|
| E_T^{miss} trigger | Passed | | | |
| Number of leptons | = 0 | | | |
| Number of jets ($p_T > 20$ GeV) | ≥ 1 | | | |
| Leading jet p_T | > 100 GeV | | | |
| $ \Delta\phi(j_1, \vec{p}_T^{\text{miss}}) $ | > 1.0 | | | |
| Number of four-layer tracklets | ≥ 1 | | | = 0 |
| Number of three-layer tracklets | - | | | ≥ 1 |
| Number of charged pions | - | | ≥ 1 | = 0 |
| Tracklet p_T | > 60 GeV | > 60 GeV | > 60 GeV | > 60 GeV |
| Tracklet $ \eta $ | 0.1–1.9 | 0.1–1.9 | 0.1–1.9 | 0.1–1.7 |
| E_T^{miss} | > 300 GeV | 150–300 GeV | > 240 GeV | > 280 GeV |

radiation (ISR) jet to boost the SUSY particle system and achieve enough E_T^{miss} to exceed the trigger threshold. Signal regions (SRs) are defined using kinematic variable selections to enhance the contribution from signal processes relative to the background processes. All SRs require events to have zero leptons, at least one jet, and a large azimuthal separation between the highest- p_T jet and the \vec{p}_T^{miss} , denoted by $(|\Delta\phi(j_1, \vec{p}_T^{\text{miss}})|)$. Four orthogonal SRs are defined in the analysis, two requiring the presence of a tracklet reconstructed from four pixel layers, and another two requiring the presence of a tracklet reconstructed from three pixel layers and differing mainly in whether or not a low-energy charged pion is required. Table 1 provides a summary of all SR selections used in the analysis.

The four-hit SRs (SR^{4High} and SR^{4Mid}) require events to contain a tracklet that is reconstructed from four pixel-detector hits and has tracklet $p_T > 60$ GeV. Tracklets with hits in four layers provide sensitivity to a wide range of $\tilde{\chi}_1^\pm/\tau$ -slepton lifetimes, from 0.02 to 10 ns. No requirement is placed on the presence of a low-energy charged pion. SR^{4High} requires high E_T^{miss} , whereas SR^{4Mid} selects events with lower E_T^{miss} . The two SRs containing tracklets reconstructed from hits in three layers are defined in order to target very short-lived charged SUSY particles, which is the phase space of interest for the higgsino-like case, where $\tau(\tilde{\chi}_1^\pm) \sim 0.02\text{--}0.2$ ns. A tracklet $p_T > 60$ GeV requirement is applied for both three-layer tracklet SRs and the main difference between the two is the absence or presence of a low-energy charged pion. SR^{3High1 π} requires the presence of at least one low-energy charged pion and requires $E_T^{\text{miss}} > 240$ GeV, whereas SR^{3High0 π} applies a low-energy charged-pion veto and applies a slightly tighter $E_T^{\text{miss}} > 280$ GeV selection.

In all regions, the backgrounds arise either from events containing particles that are misidentified as tracklets or from unrelated coincidental pixel-layer hits that form a tracklet. Figure 3 presents schematically how background events might be mis-reconstructed and satisfy the SR selections. The $\tilde{\chi}_1^\pm$ signal scenario is also shown, in the case where the charged pion is reconstructed from the track it leaves in the SCT detector, and in the case where the charged pion does not have enough energy to reach the SCT and leave any hits. Background events may have tracklets reconstructed from pixel hits which belong to known SM particles (electrons, muons, hadrons) or from coincidentally combined hits (referred to as the ‘fake’ background).

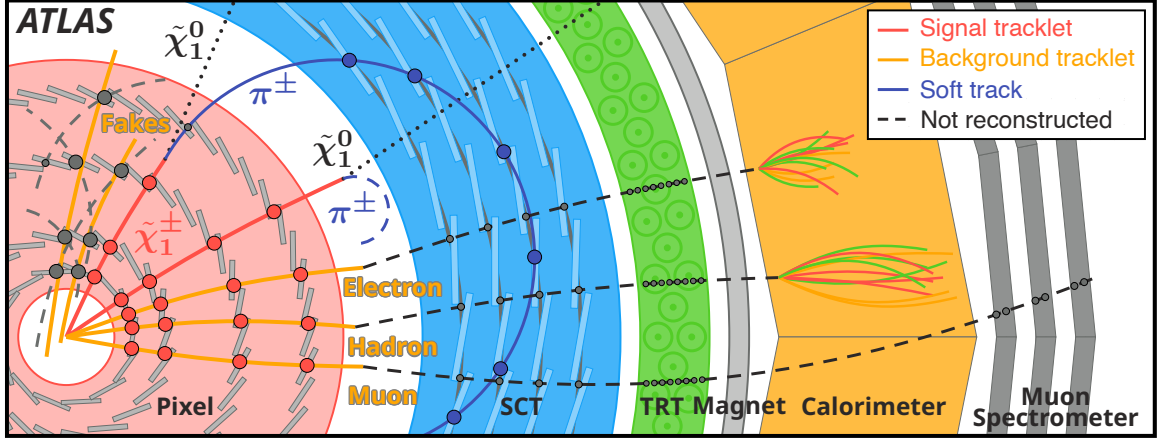


Figure 3: Schematic diagram illustrating how the signal scenarios are detected and how the background processes may enter the SR selections. The detector layers are not shown to scale. Taken from Ref. [43].

6 Background estimation

Data-driven methods are used to estimate all backgrounds in the analysis and a similar approach is used for all backgrounds sources. Template regions (TRs) are used to calculate an initial tracklet p_T distribution/template by selecting events containing the background under consideration. A set of alternative regions, with relaxed reconstruction selections, are used to calculate transfer factors (TFs) that are then applied to the tracklet p_T template to correct for the rate of electrons, muons, hadrons, and spurious signals/fakes misidentified as tracklets. This approach produces a purely data-driven estimate of the SR background from electrons and muons. However, MC simulation is used to calculate the TFs for the hadronic and fake backgrounds, so control regions (CRs) are used to normalise the tracklet p_T distribution and predict the expected yields in the SRs.

The electron and muon backgrounds arise due to bremsstrahlung from interactions with the inner-detector material resulting in an abrupt increase in the electron/muon track curvature. This causes the lepton to not satisfy the standard tracking requirements for lepton reconstruction and it is instead incorrectly reconstructed as a tracklet. Hadrons can also be misidentified as tracklets because of similar sudden increases in track curvature due to bremsstrahlung or hadronic interactions in the inner-detector material, or charged hadron decays inside the inner detector. Fake tracklets can be formed with spurious pixel hits from low- p_T particles that do not belong to the primary interaction (pile-up), from the underlying event, or from detector noise. The methods described below are used to estimate the expected tracklet p_T distributions (f_{SR}^{bkg}) in each SR.

The dominant background contribution in all SRs is due to fake tracklets. From MC studies it is found that true tracklets usually exhibit a correlation between the true particle p_T and the tracklet p_T , whereas fake tracklets do not have this correlation. For each SR the p_T distribution of fake tracklets is estimated by

$$f_{SR}^{fake}(p_T) = N^{TRfake}(p_T) \times TF_{d_0\text{-correction}}^{fake}(d_0) \times TF_{\text{hybrid}}^{fake}(p_T) \times SF_{z_0}^{fake} \times SF_{E_T^{miss}}^{fake},$$

using the yields in TRs modified by TFs and scale factors (SFs), which are described further below. In total, three tracklet p_T templates ($N^{TRfake}(p_T)$) are extracted from three TRs (TRfake), each defined with

the same selection as the SRs, but with orthogonal selections of $E_T^{\text{miss}} < 150 \text{ GeV}$ and $|z_0 \sin \theta| > 2.5 \text{ mm}$. Due to this inverted E_T^{miss} selection, the same TRfake is used for SR^{4High} and SR^{4Mid}. The E_T^{miss} trigger can be safely used with this lower selection because the trigger efficiency does not need to be well understood in this region since it is not used to predict the overall event yield. Furthermore, because the tracklets are not included in the E_T^{miss} calculation, the shape of the p_T distribution is independent of E_T^{miss} . All three TRs select tracklets reconstructed from hits in three layers to ensure a high-statistics p_T template. Figure 4(a) presents an example of the $N^{\text{TRfake}}(p_T)$ distribution extracted from the TR associated with SR^{4High} and SR^{4Mid}.

From studies using V +jets MC events, it is found that extrapolating from the high- $|z_0 \sin \theta|$ TR to regions with low $|z_0 \sin \theta|$ introduces a $|d_0|/\sigma(d_0)$ dependence. This is corrected for by using $|d_0|/\sigma(d_0)$ -binned correction factors, $\text{TF}_{d_0\text{-correction}}^{\text{fake}}$, defined as the ratio of the $|d_0|/\sigma(d_0)$ distribution shape for tracklets with $|z_0 \sin \theta| < 0.2 \text{ mm}$ to that for those with $|z_0 \sin \theta| > 2.5 \text{ mm}$ and are taken directly from data. Figure 4(b) shows the difference in $|d_0|/\sigma(d_0)$ between the TR and a low- $|z_0 \sin \theta|$ region, with the $\text{TF}_{d_0\text{-correction}}^{\text{fake}}$ shown in the lower panel.

Studies of V +jets MC events show that the fake-tracklet background has two sources: ‘pure’ fakes, where the tracklet is reconstructed from unrelated coincidental hits in the pixel layers, and ‘hybrid’ fakes, where at least one hit is not from a true hadron. In these studies it is found that at low E_T^{miss} the dominant component comes from pure fakes, while at higher E_T^{miss} there is a mixture of both contributions. To account for the different contributions when extrapolating from low- to high- E_T^{miss} regions, the tracklet p_T template is adjusted by a p_T -dependent transfer factor, $\text{TF}_{\text{hybrid}}^{\text{fake}}$, derived from V +jets MC samples and calculated as the ratio of the tracklet p_T distributions for pure fakes and hybrid fakes. The TFs are used to scale the pure fake p_T distribution to the hybrid fake distribution, and the sum of the pure fakes and hybrid fakes is then used for the final tracklet p_T shape. Figure 4(c) shows the relative contributions of pure fakes and hybrid fakes from MC simulation studies, and the ratio of the two is fitted with a falling exponential-plus-constant distribution as shown in the bottom panel.

To scale the template to data, a set of regions enriched in fake tracklets are used; these select events with a low- p_T tracklet ($p_T < 35 \text{ GeV}$), low E_T^{miss} ($E_T^{\text{miss}} < 150 \text{ GeV}$), and a high- p_T ‘unconstrained’ tracklet ($p_T > 100 \text{ GeV}$), while keeping all other SR selections the same. The unconstrained tracklet is produced from the same hits as a typical tracklet, but there is no requirement to re-fit this tracklet to the primary vertex, so a significantly different p_T measurement can result. A set of scale factors, $\text{SF}_{z_0}^{\text{fake}}$, are calculated as the ratio of events in the fake tracklet enhanced regions to the events in the associated TRfake region but with an alternative selection of tracklet $p_T < 35 \text{ GeV}$ and unconstrained-tracklet $p_T < 100 \text{ GeV}$ ensuring orthogonality.

A final set of scale factors, $\text{SF}_{E_T^{\text{miss}}}^{\text{fake}}$, are used to extrapolate the template from the low- E_T^{miss} region to the SRs with tighter E_T^{miss} selections. The scale factors are derived from CRs which use high values of the tracklet $|d_0|/\sigma(d_0)$ (>1.5), a loosened tracklet p_T selection ($>20 \text{ GeV}$), but otherwise the same selections as the SRs. MC simulation shows the normalisation regions are $>99\%$ pure in fake tracklets, with a ratio of pure to hybrid fakes similar to that in the SRs. Table 2 defines the control regions CR^{4Low} and CR^{4High}, with the ratio of events in the low-CR to the high-CR used to derive the fake background $\text{SF}_{E_T^{\text{miss}}}^{\text{fake}}$ in the signal regions SR^{4High} and SR^{4Mid}. Table 3 defines the control regions CR^{3Low1 π} and CR^{3High1 π} used to calculate $\text{SF}_{E_T^{\text{miss}}}^{\text{fake}}$ for the fake background in SR^{3High1 π} , and Table 4 defines CR^{3Low0 π} and CR^{3High0 π} , which are used to scale this background in SR^{3High0 π} . The remaining two CRs, CR^{3Mid1 π} and CR^{3Mid0 π} , are used to calculate $\text{SF}_{E_T^{\text{miss}}}^{\text{fake}}$ for the validation regions, introduced later in the section.

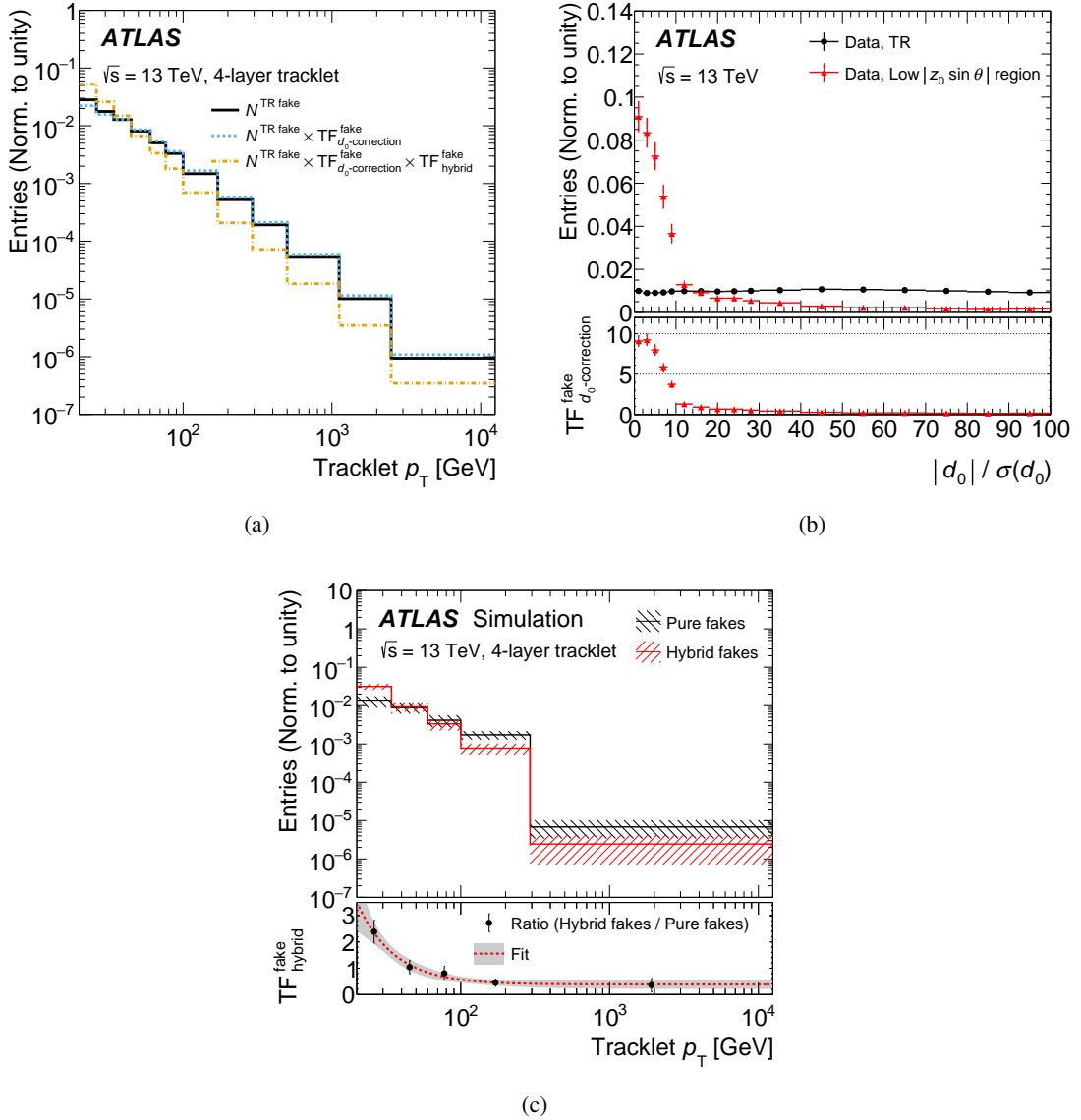


Figure 4: Individual components used in the estimation of the fake background: (a) shows the original template, $N^{\text{TR fake}}(p_T)$, as a solid line. The templates after the application of the transfer factors are shown as dashed lines; (b) shows the $|d_0|/\sigma(d_0)$ dependence introduced when extrapolating over $|z_0 \sin \theta|$ and the binwise, with respect to $|d_0|/\sigma(d_0)$, transfer factors $\text{TF}_{d_0\text{-correction}}^{\text{fake}}(d_0)$ used to remove the dependence; and (c) shows a comparison between the pure fake and hybrid fake contributions and the p_T -dependent transfer factors $\text{TF}_{\text{hybrid}}^{\text{fake}}(p_T)$ used to extrapolate from the template region that contains pure fakes to the SR, which contains a mixture of hybrid and pure fake components.

The background from electrons reconstructed as tracklets is given by

$$f_{\text{SR}}^e(p_T, \eta) = N^{\text{TR}e}(p_T, \eta) \times \text{TF}_{\text{tracklet}}^e(p_T, \eta) \times \text{TF}_{\text{calo-veto}}^e(p_T, \eta) \times f_{\text{smear}}^e(p_T),$$

which uses the yields in TRs modified by TFs and a smearing function that is described further below. Four electron-enriched TRs (TR e), with the same selections as the associated SRs but with the presence of

exactly one electron instead of a tracklet, are used to extract a set of templates for the tracklet p_T spectrum ($N^{\text{TR}e}(p_T, \eta)$). An example of the template p_T spectrum is presented in Figure 5(a) for the $\text{TR}e$ associated with SR^{4High} . The $\text{TR}e$ events must fire the single-electron trigger, with an offline p_T requirement of 27 GeV. To mimic the expected E_T^{miss} distribution in the SR, the electrons are removed from the E_T^{miss} calculation in this region, allowing the same E_T^{miss} selection as in the SR to be applied. A data-driven tag-and-probe method using $Z \rightarrow ee$ events is used to derive correction factors to estimate the likelihood that a standard electron is reconstructed as a tracklet ($\text{TF}_{\text{tracklet}}^e$) by identifying probe electrons that have a calorimeter energy cluster but no associated standard track. Figure 5(b) shows the p_T dependence of the $\text{TF}_{\text{tracklet}}^e$ distributions. A further transfer factor ($\text{TF}_{\text{calo-veto}}^e$) is calculated, again using a data-driven tag-and-probe method in $Z \rightarrow ee$ events, to estimate the likelihood that an electron with a standard track does not have an associated calorimeter energy cluster. Figure 5(c) shows the p_T dependence of $\text{TF}_{\text{calo-veto}}^e$ for three- and four-layer tracklets, where both TFs are calculated in bins of tracklet p_T and η . A transfer

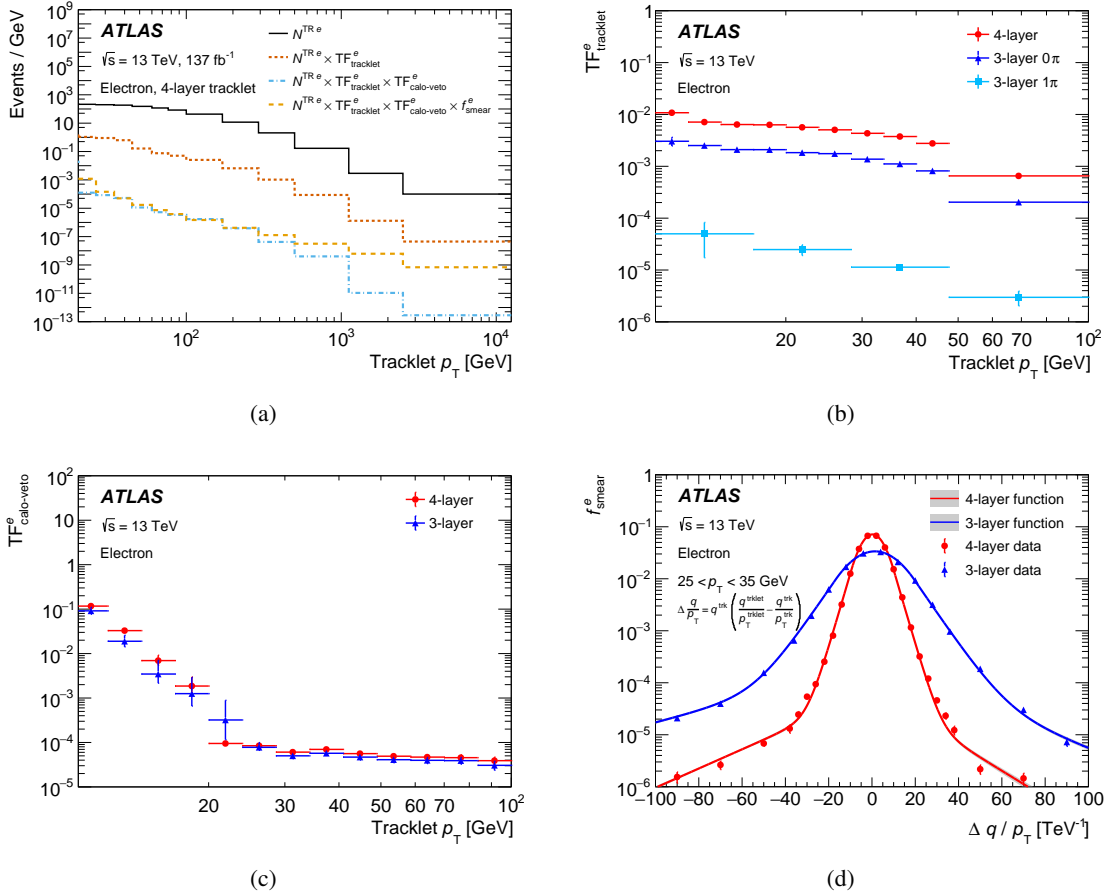


Figure 5: Individual contributions used in the estimation of the electron background: (a) presents the original electron p_T template, $N^{\text{TR}e}(p_T)$, as a solid line, with the templates also shown after the application of each transfer/smearing factor as dashed lines; (b) shows the transfer factor, $\text{TF}_{\text{tracklet}}^e$, used to correct for the likelihood of reconstructing an electron track as a tracklet; (c) shows the transfer factors, $\text{TF}_{\text{calo-veto}}^e$, used to correct for the likelihood of an electron not being associated with a calorimeter energy cluster; and (d) shows the smearing functions, f_{smeare}^e , used to correct the measured electron track p_T to the tracklet p_T (defined on the figure). While the tracklet p_T template and the TFs are dependent upon both p_T and η , the components are shown with their dependence upon the tracklet p_T distribution as a representative distribution.

factor ($\text{TF}_{\text{tracklet}+\pi}^e$) is calculated and used specifically for the regions where the electron is associated with a low-energy charged-pion track and is used instead of $\text{TF}_{\text{tracklet}}^e$ when considering the regions requiring the presence of a pion. The application of these TFs allows the electron p_T template taken from the TR to be scaled in a way that takes into account the likelihood that an electron may not satisfy both of the tracking and calorimeter requirements, and thus is reconstructed as a tracklet. To account for the differences between a standard reconstructed electron track and a reconstructed tracklet, a p_T -dependent smearing function (f_{smear}^e) is applied. To calculate the smearing function, the tracklet reconstruction is applied to a standard track associated with an electron (again using $Z \rightarrow ee$ data) and the difference between the charge and p_T values of the standard track and tracklet are calculated. This function is fitted using a Gaussian core with exponential tails. Figure 5(d) shows the smearing functions used for three- and four-layer tracklets.

A similar method is used to constrain the muon backgrounds. The tracklet p_T distribution due to muons in a SR is calculated as

$$f_{\text{SR}}^\mu(p_T, \eta) = N^{\text{TR}\mu}(p_T, \eta) \times \text{TF}_{\text{tracklet}}^\mu(p_T, \eta) \times \text{TF}_{\text{MS-veto}}^\mu(p_T, \eta) \times f_{\text{smear}}^\mu(p_T).$$

This is used in the same way as for the electron background and the individual terms are derived in a similar manner as discussed below. Four muon-enriched TRs ($\text{TR}\mu$) are defined and the tracklet p_T template is taken from events passing the same selection as in the SRs but containing exactly one muon instead of a tracklet. The $\text{TR}\mu$ events must fire the single-muon trigger, with an offline p_T requirement of 27 GeV. As with the electrons, the expected E_T^{miss} distribution in the SR is emulated by removing the muons from the E_T^{miss} calculation. Correction factors to account for muons reconstructed as tracklets ($\text{TF}_{\text{tracklet}}^\mu$), and muons that do not have an associated track in the MS ($\text{TF}_{\text{MS-veto}}^\mu$), are calculated in bins of tracklet p_T and η using a tag-and-probe method in $Z \rightarrow \mu\mu$ events. A transfer factor ($\text{TF}_{\text{tracklet}+\pi}^\mu$) is calculated specifically for the cases where the muon is associated with a low-energy charged-pion track and is used instead of $\text{TF}_{\text{tracklet}}^\mu$ in the regions requiring the presence of a pion. A p_T -dependent smearing function (f_{smear}^μ) is applied to account for differences between the measured muon track p_T in the TR and the reconstructed tracklet p_T .

The final background considered in the analysis, the one due to hadronic interactions, is calculated as

$$f_{\text{SR}}^{\text{had}}(p_T, \eta) = N^{\text{TRhad}}(p_T, \eta) \times \text{TF}_{\text{tracklet}}^{\text{had}}(p_T, \eta) \times \text{TF}_{\text{calo-veto}}^{\text{had}}(p_T, \eta) \times f_{\text{smear}}^{\text{had}}(p_T).$$

Similarly to the other backgrounds, yields in TRs are modified by TFs and a smearing function, which is described below. Four hadronic TRs (TRhad) are defined to extract the tracklet p_T template ($N^{\text{TRhad}}(p_T, \eta)$) by applying the same selections as the associated SR, but with changed tracklet reconstruction requirements. In the TRs the track with the highest p_T is required to have at least 14 hits in the TRT detector, at least five hits in the SCT, and be matched, within $\Delta R < 0.2$, to a calorimeter energy cluster with $E_T^{\text{clus}} > 3$ GeV, and $E_T^{\text{topoclus40}}/p_T^{\text{track}} > 0.5$, resulting in a pure sample of hadronic tracks. Due to the unavailability of a data-driven tag-and-probe method to calculate the transfer factors, pion and electron ‘particle gun’ simulation is used to estimate the probability to misidentify a hadron as a short track ($\text{TF}_{\text{tracklet}}^{\text{had}}$) by calculating the ratio of hadron MC events reconstructed as tracklets to electron MC events reconstructed as tracklets and multiplying this by the $\text{TF}_{\text{tracklet}}^e$ value calculated from data as described above. A similar procedure is followed to calculate $\text{TF}_{\text{tracklet}+\pi}^{\text{had}}$, which is subsequently used instead of $\text{TF}_{\text{tracklet}}^{\text{had}}$ to calculate the SR contribution containing a low-energy pion. A transfer factor $\text{TF}_{\text{calo-veto}}^{\text{had}}$ is applied to estimate the likelihood of reconstructing a hadron without an associated calorimeter energy cluster; it is calculated as the ratio of MC events containing a tracklet associated with a calorimeter energy cluster within $\Delta R = 0.4$

Table 2: Summary of the event and tracklet selection requirements for the CRs associated with the four-layer SRs.

| Variable | CR ^{4Low} | CR ^{4High} | CR ^{4LowS} | CR ^{4MidS} |
|--|--------------------|---------------------|---------------------|---------------------|
| E_T^{miss} trigger | Passed | | | |
| Number of leptons | = 0 | | | |
| Number of jets ($p_T > 20$ GeV) | = 1 | | | |
| Leading jet p_T | > 100 GeV | | | |
| $ \Delta\phi(j_1, \vec{p}_T^{\text{miss}}) $ | > 1.0 | | | |
| Number of four-layer tracklets | ≥ 1 | | | |
| Tracklet p_T | > 20 GeV | 20–60 GeV | > 20 GeV | 20–60 GeV |
| Tracklet E_T^{clus} | < 5 GeV | < 5 GeV | > 5 GeV | > 5 GeV |
| E_T^{miss} | < 150 GeV | > 300 GeV | < 150 GeV | 150–300 GeV |

of the tracklet (when requiring $E_T^{\text{clus}} > 10$ GeV) to those without (when requiring $E_T^{\text{clus}} < 5$ GeV). Both TFs are dependent upon p_T and η . A p_T -dependent smearing function ($f_{\text{smear}}^{\text{had}}$) is applied to take into account differences between the hadronic track and the reconstructed tracklet.

After evaluating the tracklet p_T distributions for the electron, muon, hadron and fake backgrounds, they are used as the input to a binned likelihood fit (as described in Section 8) to provide a final estimate of the background distributions in the SRs, performing an extrapolation to higher values of E_T^{miss} . The hadronic background tracklet distributions are normalised using ‘sideband’ CRs: CR^{4LowS} and CR^{4MidS} (defined in Table 2) for the four-layer SRs, and CR^{3Low1 π S} and CR^{3Mid1 π S} (defined in Table 3) for both three-layer SRs, where the ‘S’ in the superscript denotes the sideband CR for the region. Applying this normalisation mitigates the MC dependence introduced when calculating the hadronic transfer factors. Figure 6 presents a schematic overview of the general background estimation strategy with the usage of CRs to normalise the hadronic background while the remaining backgrounds are taken from their templates as described above.

To evaluate the fit procedure and background modelling, orthogonal validation regions (VRs) are constructed by selecting events kinematically closer to the SR, and an extrapolation of the CR backgrounds to the VRs is performed. Five VRs are defined, as shown in Table 5, with reversed selections on the tracklet p_T , tracklet E_T^{clus} , or E_T^{miss} in order to remain orthogonal to both the SRs and CRs.

Table 3: Summary of the event and tracklet selection requirements for the CRs associated with the three-layer SRs that contain a low-energy charged pion.

| Variable | CR ^{3Low1π} | CR ^{3Mid1π} | CR ^{3High1π} | CR ^{3Low1πS} | CR ^{3Mid1πS} |
|--|-------------------------------------|-------------------------------------|--------------------------------------|--------------------------------------|--------------------------------------|
| E_T^{miss} trigger | Passed | | | | |
| Number of leptons | = 0 | | | | |
| Number of jets ($p_T > 20$ GeV) | = 1 | | | | |
| Leading jet p_T | > 100 GeV | | | | |
| $ \Delta\phi(j_1, \vec{p}_T^{\text{miss}}) $ | > 1.0 | | | | |
| Number of three-layer tracklets | ≥ 1 | | | | |
| Number of charged pions | ≥ 1 | | | | |
| Tracklet p_T | > 20 GeV | 20–60 GeV | 20–60 GeV | > 20 GeV | 20–60 GeV |
| Tracklet E_T^{clus} | < 5 GeV | < 5 GeV | < 5 GeV | > 5 GeV | > 5 GeV |
| E_T^{miss} | < 150 GeV | 150–240 GeV | > 240 GeV | < 150 GeV | 150–240 GeV |

Table 4: Summary of the event and tracklet selection requirements for the CRs associated with the three-layer SRs that veto a low-energy charged pion.

| Variable | CR ^{3Low0π} | CR ^{3Mid0π} | CR ^{3High0π} |
|--|-------------------------------------|-------------------------------------|--------------------------------------|
| E_T^{miss} trigger | Passed | | |
| Number of leptons | = 0 | | |
| Number of jets ($p_T > 20$ GeV) | = 1 | | |
| Leading jet p_T | > 100 GeV | | |
| $ \Delta\phi(j_1, \vec{p}_T^{\text{miss}}) $ | > 1.0 | | |
| Number of three-layer tracklets | ≥ 1 | | |
| Number of charged pions | = 0 | | |
| Tracklet p_T | > 20 GeV | 20–60 GeV | 20–60 GeV |
| Tracklet E_T^{clus} | < 5 GeV | < 5 GeV | < 5 GeV |
| E_T^{miss} | < 150 GeV | 150–280 GeV | > 280 GeV |

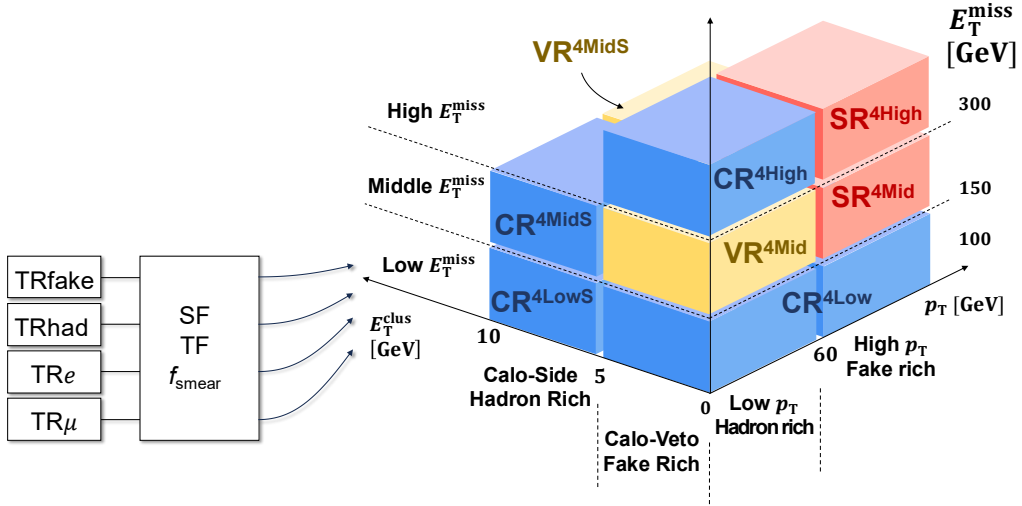


Figure 6: Schematic diagram for the background estimation strategy, describing the usage of template regions (TRs), and relaxed selections to calculate transfer factors (TFs) before performing the fit using control regions (CRs). The kinematic regions are orthogonal due to selections on E_T^{miss} , tracklet p_T , and tracklet E_T^{clus} , with high calorimeter energies (‘calo-side’) dominated by the hadron background, and low calorimeter energies (‘calo-veto’) dominated by the fake background.

Table 5: Summary of the event and tracklet selection requirements for the validation regions.

| Variable | VR ^{4Mid} | VR ^{4MidS} | VR ^{3Mid1π} | VR ^{3Mid1πS} | VR ^{3High0π} |
|--|--------------------|---------------------|-------------------------------------|--------------------------------------|--------------------------------------|
| E_T^{miss} trigger | Passed | | | | |
| Number of leptons | = 0 | | | | |
| Number of jets ($p_T > 20$ GeV) | = 1 | | | | |
| Leading jet p_T | > 100 GeV | | | | |
| $ \Delta\phi(j_1, \vec{p}_T^{\text{miss}}) $ | > 1.0 | | | | |
| Number of four-layer tracklets | ≥ 1 | | | | = 0 |
| Number of three-layer tracklets | - | | | | ≥ 1 |
| Number of charged pions | - | | | | = 0 |
| Tracklet p_T | < 60 GeV | > 60 GeV | > 60 GeV | > 60 GeV | > 60 GeV |
| Tracklet E_T^{clus} | < 5 GeV | > 5 GeV | < 5 GeV | > 5 GeV | < 5 GeV |
| E_T^{miss} | 150–300 GeV | 150–300 GeV | 150–240 GeV | 150–240 GeV | > 280 GeV |

7 Systematic uncertainties

Systematic uncertainties in the background estimates are driven by the uncertainties in the transfer factors, normalisations and shape of the tracklet p_T templates for the electron, muon, hadron and fake backgrounds. These uncertainties are dominated by the statistical uncertainties of the data in regions used to derive the background estimates, and are always below 10%. When calculating values of parameters which are based on data, such as the TFs and smearing functions, the statistical uncertainty of the data is used as a $\pm 1\sigma$ variation. When performing the statistical fit, the values of the transfer factors and the individual bins of each tracklet p_T template are allowed to vary within their statistical uncertainties. Each source of background uncertainty (p_T template statistical uncertainties, TFs, and smearing functions) is treated as correlated across each set of associated CRs and SRs but uncorrelated between backgrounds, except $\text{TF}_{\text{tracklet}}^{\text{had}}$, which is correlated with $\text{TF}_{\text{tracklet}}^e$ since both TFs are used in the estimation of the hadronic background. No dedicated uncertainty is associated with the overall background estimation methodology as, within other sources of uncertainties including the statistics of the data, the predicted post-fit tracklet p_T distributions in the VRs are consistent with the data.

Several sources of experimental uncertainty in the SUSY signal estimates are considered. The uncertainties are included in the likelihood fit as Gaussian nuisance parameters that affect the expectation values for each SR bin. Jet energy scale and resolution uncertainties are derived as a function of the jet p_T , η , and flavour, using data and simulated events, as detailed in Ref. [104]. Lepton reconstruction and identification uncertainties [97, 98] are included in the fit, but are found to have negligible impact. Uncertainties in the tracklet reconstruction efficiency are estimated to be 10% due to inactive pixel modules and 6% due to selection differences between data and MC $V+$ jets events. An uncertainty related to the low-energy charged pions is also applied, combining uncertainties of 10% in the reconstruction efficiency, taken from Ref. [109], and 6% in the BDT selection efficiency, evaluated by varying the BDT input parameters by 1σ and examining the effect on the output score. All uncertainties in the final-state object reconstruction are propagated to the E_T^{miss} calculation, including an additional term taking into account uncertainties in the scale and resolution of the soft term [106]. In the SR^{4Mid} region, the E_T^{miss} selection used is in the ‘turn-on’ region of the E_T^{miss} trigger where the trigger is found to be between 85% and 90% efficient for the signal event topology. Therefore, a trigger efficiency uncertainty is also applied, as an uncertainty in the signal yield.

The theoretical uncertainties originating from the choice of factorisation and renormalisation scales for the SUSY signal samples are evaluated by varying the corresponding MC generator parameters by a factor of two around their nominal values. The uncertainties associated with the choice of PDF set [71] and the value of the strong coupling constant are also considered. Finally, five variations of the A14 tune of PYTHIA are used to account for ISR modelling effects due to the underlying event, jet structure, and different aspects of extra jet production. The total uncertainty from experimental sources is found to be $\sim 5\%$ for all signal scenarios. The theoretical modelling uncertainties contribute up to 20%, increasing with increasing $\tilde{\chi}_1^\pm/\tau$ -slepton mass, and are primarily driven by the ISR modelling uncertainty.

Figure 7 presents a breakdown of systematic uncertainties affecting the background estimates in the SRs, grouped by the source of the uncertainty. The total uncertainty may not simply be the sum in quadrature of the individual uncertainties, because the fit can induce correlations between the components. In all SRs, the dominant uncertainty comes from the normalisation of the fake background, and the subdominant uncertainty in most regions arises from the shape of the fake background. Due to the limited number of tracklets available for the tracklet p_T templates in the $\text{SR}^{\text{3High1}\pi}$ region, the statistical uncertainty of the template shape contributes significantly to the background uncertainty in this region.

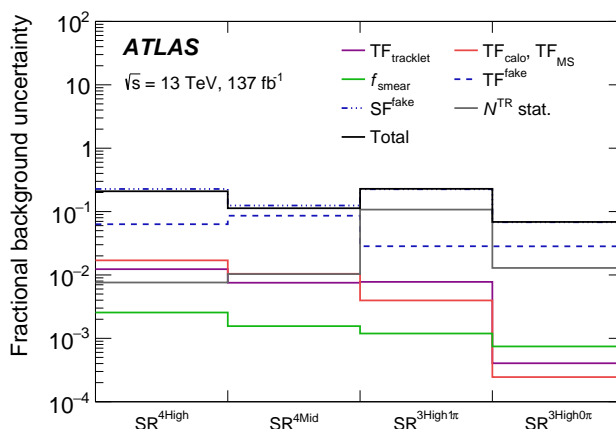


Figure 7: A summary of the systematic uncertainties affecting the background estimates in the SRs after the likelihood fit to data in the CRs is performed (‘Post-fit’). The total uncertainty is indicated by a solid black line. The individual uncertainties may not sum in quadrature to the total uncertainty, due to correlations between the different components. The uncertainties arising from the estimation of the fake-tracklet background, which are the dominant uncertainties, are shown as blue dashed lines.

8 Results

Three profile likelihood fits are performed: to assess the accuracy of the SM background determination (*background-only* fit), to compute the p -value of the SM-only hypothesis (*model-independent* fit), and to evaluate the confidence level (CL) for excluding a specific new-physics hypothesis (*model-dependent* fit) [110]. Due to the low event yields in the SRs, pseudoexperiments are used for statistical interpretation of the results when performing the model-independent fit, while the asymptotic approximation [111] is used when performing the model-dependent fit.

When performing the background-only fit, the hadronic background yield is allowed to float in the CRs, resulting in a set of normalisation factors which are uncorrelated between SRs. One hadronic normalisation factor is calculated for each SR and is propagated as a general scaling factor to the SR’s tracklet p_T distribution. Only the CRs, and not the SRs, are used to constrain the SM background. The electron, muon and fake-tracklet background yields are allowed to vary within their uncertainties when the fit is performed, but no overall normalisation is derived for these backgrounds.

Figure 8 presents an overview of the CRs after the background-only fit. The CRs that are used to normalise the hadronic backgrounds have, by design, a ratio of data to background event yield of one, whereas the other CRs that are used to derive the tracklet p_T distribution for the fake background are not normalised and the data–MC difference is applied as the $SF_{E_T^{\text{miss}}}^{\text{fake}}$ value from the fake-background estimation procedure before performing the fit.

To evaluate the fit procedure and background modelling, the CR normalisations are extrapolated to the VRs and the results are compared with data and validated before performing the same extrapolation to the SRs. Good agreement is seen between the data and prediction when examining the modelling of the tracklet p_T shape in three of the VRs as shown in Figure 9. The tracklet p_T distribution differs between the electron and muon backgrounds because an electron is more likely to undergo bremsstrahlung than a muon.

The level of post-fit agreement in the VRs and SRs is shown in Figure 10, which also shows the statistical significance [112] of the observed data yields and the background prediction in each of the regions. Good

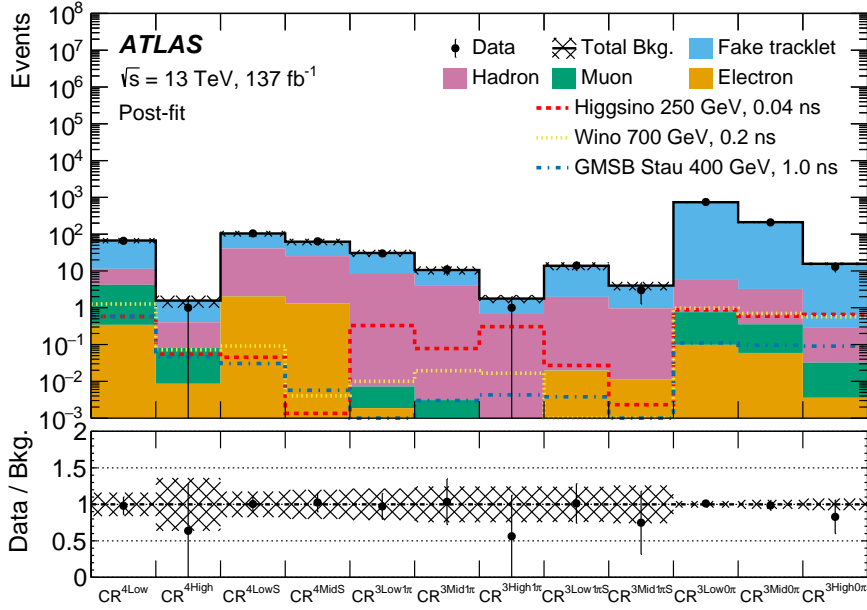


Figure 8: The post-fit yields in the CRs. All statistical and systematic uncertainties are considered in the error bands. Three representative pre-fit signal yields are indicated with dashed lines.

agreement is seen in the VRs. Small excesses are seen in $\text{SR}^{4\text{High}}$ and $\text{SR}^{3\text{High}1\pi}$, corresponding to local significances of 1.9σ and 1.0σ respectively. These discrepancies and how the events compare with the previous analysis are discussed further at the end of this section.

Figure 11 presents post-fit distributions of the tracklet p_T in each SR. In the regions where a relatively high number of background events are expected ($\text{SR}^{4\text{Mid}}$ and $\text{SR}^{3\text{High}0\pi}$), the data are in good agreement with the background estimates, with the distributions agreeing within uncertainties. Due to the small number of events in $\text{SR}^{4\text{High}}$ and $\text{SR}^{3\text{High}1\pi}$, less can be discerned from the level of agreement of the tracklet p_T distributions. Figure 11(a) shows the presence of three data events in a single $\text{SR}^{4\text{High}}$ bin, corresponding to tracklet p_T values of 139 GeV, 142 GeV and 152 GeV.

Table 6 shows the observed and expected yields in the SRs, as well as the model-independent fit results in each SR. The model-independent fit uses the same CRs as the background-only fit. A single-bin SR is also included in the fit by summing the individual tracklet- p_T bins in a given region. The hadronic background is then allowed to float in the CRs and the single-bin SR. This method uses a profile-likelihood-ratio test statistic [111], where a generic new-physics signal of intensity μ_{sig} is assumed to contribute exclusively to each individual, single-bin SR, and is used to assess the p -value of the background-only hypothesis (corresponding to $\mu_{\text{sig}} = 0$) and to extract S_{exp}^{95} and S_{obs}^{95} , i.e. the expected and observed 95% CL limits on the number of signal events in the SR, using the CL_s prescription [113]. The S_{obs}^{95} limit is also converted to a limit on the visible cross-section σ_{obs}^{95} by dividing by the total integrated luminosity.

In the absence of a significant excess in the observed data, 95% CL exclusion limits are placed on the SUSY signal scenarios by statistically combining all SRs, binned in tracklet p_T , which provides greater sensitivity than simply considering only one SR at a time. The binning is chosen such that the low tracklet- p_T bins retain sufficient granularity to ensure fit stability and signal sensitivity, with wider bins used as tracklet p_T increases, reflecting the poorer tracklet p_T resolution and limited discrimination power of the highest

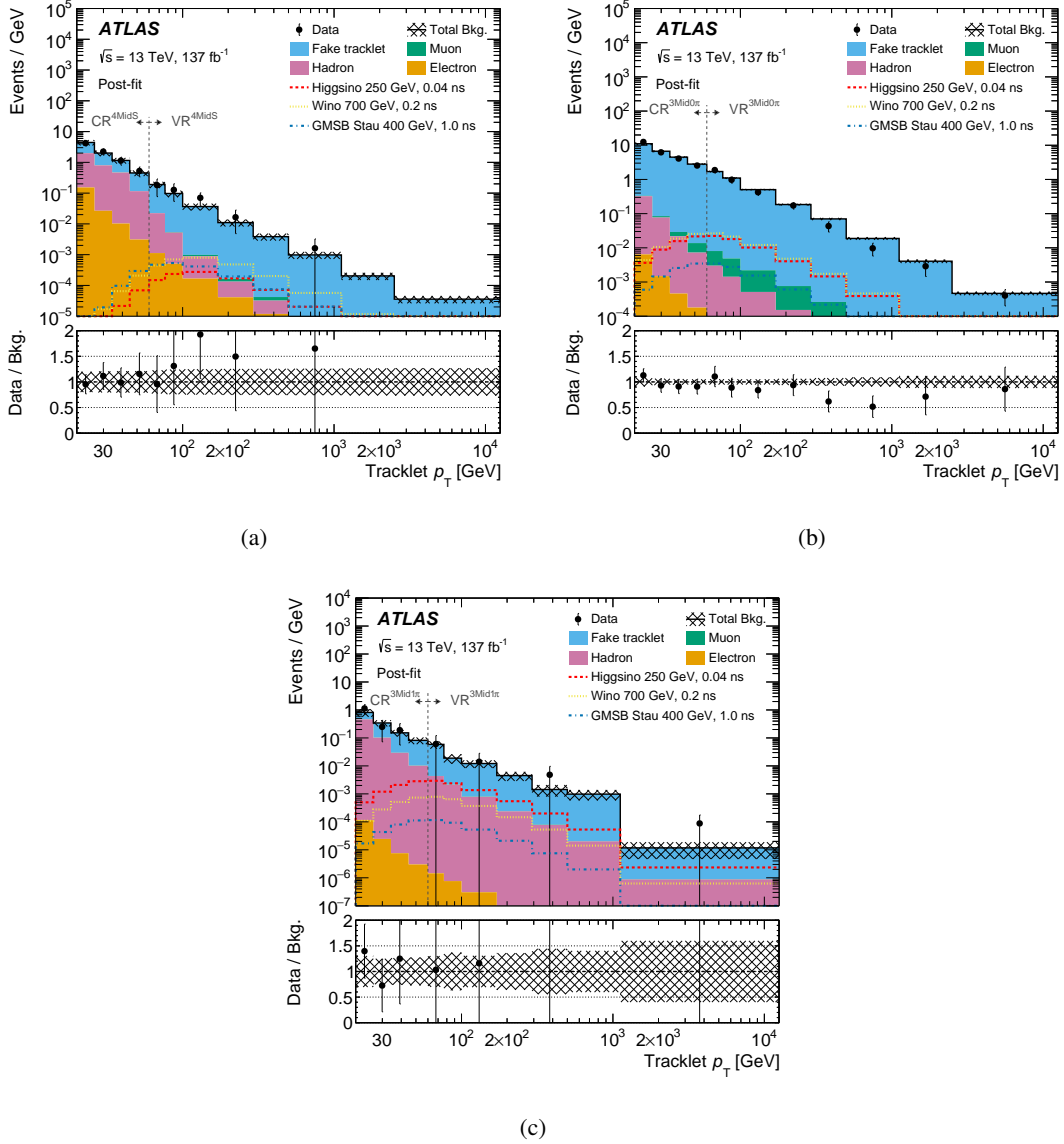


Figure 9: The post-fit tracklet p_T distributions in (a) $\text{VR}^{4\text{Mid}S}$, (b) $\text{VR}^{3\text{High}0\pi}$, and (c) $\text{VR}^{3\text{Mid}1\pi}$. The dashed vertical line denotes the boundary between the CR and VR selections. The pre-fit signal distributions are indicated with dashed lines. The lower pad shows the ratio of the observed yields to the post-fit predicted background yields. The last bin includes overflow events. All statistical and systematic uncertainties are considered in the error bands.

bins. A model-dependent fit is used, where each signal scenario is introduced and a fit to the tracklet p_T distribution is performed, with CRs and SRs used to normalise the hadronic background and determine the signal strength for a specific signal model. The four-layer regions dominate the sensitivity, and although the expected sensitivity in the SUSY models is significantly better than in the previous analysis [43], by around 100 GeV in SUSY particle masses, the small excess in $\text{SR}^{4\text{High}}$ weakens the observed exclusion limit.

The model-dependent limits for wino pair production are shown in Figure 12, where wino-like charginos with lifetimes of 1 ns and masses up to 1020 GeV are expected to be excluded. The small excess observed in the signal regions results in a weaker observed mass exclusion limit of 880 GeV. Figure 13 shows

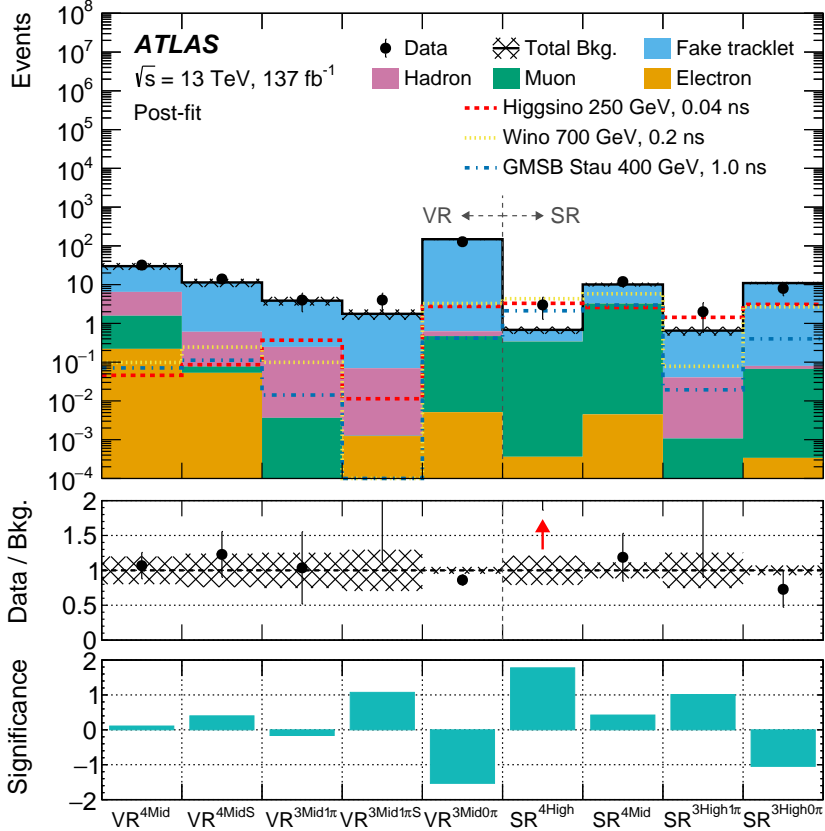


Figure 10: The observed and expected event yields in the VRs and SRs. The lower pads show the ratio of the observed yields to the post-fit predicted background yields and the statistical significance [112] of the observed data. A red arrow is used to indicate that a ratio value is outside the displayed interval. The background estimates are calculated from the background-only fit. All statistical and systematic uncertainties are considered in the error bands. Three representative pre-fit signal yields are indicated with dashed lines.

the model-dependent limits for higgsino pair production, where in the long-lifetime region of ~ 1 ns, the sensitivity extends up to masses of 720 GeV (840 GeV expected). Figures 12 and 13 also show the exclusion sensitivities when converting the chargino lifetime to the mass-splitting between the electroweakinos and when comparing it with the theoretical expectation for mass splitting in wino- or higgsino-like scenarios. In the wino-like case, charginos are excluded for masses up to 670 GeV (770 GeV expected), while in the higgsino-like case, charginos are excluded for masses up to 225 GeV (250 GeV expected), improving upon previous results by 15 GeV. Compared to the previous analysis, this search is able to exclude smaller values of the signal cross-section. For example, when considering a higgsino signal scenario of $m(\tilde{\chi}_1^\pm) = 300$ GeV and $\tau(\tilde{\chi}_1^\pm) = 0.05$ ns the signal cross-section exclusion limit is a factor of 2.5 times lower than the previous result. When considering $m(\tilde{\chi}_1^\pm) = 500$ GeV and $\tau(\tilde{\chi}_1^\pm) = 0.1$ ns the signal cross-section exclusion limit is a factor of 1.8 lower than in the previous analysis.

The 95% CL exclusion limits in the τ -slepton scenarios are presented in Figure 14. Due to the small cross-section for $\tilde{\tau}\tilde{\tau}$ production, the signal yield is too low in the three-layer SRs to offer sensitivity, so only the four-layer SRs and associated CRs are used in the model-dependent fit. The sensitivity in CMSSM- and GMSB-inspired scenarios is comparable, with τ -sleptons excluded for masses up to around 320 GeV and 300 GeV (390 GeV and 380 GeV expected), respectively, for a mass difference of ~ 2 GeV between the

τ -slepton and $\tilde{\chi}_1^0/\tilde{G}$ (corresponding to τ -slepton lifetimes of ~ 1 ns).

Due to changes in the analysis strategy since the previous analysis in Ref. [43], particularly in the reconstruction of the tracklets, a direct comparison of the SRs is non-trivial, as the previous analyses used five-layer tracking and did not use the additional SCT data quality veto. Despite this, it is found that one of the events selected by SR^{4High} was also one of the three events selected by the previous analysis. The two new events in SR^{4High} are selected because of improvements in track reconstruction. The two events selected by SR^{3High1 π} are likely to stem from a hadronic interaction in the ID material as a secondary vertex is reconstructed in a region with known material. The resulting kink in the particle path results in a reconstructed tracklet rather than a standard track. A ‘material veto’ was considered in the analysis design to avoid such events, but was not adopted as it had a highly detrimental impact on the signal acceptance.

Table 6: Summary of the observed and post-fit expected SR yields, with ‘Bkg.’ denoting background, and the model-independent fit results. All systematic and statistical uncertainties are considered. The calculated p_0 -value is capped at 0.5 and shown together with the corresponding significance in standard deviations (Z).

| | SR ^{4High} | SR ^{4Mid} | SR ^{3High1π} | SR ^{3High0π} |
|---------------------------------|--------------------------------|--------------------------------|--------------------------------------|--------------------------------------|
| Fake Bkg. | 0.33 ± 0.14 | 6.8 ± 1.1 | 0.62 ± 0.16 | 10.9 ± 0.8 |
| Hadron Bkg. | $(5 \pm 4) \times 10^{-4}$ | $(7 \pm 7) \times 10^{-3}$ | 0.029 ± 0.014 | 0.011 ± 0.021 |
| Electron Bkg. | $(3.7 \pm 2.1) \times 10^{-4}$ | $(4.6 \pm 2.7) \times 10^{-3}$ | $(10 \pm 9) \times 10^{-6}$ | $(2.5 \pm 1.3) \times 10^{-4}$ |
| Muon Bkg. | 0.342 ± 0.015 | 3.28 ± 0.14 | $(1.1 \pm 0.6) \times 10^{-3}$ | 0.068 ± 0.009 |
| Total Bkg. | 0.68 ± 0.14 | 10.1 ± 1.1 | 0.65 ± 0.16 | 11.0 ± 0.8 |
| Observed | 3 | 12 | 2 | 8 |
| p_0 (Z) | 0.033 (1.9) | 0.26 (0.6) | 0.14 (1.1) | 0.5 (0) |
| S_{exp}^{95} | $3.7^{+0.8}_{-0.6}$ | $12.3^{+3.6}_{-2.9}$ | $3.2^{+1.0}_{-0.2}$ | $8.3^{+2.8}_{-2.6}$ |
| S_{obs}^{95} | 6.0 | 12.4 | 5.0 | 5.8 |
| σ_{obs}^{95} [fb] | 0.044 | 0.090 | 0.037 | 0.043 |

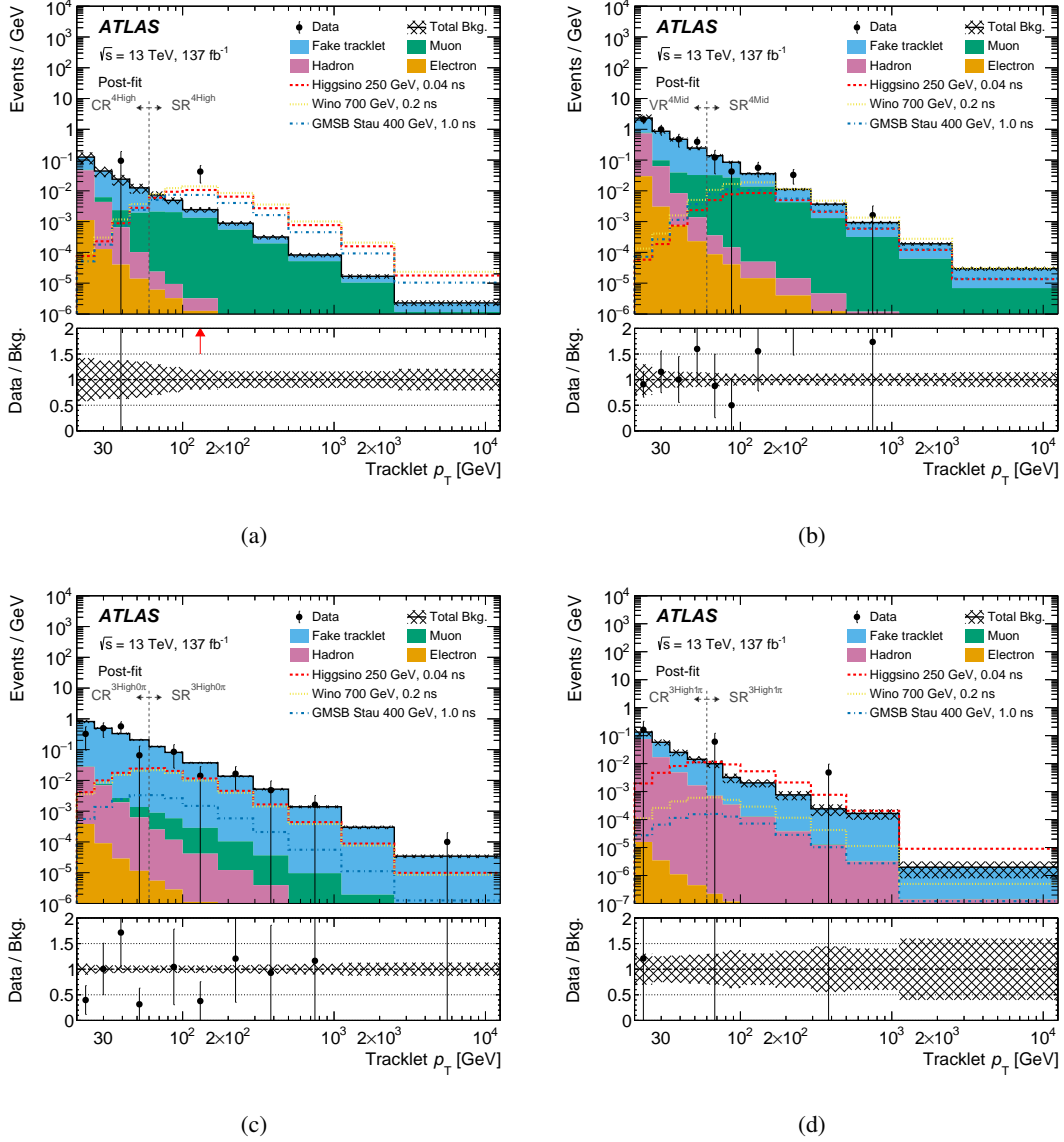


Figure 11: The post-fit tracklet p_T distributions in (a) SR^{4High} , (b) SR^{4Mid} , (c) $SR^{3High0\pi}$, and (d) $SR^{3High1\pi}$. The dashed vertical line denotes the boundary between the CR/VR and SR selections. The lower pad shows the ratio of the observed data yields to the post-fit predicted background estimates. A red arrow is used to indicate that a ratio value is outside the displayed interval. The last bin includes overflow events. All statistical and systematic uncertainties are considered in the error bands. Three representative pre-fit signal yields are indicated with dashed lines.

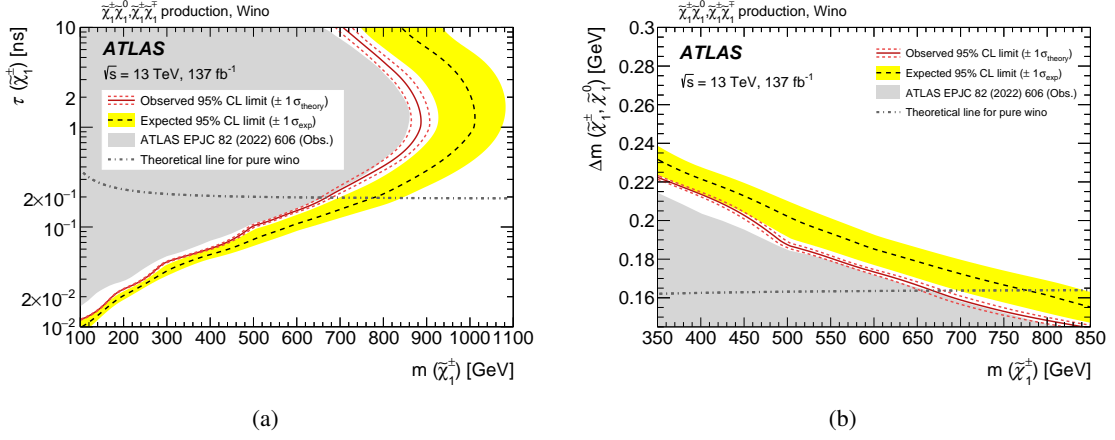


Figure 12: The expected (dashed line) and observed (solid line) 95% CL exclusion contours for wino production as a function of the chargino mass and (a) lifetime, or (b) mass splitting of the electroweakinos. The dotted lines indicates the $\pm\sigma_{\text{theory}}$ from signal cross-section uncertainties, while the solid band indicates the $\pm\sigma_{\text{exp}}$ from experimental systematic uncertainties and statistical uncertainties on the data yields. The solid grey area shows the region excluded by Ref. [43]. The dashed-dotted line is the prediction of the chargino lifetime or wino mass splitting as a function of the chargino mass as predicted by the SM loop corrections [14].

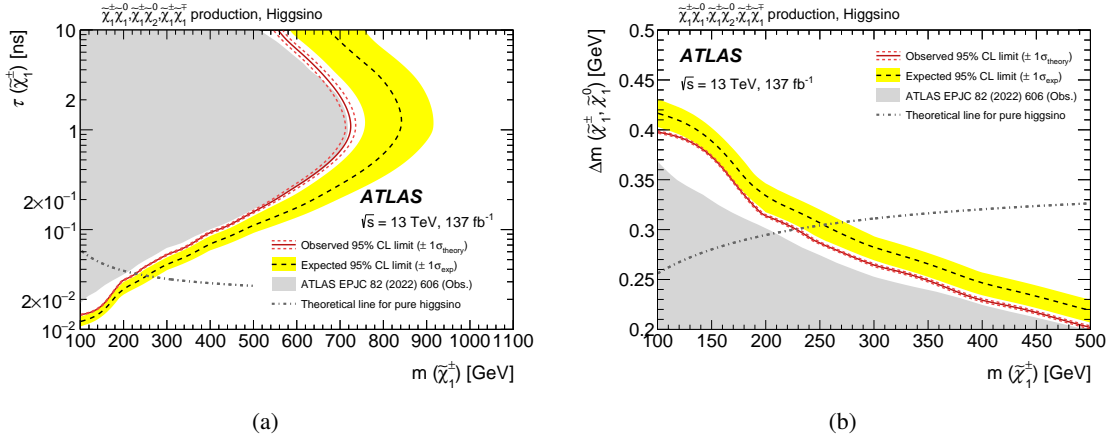


Figure 13: The expected (dashed line) and observed (solid line) 95% CL exclusion contours for higgsino production as a function of the chargino mass and (a) lifetime, or (b) mass splitting of the electroweakinos. The dotted lines indicates the $\pm\sigma_{\text{theory}}$ from signal cross-section uncertainties, while the solid band indicates the $\pm\sigma_{\text{exp}}$ from experimental systematic uncertainties and statistical uncertainties on the data yields. The solid grey area shows the region excluded by Ref. [43]. The dashed-dotted line is the prediction of the chargino lifetime or higgsino mass splitting as a function of the chargino mass as predicted by the SM loop corrections [21].

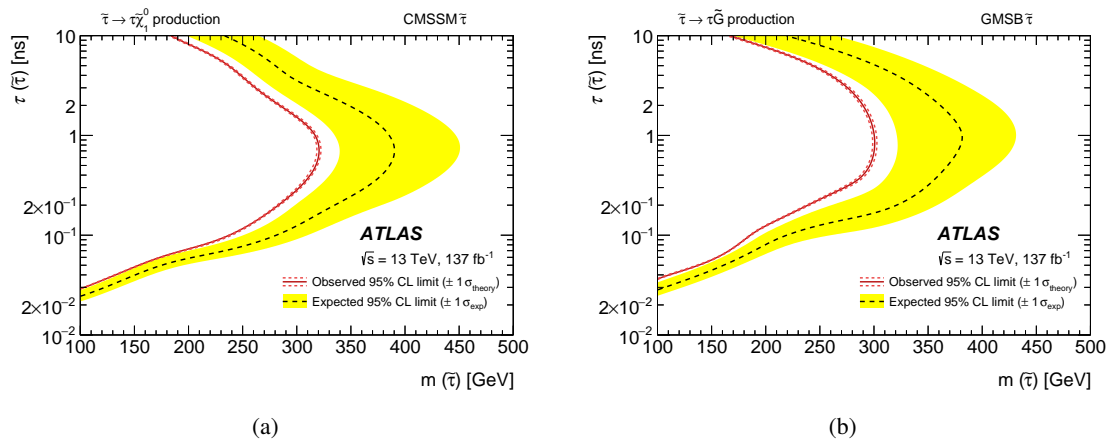


Figure 14: The expected (dashed line) and observed (solid line) 95% CL exclusion contours for τ -slepton production in (a) CMSSM-inspired scenarios and (b) GMSB-inspired scenario. The dotted lines indicates the $\pm 1 \sigma_{\text{theory}}$ from signal cross-section uncertainties, while the solid band indicates the $\pm 1 \sigma_{\text{exp}}$ from experimental systematic uncertainties and statistical uncertainties on the data yields.

9 Conclusion

A search for new physics in final states containing a disappearing track and E_T^{miss} , indicative of a heavy charged particle decaying after traversing only the innermost layers of the ATLAS detector, has been performed using 137 fb^{-1} of data from $\sqrt{s} = 13 \text{ TeV}$ pp collisions at the LHC. Two BSM scenarios are considered, the first being electroweakino pair production with at least one chargino, where $\tilde{\chi}_1^\pm \rightarrow \pi^\pm \tilde{\chi}_1^0$. The second set of scenarios considered are those of τ -slepton pair production: a CMSSM-inspired scenario where the τ -slepton decays as $\tilde{\tau} \rightarrow \tau \tilde{\chi}_1^0$, and a GMSB-inspired scenario where it decays as $\tilde{\tau} \rightarrow \tau \tilde{G}$. The analysis uses four signal regions for a final state with zero leptons, one jet, high E_T^{miss} , and a tracklet. Improvements in the analysis techniques, including the reconstruction of tracklets from hits in only three pixel layers and a dedicated BDT to reconstruct low-energy pions, increased the sensitivity compared to the previous Run-2 analysis. Data-driven methods are used to estimate the backgrounds, which arise when a stable particle is incorrectly reconstructed as a tracklet or when random combinations of inner-detector hits are incorrectly identified as a tracklet.

The data observations agree with the SM expectation to within 2σ . The results are interpreted in simplified SUSY models. For higgsino production, chargino masses of up to 225 GeV (250 GeV) are observed (expected) to be excluded at 95% CL in the lifetime regime $\tau < 0.03 \text{ ns}$ where the electroweakino mass splitting is motivated by loop corrections due to SM bosons. These are currently the strongest exclusion limits in this region of phase space. For longer lifetimes up to 1 ns, exclusion limits of up to 720 GeV (840 GeV) are set. For wino production, charginos with masses of up to 880 GeV (1020 GeV) are excluded for lifetimes of around 1 ns. In CMSSM- and GMSB-inspired τ -slepton production scenarios, the observed (expected) τ -slepton mass exclusion limits reach 320 GeV (390 GeV) and 300 GeV (380 GeV) respectively, in the case of τ -slepton lifetimes of around 1 ns.

Acknowledgements

We thank CERN for the very successful operation of the LHC and its injectors, as well as the support staff at CERN and at our institutions worldwide without whom ATLAS could not be operated efficiently.

The crucial computing support from all WLCG partners is acknowledged gratefully, in particular from CERN, the ATLAS Tier-1 facilities at TRIUMF/SFU (Canada), NDGF (Denmark, Norway, Sweden), CC-IN2P3 (France), KIT/GridKA (Germany), INFN-CNAF (Italy), NL-T1 (Netherlands), PIC (Spain), RAL (UK) and BNL (USA), the Tier-2 facilities worldwide and large non-WLCG resource providers. Major contributors of computing resources are listed in Ref. [114].

We gratefully acknowledge the support of ANPCyT, Argentina; YerPhI, Armenia; ARC, Australia; BMWFW and FWF, Austria; ANAS, Azerbaijan; CNPq and FAPESP, Brazil; NSERC, NRC and CFI, Canada; CERN; ANID, Chile; CAS, MOST and NSFC, China; Minciencias, Colombia; MEYS CR, Czech Republic; DNRf and DNSRC, Denmark; IN2P3-CNRS and CEA-DRF/IRFU, France; SRNSFG, Georgia; BMFTR, HGF and MPG, Germany; GSRI, Greece; RGC and Hong Kong SAR, China; ICHEP and Academy of Sciences and Humanities, Israel; INFN, Italy; MEXT and JSPS, Japan; CNRST, Morocco; NWO, Netherlands; RCN, Norway; MNiSW, Poland; FCT, Portugal; MNE/IFA, Romania; MSTDI, Serbia; MSSR, Slovakia; ARIS and MVZI, Slovenia; DSI/NRF, South Africa; MICIU/AEI, Spain; SRC and Wallenberg Foundation, Sweden; SERI, SNSF and Cantons of Bern and Geneva, Switzerland; NSTC, Taipei; TENMAK, Türkiye; STFC/UKRI, United Kingdom; DOE and NSF, United States of America.

Individual groups and members have received support from BCKDF, CANARIE, CRC and DRAC, Canada; CERN-CZ, FORTE and PRIMUS, Czech Republic; COST, ERC, ERDF, Horizon 2020 and Marie Skłodowska-Curie Actions, European Union; Investissements d’Avenir Labex, Investissements d’Avenir IDEX and ANR, France; DFG and AvH Foundation, Germany; Herakleitos, Thales and Aristeia programmes co-financed by EU-ESF and the Greek NSRF, Greece; BSF-NSF and MINERVA, Israel; NCN and NAWA, Poland; La Caixa Banking Foundation, CERCA and AGAUR programs from Generalitat de Catalunya and PROMETEO and GenT Programmes Generalitat Valenciana, Spain; Göran Gustafssons Stiftelse, Sweden; The Royal Society and Leverhulme Trust, United Kingdom; United States of America.

In addition, individual members wish to acknowledge support from Chile: Agencia Nacional de Investigación y Desarrollo (ANID FONDECYT reg. 1230987, FONDECYT 1230812, FONDECYT 1240864, Fondecyt 3240661, Fondecyt Regular 1240721); China: Chinese Ministry of Science and Technology (MOST-2023YFA1605700, MOST-2023YFA1609300), National Natural Science Foundation of China (NSFC 12275265, NSFC-W2543005); Czech Republic: Czech Science Foundation (GACR - 24-11373S), Ministry of Education Youth and Sports (ERC-CZ-LL2327, FORTE CZ.02.01.01/00/22_008/0004632), PRIMUS Research Programme (PRIMUS/21/SCI/017); EU: H2020 European Research Council (ERC - 101002463); European Union: European Research Council (BARD No. 101116429, ERC - 948254, ERC 101089007), European Regional Development Fund (HE COFUND GA No.101081355, ERDF), Marie Skłodowska-Curie Actions (GAP-101168829); France: Agence Nationale de la Recherche (ANR-21-CE31-0013, ANR-22-EDIR-0002, ANR-24-CE31-0504-01); Germany: Deutsche Forschungsgemeinschaft (DFG - 469666862); China: Research Grants Council (GRF); Italy: Ministero dell’Università e della Ricerca (NextGenEU 153D23001490006 M4C2.1.1, NextGenEU 153D23000820006 M4C2.1.1, NextGenEU 153D23001490006 M4C2.1.1, SOE2024_0000023); Japan: Japan Society for the Promotion of Science (JSPS KAKENHI JP25H0063, JSPS KAKENHI JP22H01227, JSPS KAKENHI JP22H04944, JSPS KAKENHI JP22KK0227, JSPS KAKENHI JP24K23939, JSPS KAKENHI JP24KK0251, JSPS KAKENHI JP25H00650, JSPS KAKENHI JP25H01291, JSPS KAKENHI JP25K01023); Norway: Research Council of Norway (RCN-314472); Poland: Polish National Science Centre (NCN 2021/42/E/ST2/00350, NCN OPUS 2023/51/B/ST2/02507, NCN OPUS nr 2022/47/B/ST2/03059, NCN UMO-2019/34/E/ST2/00393, UMO-2022/47/O/ST2/00148, UMO-2023/49/B/ST2/04085, UMO-2023/51/B/ST2/00920, UMO-2024/53/N/ST2/00869); Spain: Agencia de Gestión de Ayudas Universitarias y de Investigación (AGAUR - 2023 BP 00141), Ministry of Science and Innovation (RYC2019-028510-I, RYC2020-030254-I, RYC2021-031273-I, RYC2022-038164-I), Ministerio de Ciencia, Innovación y Universidades/Agencia Estatal de Investigación (PID2022-142604OB-C22); Sweden: Carl Trygger Foundation (Carl Trygger Foundation CTS 22:2312), Swedish Research Council (Swedish Research Council 2023-04654, VR 2021-03651, VR 2022-03845, VR 2022-04683, VR 2023-03403, VR 2024-05451, VR 2025-05940), Knut and Alice Wallenberg Foundation (KAW 2023.0366); Switzerland: Swiss National Science Foundation (SNSF - PCEFP2_194658); United Kingdom: The Binks Trust, Royal Society (NIF-R1-231091); United States of America: U.S. Department of Energy (ECA DE-AC02-76SF00515), John Templeton Foundation (John Templeton Foundation 63206), Neubauer Family Foundation.

References

- [1] Y. Gol'fand and E. Likhtman, *Extension of the Algebra of Poincare Group Generators and Violation of P Invariance*, [JETP Lett. **13** \(1971\) 323](#), [*Pisma Zh. Eksp. Teor. Fiz.* **13** (1971) 452].
- [2] D. V. Volkov and V. P. Akulov, *Is the neutrino a goldstone particle?*, [Phys. Lett. B **46** \(1973\) 109](#).
- [3] J. Wess and B. Zumino, *Supergauge transformations in four dimensions*, [Nucl. Phys. B **70** \(1974\) 39](#).
- [4] J. Wess and B. Zumino, *Supergauge invariant extension of quantum electrodynamics*, [Nucl. Phys. B **78** \(1974\) 1](#).
- [5] S. Ferrara and B. Zumino, *Supergauge invariant Yang-Mills theories*, [Nucl. Phys. B **79** \(1974\) 413](#).
- [6] A. Salam and J. Strathdee, *Super-symmetry and non-Abelian gauges*, [Phys. Lett. B **51** \(1974\) 353](#).
- [7] N. Sakai, *Naturalness in supersymmetric GUTS*, [Z. Phys. C **11** \(1981\) 153](#).
- [8] S. Dimopoulos, S. Raby and F. Wilczek, *Supersymmetry and the scale of unification*, [Phys. Rev. D **24** \(1981\) 1681](#).
- [9] L. E. Ibáñez and G. G. Ross, *Low-energy predictions in supersymmetric grand unified theories*, [Phys. Lett. B **105** \(1981\) 439](#).
- [10] S. Dimopoulos and H. Georgi, *Softly broken supersymmetry and SU(5)*, [Nucl. Phys. B **193** \(1981\) 150](#).
- [11] G. R. Farrar and P. Fayet, *Phenomenology of the production, decay, and detection of new hadronic states associated with supersymmetry*, [Phys. Lett. B **76** \(1978\) 575](#).
- [12] H. Goldberg, *Constraint on the Photino Mass from Cosmology*, [Phys. Rev. Lett. **50** \(1983\) 1419](#), Erratum: [Phys. Rev. Lett. **103** \(2009\) 099905](#).
- [13] J. Ellis, J. Hagelin, D. V. Nanopoulos, K. A. Olive and M. Srednicki, *Supersymmetric relics from the big bang*, [Nucl. Phys. B **238** \(1984\) 453](#).
- [14] M. Ibe, S. Matsumoto and R. Sato, *Mass Splitting between Charged and Neutral Winos at Two-Loop Level*, [Phys. Lett. B **721** \(2013\) 252](#), arXiv: [1212.5989 \[hep-ph\]](#).
- [15] H. Fukuda, N. Nagata, H. Otono and S. Shirai, *Higgsino Dark Matter or Not: Role of Disappearing Track Searches at the LHC and Future Colliders*, [Phys. Lett. B **781** \(2018\) 306](#), arXiv: [1703.09675 \[hep-ph\]](#).
- [16] G. F. Giudice, M. A. Luty, H. Murayama and R. Rattazzi, *Gaugino mass without singlets*, [JHEP **12** \(1998\) 027](#), arXiv: [hep-ph/9810442](#).
- [17] L. Randall and R. Sundrum, *Out of this world supersymmetry breaking*, [Nucl. Phys. B **557** \(1999\) 79](#), arXiv: [hep-th/9810155](#).
- [18] M. Papucci, J. T. Ruderman and A. Weiler, *Natural SUSY Endures*, [JHEP **09** \(2012\) 035](#), arXiv: [1110.6926 \[hep-ph\]](#).
- [19] R. Barbieri and G. F. Giudice, *Upper bounds on supersymmetric particle masses*, [Nucl. Phys. B **306** \(1988\) 63](#).
- [20] B. de Carlos and J. A. Casas, *One-loop analysis of the electroweak breaking in supersymmetric models and the fine-tuning problem*, [Phys. Lett. B **309** \(1993\) 320](#), arXiv: [hep-ph/9303291](#).

- [21] S. D. Thomas and J. D. Wells, *Phenomenology of Massive Vectorlike Doublet Leptons*, *Phys. Rev. Lett.* **81** (1998) 34, arXiv: [hep-ph/9804359](#).
- [22] N. Nagata and S. Shirai, *Higgsino Dark Matter in High-Scale Supersymmetry*, *JHEP* **01** (2015) 029, arXiv: [1410.4549 \[hep-ph\]](#).
- [23] D. Albornoz Vásquez, G. Bélanger and C. Boehm, *Revisiting light neutralino scenarios in the MSSM*, *Phys. Rev. D* **84** (2011) 095015, arXiv: [1108.1338 \[hep-ph\]](#).
- [24] G. Belanger, F. Boudjema, A. Cottrant, A. Pukhov and A. Semenov, *WMAP constraints on SUGRA models with non-universal gaugino masses and prospects for direct detection*, *Nucl. Phys. B* **706** (2005) 411, arXiv: [hep-ph/0407218](#).
- [25] S. King, J. Roberts and D. Roy, *Natural dark matter in SUSY GUTs with non-universal gaugino masses*, *JHEP* **10** (2007) 106, arXiv: [0705.4219 \[hep-ph\]](#).
- [26] J. R. Ellis, T. Falk and K. A. Olive, *Neutralino - Stau coannihilation and the cosmological upper limit on the mass of the lightest supersymmetric particle*, *Phys. Lett. B* **444** (1998) 367, arXiv: [hep-ph/9810360](#).
- [27] T. Jittoh, J. Sato, T. Shimomura and M. Yamanaka, *Long life stau in the minimal supersymmetric standard model*, *Phys. Rev. D* **73** (2006) 055009, [Erratum: *Phys. Rev. D* **87** (2013) 019901], arXiv: [hep-ph/0512197](#).
- [28] S. Kaneko, J. Sato, T. Shimomura, O. Vives and M. Yamanaka, *Measuring lepton flavor violation at LHC with a long-lived slepton in the coannihilation region*, *Phys. Rev. D* **78** (2008) 116013, [Erratum: *Phys. Rev. D* **87** (2013) 039904], arXiv: [0811.0703 \[hep-ph\]](#).
- [29] M. Dine and W. Fischler, *A phenomenological model of particle physics based on supersymmetry*, *Phys. Lett. B* **110** (1982) 227.
- [30] L. Alvarez-Gaumé, M. Claudson and M. B. Wise, *Low-energy supersymmetry*, *Nucl. Phys. B* **207** (1982) 96.
- [31] C. R. Nappi and B. A. Ovrut, *Supersymmetric extension of the $SU(3) \times SU(2) \times U(1)$ model*, *Phys. Lett. B* **113** (1982) 175.
- [32] A. H. Chamseddine, R. L. Arnowitt and P. Nath, *Locally Supersymmetric Grand Unification*, *Phys. Rev. Lett.* **49** (1982) 970.
- [33] R. Barbieri, S. Ferrara and C. A. Savoy, *Gauge Models with Spontaneously Broken Local Supersymmetry*, *Phys. Lett. B* **119** (1982) 343.
- [34] G. L. Kane, C. F. Kolda, L. Roszkowski and J. D. Wells, *Study of constrained minimal supersymmetry*, *Phys. Rev. D* **49** (1994) 6173, arXiv: [hep-ph/9312272](#).
- [35] M. Cirelli, N. Fornengo and A. Strumia, *Minimal dark matter*, *Nucl. Phys. B* **753** (2006) 178, arXiv: [hep-ph/0512090](#).
- [36] X. Cid Vidal et al., *Report from Working Group 3: Beyond the Standard Model physics at the HL-LHC and HE-LHC*, *CERN Yellow Rep. Monogr.* **7** (2019) 585, ed. by A. Dainese et al., arXiv: [1812.07831 \[hep-ph\]](#).

- [37] M. Saito, R. Sawada, K. Terashi and S. Asai, *Discovery reach for wino and higgsino dark matter with a disappearing track signature at a 100 TeV pp collider*, *Eur. Phys. J. C* **79** (2019) 469, arXiv: [1901.02987 \[hep-ph\]](#).
- [38] R. Capdevilla, F. Meloni, R. Simoniello and J. Zurita, *Hunting wino and higgsino dark matter at the muon collider with disappearing tracks*, *JHEP* **06** (2021) 133, arXiv: [2102.11292 \[hep-ph\]](#).
- [39] R. Capdevilla, F. Meloni and J. Zurita, *Discovering Electroweak Interacting Dark Matter at Muon Colliders Using Soft Tracks*, *Phys. Rev. Lett.* **134** (2025) 181802, arXiv: [2405.08858 \[hep-ph\]](#).
- [40] J. Alwall, M.-P. Le, M. Lisanti and J. G. Wacker, *Searching for directly decaying gluinos at the Tevatron*, *Phys. Lett. B* **666** (2008) 34, arXiv: [0803.0019 \[hep-ph\]](#).
- [41] J. Alwall, P. C. Schuster and N. Toro, *Simplified models for a first characterization of new physics at the LHC*, *Phys. Rev. D* **79** (2009) 075020, arXiv: [0810.3921 \[hep-ph\]](#).
- [42] D. Alves et al., *Simplified models for LHC new physics searches*, *J. Phys. G* **39** (2012) 105005, arXiv: [1105.2838 \[hep-ph\]](#).
- [43] ATLAS Collaboration, *Search for long-lived charginos based on a disappearing-track signature using 136fb^{-1} of pp collisions at $\sqrt{s} = 13\text{ TeV}$ with the ATLAS detector*, *Eur. Phys. J. C* **82** (2022) 606, arXiv: [2201.02472 \[hep-ex\]](#).
- [44] ATLAS Collaboration, *Search for long-lived charginos based on a disappearing-track signature in pp collisions at $\sqrt{s} = 13\text{ TeV}$ with the ATLAS detector*, *JHEP* **06** (2018) 022, arXiv: [1712.02118 \[hep-ex\]](#).
- [45] ATLAS Collaboration, *Search for direct pair production of higgsinos by reinterpretation of the disappearing track analysis with 36.1fb^{-1} of $\sqrt{s} = 13\text{ TeV}$ data collected with the ATLAS experiment*, ATL-PHYS-PUB-2017-019, 2017, URL: <https://cds.cern.ch/record/2297480>.
- [46] ATLAS Collaboration, *Search for charginos nearly mass degenerate with the lightest neutralino based on a disappearing-track signature in pp collisions at $\sqrt{s} = 8\text{ TeV}$ with the ATLAS detector*, *Phys. Rev. D* **88** (2013) 112006, arXiv: [1310.3675 \[hep-ex\]](#).
- [47] CMS Collaboration, *Search for disappearing tracks in proton–proton collisions at $\sqrt{s} = 13\text{ TeV}$* , *Phys. Lett. B* **806** (2020) 135502, arXiv: [2004.05153 \[hep-ex\]](#).
- [48] ATLAS Collaboration, *Search for long-lived charged particles using large specific ionisation loss and time of flight in 140fb^{-1} of pp collisions at $\sqrt{s} = 13\text{ TeV}$ with the ATLAS detector*, *JHEP* **07** (2025) 140, arXiv: [2502.06694 \[hep-ex\]](#).
- [49] CMS Collaboration, *Search for heavy long-lived charged particles with large ionization energy loss in proton–proton collisions at $\sqrt{s} = 13\text{ TeV}$* , *JHEP* **04** (2024) 109, arXiv: [2410.09164 \[hep-ex\]](#).
- [50] ATLAS Collaboration, *The ATLAS Experiment at the CERN Large Hadron Collider*, *JINST* **3** (2008) S08003.

- [51] ATLAS Collaboration, *ATLAS Insertable B-Layer: Technical Design Report*, ATLAS-TDR-19; CERN-LHCC-2010-013, 2010, URL: <https://cds.cern.ch/record/1291633>, Addendum: ATLAS-TDR-19-ADD-1; CERN-LHCC-2012-009, 2012, URL: <https://cds.cern.ch/record/1451888>.
- [52] B. Abbott et al., *Production and integration of the ATLAS Insertable B-Layer*, *JINST* **13** (2018) T05008, arXiv: [1803.00844](https://arxiv.org/abs/1803.00844) [[physics.ins-det](#)].
- [53] G. Avoni et al., *The new LUCID-2 detector for luminosity measurement and monitoring in ATLAS*, *JINST* **13** (2018) P07017.
- [54] ATLAS Collaboration, *Performance of the ATLAS trigger system in 2015*, *Eur. Phys. J. C* **77** (2017) 317, arXiv: [1611.09661](https://arxiv.org/abs/1611.09661) [[hep-ex](#)].
- [55] ATLAS Collaboration, *Software and computing for Run 3 of the ATLAS experiment at the LHC*, *Eur. Phys. J. C* **85** (2025) 234, arXiv: [2404.06335](https://arxiv.org/abs/2404.06335) [[hep-ex](#)], Erratum: *Eur. Phys. J. C* **85** (2025) 907.
- [56] ATLAS Collaboration, *ATLAS data quality operations and performance for 2015–2018 data-taking*, *JINST* **15** (2020) P04003, arXiv: [1911.04632](https://arxiv.org/abs/1911.04632) [[physics.ins-det](#)].
- [57] ATLAS Collaboration, *Luminosity determination in pp collisions at $\sqrt{s} = 13$ TeV using the ATLAS detector at the LHC*, *Eur. Phys. J. C* **83** (2023) 982, arXiv: [2212.09379](https://arxiv.org/abs/2212.09379) [[hep-ex](#)].
- [58] ATLAS Collaboration, *2015 start-up trigger menu and initial performance assessment of the ATLAS trigger using Run-2 data*, ATL-DAQ-PUB-2016-001, 2016, URL: <https://cds.cern.ch/record/2136007>.
- [59] ATLAS Collaboration, *Performance of the missing transverse momentum triggers for the ATLAS detector during Run-2 data taking*, *JHEP* **08** (2020) 080, arXiv: [2005.09554](https://arxiv.org/abs/2005.09554) [[hep-ex](#)].
- [60] ATLAS Collaboration, *Performance of the ATLAS muon triggers in Run 2*, *JINST* **15** (2020) P09015, arXiv: [2004.13447](https://arxiv.org/abs/2004.13447) [[physics.ins-det](#)].
- [61] ATLAS Collaboration, *Performance of electron and photon triggers in ATLAS during LHC Run 2*, *Eur. Phys. J. C* **80** (2020) 47, arXiv: [1909.00761](https://arxiv.org/abs/1909.00761) [[hep-ex](#)].
- [62] ATLAS Collaboration, *The ATLAS Simulation Infrastructure*, *Eur. Phys. J. C* **70** (2010) 823, arXiv: [1005.4568](https://arxiv.org/abs/1005.4568) [[physics.ins-det](#)].
- [63] S. Agostinelli et al., *GEANT4 – a simulation toolkit*, *Nucl. Instrum. Meth. A* **506** (2003) 250.
- [64] T. Sjöstrand, S. Mrenna and P. Skands, *A brief introduction to PYTHIA 8.1*, *Comput. Phys. Commun.* **178** (2008) 852, arXiv: [0710.3820](https://arxiv.org/abs/0710.3820) [[hep-ph](#)].
- [65] NNPDF Collaboration, R. D. Ball et al., *Parton distributions with LHC data*, *Nucl. Phys. B* **867** (2013) 244, arXiv: [1207.1303](https://arxiv.org/abs/1207.1303) [[hep-ph](#)].
- [66] ATLAS Collaboration, *The Pythia 8 A3 tune description of ATLAS minimum bias and inelastic measurements incorporating the Donnachie–Landshoff diffractive model*, ATL-PHYS-PUB-2016-017, 2016, URL: <https://cds.cern.ch/record/2206965>.
- [67] J. Alwall et al., *The automated computation of tree-level and next-to-leading order differential cross sections, and their matching to parton shower simulations*, *JHEP* **07** (2014) 079, arXiv: [1405.0301](https://arxiv.org/abs/1405.0301) [[hep-ph](#)].

- [68] T. Sjöstrand et al., *An introduction to PYTHIA 8.2*, *Comput. Phys. Commun.* **191** (2015) 159, arXiv: [1410.3012 \[hep-ph\]](#).
- [69] ATLAS Collaboration, *ATLAS Pythia 8 tunes to 7 TeV data*, ATL-PHYS-PUB-2014-021, 2014, URL: <https://cds.cern.ch/record/1966419>.
- [70] L. Lönnblad and S. Prestel, *Merging Multi-leg NLO Matrix Elements with Parton Showers*, *JHEP* **03** (2013) 166, arXiv: [1211.7278 \[hep-ph\]](#).
- [71] NNPDF Collaboration, R. D. Ball et al., *Parton distributions for the LHC run II*, *JHEP* **04** (2015) 040, arXiv: [1410.8849 \[hep-ph\]](#).
- [72] W. Beenakker et al., *Production of Charginos, Neutralinos, and Stopped at Hadron Colliders*, *Phys. Rev. Lett.* **83** (1999) 3780, arXiv: [hep-ph/9906298](#),
Erratum: *Phys. Rev. Lett.* **100** (2008) 029901.
- [73] J. Debove, B. Fuks and M. Klasen,
Threshold resummation for gaugino pair production at hadron colliders,
Nucl. Phys. B **842** (2011) 51, arXiv: [1005.2909 \[hep-ph\]](#).
- [74] B. Fuks, M. Klasen, D. R. Lamprea and M. Rothering,
Gaugino production in proton-proton collisions at a center-of-mass energy of 8 TeV,
JHEP **10** (2012) 081, arXiv: [1207.2159 \[hep-ph\]](#).
- [75] B. Fuks, M. Klasen, D. R. Lamprea and M. Rothering,
Precision predictions for electroweak superpartner production at hadron colliders with RESUMMINO,
Eur. Phys. J. C **73** (2013) 2480, arXiv: [1304.0790 \[hep-ph\]](#).
- [76] J. Fiaschi and M. Klasen, *Neutralino-chargino pair production at NLO+NLL with resummation-improved parton density functions for LHC Run II*, *Phys. Rev. D* **98** (2018) 055014, arXiv: [1805.11322 \[hep-ph\]](#).
- [77] G. Bozzi, B. Fuks and M. Klasen,
Threshold resummation for slepton-pair production at hadron colliders,
Nucl. Phys. B **777** (2007) 157, arXiv: [hep-ph/0701202](#).
- [78] B. Fuks, M. Klasen, D. R. Lamprea and M. Rothering,
Revisiting slepton pair production at the Large Hadron Collider, *JHEP* **01** (2014) 168, arXiv: [1310.2621 \[hep-ph\]](#).
- [79] J. Fiaschi and M. Klasen,
Slepton pair production at the LHC in NLO+NLL with resummation-improved parton densities,
JHEP **03** (2018) 094, arXiv: [1801.10357 \[hep-ph\]](#).
- [80] J. Fiaschi, B. Fuks, M. Klasen and A. Neuwirth,
Electroweak superpartner production at 13.6 TeV with Resummino, *Eur. Phys. J. C* **83** (2023) 707, arXiv: [2304.11915 \[hep-ph\]](#).
- [81] C. Borschensky et al.,
Squark and gluino production cross sections in pp collisions at $\sqrt{s} = 13, 14, 33$ and 100 TeV,
Eur. Phys. J. C **74** (2014) 3174, arXiv: [1407.5066 \[hep-ph\]](#).
- [82] E. Bothmann et al., *Event generation with Sherpa 2.2*, *SciPost Phys.* **7** (2019) 034, arXiv: [1905.09127 \[hep-ph\]](#).
- [83] T. Gleisberg and S. Höche, *Comix, a new matrix element generator*, *JHEP* **12** (2008) 039, arXiv: [0808.3674 \[hep-ph\]](#).

- [84] F. Buccioni et al., *OpenLoops 2*, *Eur. Phys. J. C* **79** (2019) 866, arXiv: [1907.13071 \[hep-ph\]](#).
- [85] F. Cascioli, P. Maierhöfer and S. Pozzorini, *Scattering Amplitudes with Open Loops*, *Phys. Rev. Lett.* **108** (2012) 111601, arXiv: [1111.5206 \[hep-ph\]](#).
- [86] A. Denner, S. Dittmaier and L. Hofer, *COLLIER: A fortran-based complex one-loop library in extended regularizations*, *Comput. Phys. Commun.* **212** (2017) 220, arXiv: [1604.06792 \[hep-ph\]](#).
- [87] S. Schumann and F. Krauss, *A parton shower algorithm based on Catani–Seymour dipole factorisation*, *JHEP* **03** (2008) 038, arXiv: [0709.1027 \[hep-ph\]](#).
- [88] S. Höche, F. Krauss, M. Schönherr and F. Siegert, *A critical appraisal of NLO+PS matching methods*, *JHEP* **09** (2012) 049, arXiv: [1111.1220 \[hep-ph\]](#).
- [89] S. Höche, F. Krauss, M. Schönherr and F. Siegert, *QCD matrix elements + parton showers. The NLO case*, *JHEP* **04** (2013) 027, arXiv: [1207.5030 \[hep-ph\]](#).
- [90] S. Catani, F. Krauss, B. R. Webber and R. Kuhn, *QCD Matrix Elements + Parton Showers*, *JHEP* **11** (2001) 063, arXiv: [hep-ph/0109231](#).
- [91] S. Höche, F. Krauss, S. Schumann and F. Siegert, *QCD matrix elements and truncated showers*, *JHEP* **05** (2009) 053, arXiv: [0903.1219 \[hep-ph\]](#).
- [92] C. Anastasiou, L. Dixon, K. Melnikov and F. Petriello, *High-precision QCD at hadron colliders: Electroweak gauge boson rapidity distributions at next-to-next-to leading order*, *Phys. Rev. D* **69** (2004) 094008, arXiv: [hep-ph/0312266](#).
- [93] ATLAS Collaboration, *Performance of the ATLAS track reconstruction algorithms in dense environments in LHC Run 2*, *Eur. Phys. J. C* **77** (2017) 673, arXiv: [1704.07983 \[hep-ex\]](#).
- [94] ATLAS Collaboration, *Vertex Reconstruction Performance of the ATLAS Detector at $\sqrt{s} = 13$ TeV*, ATL-PHYS-PUB-2015-026, 2015, URL: <https://cds.cern.ch/record/2037717>.
- [95] ATLAS Collaboration, *Electron and photon performance measurements with the ATLAS detector using the 2015–2017 LHC proton–proton collision data*, *JINST* **14** (2019) P12006, arXiv: [1908.00005 \[hep-ex\]](#).
- [96] ATLAS Collaboration, *Electron reconstruction and identification in the ATLAS experiment using the 2015 and 2016 LHC proton–proton collision data at $\sqrt{s} = 13$ TeV*, *Eur. Phys. J. C* **79** (2019) 639, arXiv: [1902.04655 \[physics.ins-det\]](#).
- [97] ATLAS Collaboration, *Electron and photon efficiencies in LHC Run 2 with the ATLAS experiment*, *JHEP* **05** (2024) 162, arXiv: [2308.13362 \[hep-ex\]](#).
- [98] ATLAS Collaboration, *Muon reconstruction and identification efficiency in ATLAS using the full Run 2 pp collision data set at $\sqrt{s} = 13$ TeV*, *Eur. Phys. J. C* **81** (2021) 578, arXiv: [2012.00578 \[hep-ex\]](#).
- [99] ATLAS Collaboration, *Studies of the muon momentum calibration and performance of the ATLAS detector with pp collisions at $\sqrt{s} = 13$ TeV*, *Eur. Phys. J. C* **83** (2023) 686, arXiv: [2212.07338 \[hep-ex\]](#).

- [100] M. Cacciari, G. P. Salam and G. Soyez, *The anti- k_t jet clustering algorithm*, *JHEP* **04** (2008) 063, arXiv: [0802.1189 \[hep-ph\]](#).
- [101] M. Cacciari, G. P. Salam and G. Soyez, *FastJet user manual*, *Eur. Phys. J. C* **72** (2012) 1896, arXiv: [1111.6097 \[hep-ph\]](#).
- [102] ATLAS Collaboration, *Jet reconstruction and performance using particle flow with the ATLAS Detector*, *Eur. Phys. J. C* **77** (2017) 466, arXiv: [1703.10485 \[hep-ex\]](#).
- [103] ATLAS Collaboration, *Topological cell clustering in the ATLAS calorimeters and its performance in LHC Run 1*, *Eur. Phys. J. C* **77** (2017) 490, arXiv: [1603.02934 \[hep-ex\]](#).
- [104] ATLAS Collaboration, *Jet energy scale and resolution measured in proton–proton collisions at $\sqrt{s} = 13$ TeV with the ATLAS detector*, *Eur. Phys. J. C* **81** (2021) 689, arXiv: [2007.02645 \[hep-ex\]](#).
- [105] ATLAS Collaboration, *Performance of pile-up mitigation techniques for jets in pp collisions at $\sqrt{s} = 8$ TeV using the ATLAS detector*, *Eur. Phys. J. C* **76** (2016) 581, arXiv: [1510.03823 \[hep-ex\]](#).
- [106] ATLAS Collaboration, *The performance of missing transverse momentum reconstruction and its significance with the ATLAS detector using 140fb^{-1} of $\sqrt{s} = 13$ TeV pp collisions*, *Eur. Phys. J. C* **85** (2025) 606, arXiv: [2402.05858 \[hep-ex\]](#).
- [107] ATLAS Collaboration, *Performance of tracking and vertexing techniques for a disappearing track plus soft track signature with the ATLAS detector*, ATL-PHYS-PUB-2019-011, 2019, URL: <https://cds.cern.ch/record/2669015>.
- [108] A. Hoecker et al., *TMVA - Toolkit for Multivariate Data Analysis*, 2009, arXiv: [physics/0703039 \[physics.data-an\]](#).
- [109] ATLAS Collaboration, *Performance of the reconstruction of large impact parameter tracks in the inner detector of ATLAS*, *Eur. Phys. J. C* **83** (2023) 1081, arXiv: [2304.12867 \[hep-ex\]](#).
- [110] M. Baak et al., *HistFitter software framework for statistical data analysis*, *Eur. Phys. J. C* **75** (2015) 153, arXiv: [1410.1280 \[hep-ex\]](#).
- [111] G. Cowan, K. Cranmer, E. Gross and O. Vitells, *Asymptotic formulae for likelihood-based tests of new physics*, *Eur. Phys. J. C* **71** (2011) 1554, arXiv: [1007.1727 \[physics.data-an\]](#), Erratum: *Eur. Phys. J. C* **73** (2013) 2501.
- [112] R. D. Cousins, J. T. Linnemann and J. Tucker, *Evaluation of three methods for calculating statistical significance when incorporating a systematic uncertainty into a test of the background-only hypothesis for a Poisson process*, *Nucl. Instrum. Meth. A* **595** (2008) 480, arXiv: [physics/0702156 \[physics.data-an\]](#).
- [113] A. L. Read, *Presentation of search results: the CL_s technique*, *J. Phys. G* **28** (2002) 2693.
- [114] ATLAS Collaboration, *ATLAS Computing Acknowledgements*, ATL-SOFT-PUB-2026-001, 2026, URL: <https://cds.cern.ch/record/2952666>.

The ATLAS Collaboration

G. Aad ¹⁰², E. Aakvaag ¹⁷, B. Abbott ¹²², S. Abdelhameed ^{118a}, K. Abeling ⁵⁴, N.J. Abicht ⁴⁸, S.H. Abidi ³⁰, M. Aboeela ⁴⁴, A. Aboulhorma ^{36e}, H. Abramowicz ¹⁵⁵, B.S. Acharya ^{68a,68b,m}, A. Ackermann ^{62a}, C. Adam Bourdarios ⁴, L. Adamczyk ^{85a}, S.V. Addepalli ¹⁴⁷, M.J. Addison ¹⁰¹, J. Adelman ¹¹⁷, A. Adiguzel ^{22c}, T. Adye ¹³⁶, A.A. Affolder ¹³⁸, Y. Afik ³⁹, M.N. Agaras ¹³, A. Aggarwal ¹⁰⁰, C. Agheorghiesei ^{28c}, A. Ahmad ^{83a}, F. Ahmadov ^{38,ad}, S. Ahuja ⁹⁵, S. Ahuja ¹⁶⁶, X. Ai ^{113c}, G. Aielli ^{75a,75b}, A. Aikot ¹⁶⁶, M. Ait Tamlihat ^{36e}, T.P.A. Åkesson ⁹⁸, D. Akiyama ¹⁷¹, N.N. Akolkar ²⁵, S. Aktas ¹⁶⁹, G.L. Alberghi ^{24b}, J. Albert ¹⁶⁸, U. Alberti ²⁰, P. Albicocco ⁵², S. Alderweireldt ⁵¹, Z.L. Alegria ¹²³, M. Aleksa ³⁷, I.N. Aleksandrov ³⁸, C. Alexa ^{28b}, T. Alexopoulos ¹⁰, F. Alfonsi ^{24b}, M. Algren ⁵⁵, M. Alhroob ¹⁷⁰, B. Ali ¹³⁴, H.M.J. Ali ^{91,v}, S. Ali ³², S.W. Alibocus ⁹², M. Aliev ^{34c}, G. Alimonti ^{70a}, C. Allaire ⁶⁵, B.M.M. Allbrooke ¹⁵⁰, D.R. Allen ¹²³, J.S. Allen ¹⁰¹, J.F. Allen ⁵¹, C.S. Alley ¹, E.R. Almazan ¹³⁸, A. Aloisio ^{71a,71b}, F. Alonso ⁹⁰, C. Alpigliani ¹⁴¹, A. Alvarez Fernandez ¹⁰⁰, M. Alves Cardoso ⁵⁵, M.G. Alviggi ^{71a,71b}, M. Aly ¹⁰¹, Y. Amaral Coutinho ^{81b}, A. Ambler ¹⁰⁴, C. Amelung ³⁷, M. Amerl ¹⁰¹, T. Amezza ¹²⁹, B. Amini ⁵³, K. Amirie ¹⁵⁹, A. Amirkhanov ³⁸, D. Amperiadou ¹⁵⁶, S. An ⁸², C. Anastopoulos ¹⁴³, T. Andeen ¹¹, J.K. Anders ⁹², A.C. Anderson ⁵⁸, A. Andreatza ^{70a,70b}, S. Angelidakis ⁹, A. Angerami ⁴¹, A.V. Anisenkov ³⁸, A. Annovi ^{73a}, C. Antel ³⁷, E. Antipov ¹⁴⁹, M. Antonelli ⁵², F. Anulli ^{74a}, M. Aoki ⁸², T. Aoki ¹⁵⁷, M.A. Aparo ¹³, L. Aperio Bella ⁴⁷, M. Apicella ³¹, C. Appelt ¹⁵⁵, A. Apyan ²⁷, M. Arampatzi ¹⁰, S.J. Arbiol Val ⁸⁶, C. Arcangeletti ⁵², A.T.H. Arce ⁵⁰, J-F. Arguin ¹⁰⁸, S. Argyropoulos ¹⁵⁶, J.-H. Arling ⁴⁷, O. Arnaez ⁴, H. Arnold ¹⁴⁹, G. Artoni ^{74a,74b}, H. Asada ¹¹¹, S. Asatryan ¹⁷⁶, N.A. Asbah ³⁷, R.A. Ashby Pickering ¹⁷⁰, A.M. Aslam ⁹⁵, J. Assahsah ^{36d}, K. Assamagan ³⁰, R. Astalos ^{29a}, K.S.V. Astrand ⁹⁸, S. Atashi ¹⁶³, R.J. Atkin ^{34a}, H. Atmani ^{36f}, P.A. Atmasiddha ¹³⁰, K. Augsten ¹³⁴, A.D. Auriol ⁴⁰, V.A. Austrup ¹⁰¹, A.S. Avad ⁹⁴, G. Avolio ³⁷, K. Axiotis ⁵⁵, A. Azzam ¹³, D. Babal ^{29b}, H. Bachacou ¹³⁷, K. Bachas ^{156,p}, A. Bachiou ³⁵, E. Bachmann ⁴⁹, M.J. Backes ^{62a}, A. Badea ³⁹, T.M. Baer ¹⁰⁶, M. Bahmani ¹⁹, D. Bahner ⁵³, K. Bai ¹²⁵, L. Baines ⁹⁴, O.K. Baker ¹⁷⁵, D. Bakshi Gupta ⁸, L.E. Balabram Filho ^{81b}, V. Balakrishnan ¹²², R. Balasubramanian ⁴, P. Balek ^{85a}, E. Ballabene ^{24b,24a}, F. Balli ¹³⁷, L.M. Baltes ^{62a}, W.K. Balunas ¹²⁸, I. Bamwidhi ^{118b}, E. Banas ⁸⁶, M. Bandieramonte ¹³¹, A. Bandyopadhyay ²⁵, S. Bansal ²⁵, L. Barak ¹⁵⁵, M. Barakat ⁴⁷, E.L. Barberio ¹⁰⁵, D. Barberis ^{18b}, M. Barbero ¹⁰², M.Z. Barel ¹¹⁶, T. Barillari ¹¹⁰, M-S. Barisits ³⁷, T. Barklow ¹⁴⁷, P. Baron ¹³⁵, D.A. Baron Moreno ¹⁰¹, A. Baroncelli ⁶¹, A.J. Barr ¹²⁸, J.D. Barr ⁹⁶, F. Barreiro ⁹⁹, J. Barreiro Guimarães da Costa ¹⁴, M.G. Barros Teixeira ^{132a}, F. Bartels ^{62a}, R. Bartoldus ¹⁴⁷, A.E. Barton ⁹¹, P. Bartos ^{29a}, M. Baselga ⁴⁸, S. Bashiri ⁸⁶, A. Bassalat ^{65,b}, M.J. Basso ^{160a}, S. Bataju ⁴⁴, R. Bate ¹⁶⁷, R.L. Bates ⁵⁸, S. Batlamous ⁹⁹, M. Battaglia ¹³⁸, D. Battulga ¹⁹, M. Baucé ^{74a,74b}, L. Bauckhage ⁴⁷, P. Bauer ²⁵, L.T. Bayer ⁴⁷, L.T. Bazzano Hurrell ³¹, T. Beau ¹²⁹, J.Y. Beaucamp ⁹⁰, S. Beauceron ¹²⁹, P.H. Beauchemin ¹⁶², P. Bechtel ²⁵, H.P. Beck ^{20,o}, K. Becker ¹⁷⁰, A.J. Beddall ⁸⁰, V.A. Bednyakov ³⁸, C.P. Bee ¹⁴⁹, L.J. Beemster ¹⁶, M. Begalli ^{81d}, M. Beger ³⁰, J.K. Behr ⁴⁷, J.F. Beirer ³⁷, F. Beisiegel ²⁵, M. Belfkir ^{118b}, G. Bella ¹⁵⁵, L. Bellagamba ^{24b}, A. Bellerive ³⁵, C.D. Bellgraph ⁶⁷, P. Bellos ²¹, I. Benaoumeur ²¹, D. Benckekroun ^{36a}, F. Bendebba ^{36a}, Y. Benhammou ¹⁵⁵, K.C. Benkendorfer ¹⁶⁸, L. Beresford ⁴⁷, M. Beretta ⁵², E. Bergeas Kuutmann ¹⁶⁴, N. Berger ⁴, B. Bergmann ¹³⁴, J. Beringer ^{18a}, M. Berkat ¹³⁷, G. Bernardi ⁵, C. Bernius ¹⁴⁷, F.U. Bernlochner ²⁵, A. Berrocal Guardia ¹³, T. Berry ⁹⁵, P. Berta ¹³⁵, A. Berti ^{132a},

R. Bertrand [ID102](#), S. Bethke [ID110](#), A. Betti [ID74a,74b](#), T.F. Beumker [ID174](#), A.J. Bevan [ID94](#), L. Bezio [ID55](#), N.K. Bhalla [ID53](#), S. Bharthuar [ID110](#), S. Bhatta [ID149](#), P. Bhattacharai [ID147](#), Z.M. Bhatti [ID119](#), K.D. Bhide [ID53](#), V.S. Bhopatkar [ID123](#), R.M. Bianchi [ID131](#), G. Bianco [ID24b,24a](#), O. Biebel [ID109](#), M. Biglietti [ID76a](#), P. Bijl [ID53](#), C.S. Billingsley [ID44](#), Y. Bimngdi [ID36f](#), M. Bindi [ID54](#), A. Bingham [ID174](#), A. Bingul [ID22b](#), C. Bini [ID74a,74b](#), G.A. Bird [ID33](#), M. Biroš [ID135](#), S. Biryukov [ID150](#), T. Bisanz [ID48](#), E. Bisceglie [ID24b,24a](#), J.P. Biswal [ID136](#), D. Biswas [ID145](#), M. Biyabi [ID14](#), I. Bloch [ID47](#), A. Blue [ID58](#), U. Blumenschein [ID94](#), V.S. Bobrovnikov [ID38](#), L. Boccardo [ID56b,56a](#), M. Boehler [ID53](#), B. Boehm [ID169](#), D. Bogavac [ID13](#), L.S. Boggia [ID129](#), V. Boisvert [ID95](#), P. Bokan [ID164](#), T. Bold [ID85a](#), M. Bomben [ID5](#), M. Bona [ID94](#), M. Boonekamp [ID137](#), A.G. Borbély [ID58](#), G. Borissov [ID91](#), A. Borkar [ID169](#), D. Bortoletto [ID128](#), D. Boscherini [ID24b](#), M. Bosman [ID13](#), K. Bouaouda [ID36a](#), L. Boudet [ID137](#), J. Boudreau [ID131](#), E.V. Bouhova-Thacker [ID91](#), D. Boumediene [ID40](#), R. Bouquet [ID56b,56a](#), A. Boveia [ID121](#), D. Boye [ID30](#), I.R. Boyko [ID38](#), L. Bozianu [ID55](#), J. Bracinik [ID21](#), N. Brahimi [ID4](#), G. Brandt [ID174](#), O. Brandt [ID33](#), B. Brau [ID103](#), R. Brenner [ID172](#), L. Brenner [ID116](#), R. Brenner [ID164](#), S. Bressler [ID172](#), M. Brettell [ID96](#), G. Brianti [ID116](#), D. Britton [ID58](#), D. Britzger [ID110](#), I. Brock [ID25](#), R. Brock [ID107](#), H. Bronson [ID130](#), G. Brooijmans [ID41](#), A.J. Brooks [ID67](#), E.M. Brooks [ID160b](#), E. Brost [ID30](#), L.M. Brown [ID168,160a](#), L.E. Bruce [ID60](#), T.L. Bruckler [ID128](#), P.A. Bruckman de Renstrom [ID86](#), B. Brüers [ID47](#), A. Bruni [ID24b](#), G. Bruni [ID24b](#), D. Brunner [ID46a,46b](#), M. Bruschi [ID24b](#), N. Bruscinò [ID74a,74b](#), T. Buanes [ID17](#), Q. Buat [ID141](#), D. Buchin [ID110](#), A.G. Buckley [ID58](#), J. Bucko [ID135](#), M. Bühring [ID49](#), O. Bulekov [ID80](#), B.A. Bullard [ID147](#), T.O. Buratovich [ID90](#), S. Burdin [ID92](#), C.D. Burgard [ID48](#), A.M. Burger [ID89](#), B. Burghgrave [ID8](#), O. Burlayenko [ID53](#), J. Burleson [ID165](#), J.C. Burzynski [ID122](#), V. Büscher [ID100](#), P.J. Bussey [ID58](#), O. But [ID25](#), J.M. Butler [ID26](#), C.M. Buttar [ID58](#), J.M. Butterworth [ID96](#), P. Butti [ID37](#), W. Buttinger [ID136](#), C.J. Buxo Vazquez [ID107](#), A.R. Buzykaev [ID38](#), S. Cabrera Urbán [ID166](#), L. Cadamuro [ID65](#), H. Cai [ID37](#), Y. Cai [ID24b,112c,24a](#), Y. Cai [ID112a](#), M.A. Cairo [ID130](#), V.M.M. Cairo [ID37](#), O. Cakir [ID3a](#), N. Calace [ID37](#), P. Calafiura [ID18a](#), G. Calderini [ID129](#), P. Calfayan [ID35](#), L. Calic [ID98](#), G. Callea [ID58](#), L.P. Caloba [ID81b](#), D. Calvet [ID40](#), S. Calvet [ID40](#), R. Camacho Toro [ID129](#), S. Camarda [ID37](#), D. Camarero Munoz [ID27](#), P. Camarri [ID75a,75b](#), C. Camincher [ID37](#), M. Campanelli [ID96](#), A. Camplani [ID42](#), V. Canale [ID71a,71b](#), A.C. Canbay [ID3a](#), E. Canonero [ID95](#), J. Cantero [ID166](#), F. Capocasa [ID27](#), P. Cappelli [ID27](#), M. Capua [ID43b,43a](#), A. Carbone [ID70a,70b](#), R. Cardarelli [ID75a](#), J.C.J. Cardenas [ID8](#), M.P. Cardiff [ID27](#), G. Carducci [ID43b,43a](#), T. Carli [ID37](#), G. Carlino [ID71a](#), J.I. Carlotto [ID13](#), B.T. Carlson [ID131,q](#), E.M. Carlson [ID168](#), L. Carminati [ID70a,70b](#), A. Carnelli [ID4](#), M. Carnesale [ID37](#), S. Caron [ID115](#), E. Carquin [ID139g](#), I.B. Carr [ID105](#), S. Carrá [ID72a,72b](#), G. Carratta [ID24b,24a](#), C. Carrion Martinez [ID166](#), A.M. Carroll [ID125](#), N. Cartalade [ID40](#), M.P. Casado [ID13,h](#), P. Casolaro [ID71a,71b](#), M. Caspar [ID47](#), F. Cassinese [ID90](#), W.R. Castiglioni [ID39](#), F.L. Castillo [ID4](#), L. Castillo Garcia [ID13](#), V. Castillo Gimenez [ID166](#), N.F. Castro [ID132a,132e](#), A. Catinaccio [ID37](#), J.R. Catmore [ID127](#), T. Cavaliere [ID4](#), V. Cavaliere [ID30](#), E. Celebi [ID80](#), S. Cella [ID30](#), V. Cepaitis [ID55](#), K. Cerny [ID124](#), A.S. Cerqueira [ID81a](#), A. Cerri [ID73a,ap](#), L. Cerrito [ID75a,75b](#), F. Cerutti [ID18a](#), B. Cervato [ID70a,70b](#), A. Cervelli [ID24b](#), G. Cesarini [ID52](#), S.A. Cetin [ID80](#), P.M. Chabrilat [ID129](#), R. Chakkappai [ID65](#), S. Chakraborty [ID170](#), A. Chambers [ID60](#), J. Chan [ID18a](#), J.D. Chapman [ID33](#), E. Chapon [ID137](#), B. Chargeishvili [ID153b](#), D.G. Charlton [ID21](#), C. Chauhan [ID133](#), Y. Che [ID112a](#), S. Chekanov [ID6](#), G.A. Chelkov [ID38,a](#), H. Chen [ID30](#), J. Chen [ID142a](#), J. Chen [ID146](#), M. Chen [ID59](#), S. Chen [ID87](#), S.J. Chen [ID112a](#), X. Chen [ID142a](#), X. Chen [ID15,ai](#), Z. Chen [ID61](#), C.L. Cheng [ID173](#), H.C. Cheng [ID63a](#), S. Cheong [ID147](#), A. Cheplakov [ID38](#), E. Cherepanova [ID116](#), E. Cheu [ID7](#), K. Cheung [ID64](#), L. Chevalier [ID137](#), G. Chiarelli [ID73a](#), G. Chiodini [ID69a](#), A.S. Chisholm [ID21](#), J.L. Chisholm [ID167](#), A. Chitan [ID28b](#), M. Chitishvili [ID166](#), M.V. Chizhov [ID38,r](#), K. Choi [ID11](#), Y. Chou [ID141](#), E.Y.S. Chow [ID115](#), G. Christou [ID51](#), K.L. Chu [ID172](#), M.C. Chu [ID63a](#), Z. Chubinidze [ID52](#), J. Chudoba [ID133](#), J.J. Chwastowski [ID86](#), D. Cieri [ID110](#), K.M. Ciesla [ID85a](#), V. Cindro [ID93](#), A. Ciocio [ID18a](#), F. Ciotto [ID71a,71b](#), Z.H. Citron [ID172](#), M. Citterio [ID70a](#), D.A. Ciubotaru [ID28b](#), A. Clark [ID55](#), P.J. Clark [ID51](#), N. Clarke Hall [ID96](#), C. Clarry [ID159](#), S.E. Clawson [ID47](#), C. Clement [ID46a,46b](#), L. Clissa [ID24b,24a](#), Y. Coadou [ID102](#), M. Cobal [ID68a,68c](#), A. Coccaro [ID56b](#),

M.G. Cochran Branson [ID141](#), R.F. Coelho Barrue [ID132a](#), R. Coelho Lopes De Sa [ID103](#), S. Coelli [ID70a](#),
M.M. Cohen [ID130](#), L.S. Colangeli [ID159](#), B. Cole [ID41](#), P. Collado Soto [ID99](#), J. Collot [ID59](#),
M.R. Coluccia [ID69a](#), I. Combes [ID65](#), P. Conde Muiño [ID132a,132g](#), L.H.J. Condren [ID163](#), M.P. Connell [ID34c](#),
S.H. Connell [ID34c](#), E.I. Conroy [ID128](#), M. Contreras Cossio [ID11](#), F. Conventi [ID71a,ak](#),
A.M. Cooper-Sarkar [ID128](#), L. Corazzina [ID74a,74b](#), F.A. Corchia [ID24b,24a](#), A. Cordeiro Oudot Choi [ID141](#),
L.D. Corpe [ID40](#), M. Corradi [ID74a,74b](#), F. Corriveau [ID104,ab](#), A. Cortes-Gonzalez [ID157](#), M.J. Costa [ID166](#),
F. Costanza [ID4](#), D. Costanzo [ID143](#), J. Couthures [ID4](#), G. Cowan [ID95](#), K. Cranmer [ID173](#), L. Cremer [ID48](#),
D. Cremonini [ID24b,24a](#), S. Crépe-Renaudin [ID59](#), F. Crescioli [ID129](#), T. Cresta [ID72a,72b](#), M. Cristinziani [ID145](#),
M. Cristoforetti [ID77a,77b](#), T.M. Critchley [ID55](#), E. Critelli [ID96](#), A. Cueto [ID99](#), H. Cui [ID96](#), Z. Cui [ID7](#),
B.M. Cunnett [ID150](#), W.R. Cunningham [ID58](#), E. Cuppini [ID110](#), F. Curcio [ID166](#), J.R. Curran [ID51](#),
M.J. Da Cunha Sargedas De Sousa [ID56b,56a](#), J.V. Da Fonseca Pinto [ID81b](#), C. Da Via [ID101](#),
W. Dabrowski [ID85a](#), T. Dado [ID37](#), S. Dahbi [ID152](#), T. Dai [ID106](#), D. Dal Santo [ID20](#), C. Dallapiccola [ID103](#),
M. Dam [ID42](#), G. D'amen [ID30](#), V. D'Amico [ID109](#), J.R. Dandoy [ID35](#), M. D'Andrea [ID56b,56a](#),
D. Dannheim [ID37](#), G. D'anniballe [ID73a,73b](#), M. Danninger [ID146](#), V. Dao [ID149](#), G. Darbo [ID56b](#),
F. Dattola [ID47](#), S. D'Auria [ID70a,70b](#), A. D'Avanzo [ID71a,71b](#), T. Davidek [ID135](#), J. Davidson [ID170](#),
I. Dawson [ID94](#), K. De [ID8](#), C. De Almeida Rossi [ID159](#), N. De Biase [ID47](#), S. De Castro [ID24b,24a](#),
N. De Groot [ID115](#), P. de Jong [ID116](#), H. De la Torre [ID117](#), A. De Maria [ID112a](#), S. De Miranda Rimes [ID81d](#),
A. De Salvo [ID74a](#), U. De Sanctis [ID75a,75b](#), F. De Santis [ID69a,69b](#), A. De Santo [ID150](#),
J.B. De Vivie De Regie [ID59](#), K.G. De Vries [ID116](#), J. Debevc [ID93](#), D.V. Dedovich [ID38](#), J. Degens [ID92](#),
A.M. Deiana [ID44](#), J. Del Peso [ID99](#), L. Delagrangé [ID27](#), F. Deliot [ID137](#), C.M. Delitzsch [ID48](#),
M. Della Pietra [ID71a,71b](#), D. Della Volpe [ID55](#), A. Dell'Acqua [ID37](#), L. Dell'Asta [ID70a,70b](#), M. Delmastro [ID4](#),
C.C. Delogu [ID56b,56a](#), P.A. Delsart [ID59](#), S. Demers [ID175](#), M. Demichev [ID38](#), H. Denizli [ID22a,1](#),
M.G. Depala [ID92](#), L. D'Eramo [ID40](#), D. Derendarz [ID86](#), L. Derin [ID56b,56a](#), F. Derue [ID129](#), P. Dervan [ID92,*](#),
A.M. Desai [ID1](#), K. Desch [ID25](#), F.A. Di Bello [ID73a,73b](#), A. Di Ciaccio [ID75a,75b](#), L. Di Ciaccio [ID4](#),
D. Di Croce [ID37](#), C. Di Donato [ID71a,71b](#), A. Di Girolamo [ID37](#), G. Di Gregorio [ID65](#), A. Di Luca [ID77a,77b](#),
B. Di Micco [ID76a,76b](#), R. Di Nardo [ID76a,76b](#), K.F. Di Petrillo [ID39](#), M. Diamantopoulou [ID35](#), F.A. Dias [ID116](#),
M.A. Diaz [ID139a,139b](#), A.R. Didenko [ID38](#), M. Didenko [ID166](#), S.D. Diefenbacher [ID18a](#), E.B. Diehl [ID106](#),
S. Díez Cornell [ID47](#), C. Díez Pardos [ID145](#), C. Dimitriadi [ID148](#), A. Dimitrievska [ID21](#), A. Dimri [ID149](#),
Y. Ding [ID61](#), J. Dingfelder [ID25](#), T. Dingley [ID128](#), I-M. Dinu [ID28b](#), S.J. Dittmeier [ID62b](#), F. Dittus [ID37](#),
M. Divisek [ID135](#), B. Dixit [ID92](#), F. Djama [ID102](#), T. Djobava [ID153b](#), C. Doglioni [ID101,98](#), A. Dohnalova [ID29a](#),
Z. Dolezal [ID135](#), K. Domijan [ID85a](#), K.M. Dona [ID39](#), M. Donadelli [ID81d](#), B. Dong [ID107](#), J. Donini [ID40](#),
A. D'Onofrio [ID71a,71b](#), M. D'Onofrio [ID92](#), J. Dopke [ID136](#), A. Doria [ID71a](#), N. Dos Santos Fernandes [ID132a](#),
I.A. Dos Santos Luz [ID81e](#), P. Dougan [ID44](#), M.T. Dova [ID90](#), A.T. Doyle [ID58](#), M.P. Drescher [ID54](#),
E. Dreyer [ID172](#), I. Drivas-koulouris [ID10](#), M. Drnevich [ID119](#), D. Du [ID61](#), T. Du [ID39](#), T.A. du Pree [ID116](#),
Z. Duan [ID112a](#), M. Dubau [ID4](#), F. Dubinin [ID38](#), M. Dubovsky [ID29a](#), E. Duchovni [ID172](#), G. Duckeck [ID109](#),
P.K. Duckett [ID96](#), O.A. Ducu [ID28b](#), D. Duda [ID51](#), A. Dudarev [ID37](#), M.M. Dudek [ID86](#), E.R. Duden [ID27](#),
M. D'uffizi [ID101](#), L. Dufflot [ID65](#), M. Dührssen [ID37](#), I. Duminica [ID28g](#), A.E. Dumitriu [ID28b](#),
M. Dunford [ID62a](#), T. Duong [ID4](#), A. Duperrin [ID102](#), A.F. Duque Bran [ID40](#), H. Duran Yildiz [ID3a](#),
A. Durglishvili [ID153b](#), G.I. Dyckes [ID18a](#), M. Dyndal [ID85a](#), B.S. Dziedzic [ID37](#), G.H. Eberwein [ID128](#),
B. Eckerova [ID29a](#), J.C. Egan [ID96](#), S. Eggebrecht [ID54](#), E. Egidio Purcino De Souza [ID81e](#), G. Eigen [ID17](#),
K. Einsweiler [ID18a](#), T. Ekelof [ID164](#), P.A. Ekman [ID98](#), S. El Farkh [ID36b](#), Y. El Ghazali [ID61](#),
H. El Jarrari [ID104](#), A. El Moussaouy [ID36a](#), I. Elbaz [ID155](#), D. Elitez [ID37](#), M. Ellert [ID164](#),
F. Ellinghaus [ID174](#), T.A. Elliot [ID95](#), J. Elmsheuser [ID30](#), M. Elsayy [ID118a](#), M. Elsing [ID37](#),
D. Emelianov [ID136](#), Y. Enari [ID82](#), S. Epari [ID108](#), D. Ernani Martins Neto [ID86](#), F. Ernst [ID37](#),
M. Escalier [ID65](#), C. Escobar [ID166](#), R. Estevam De Paula [ID81c](#), E. Etzion [ID155](#), G. Evans [ID132a,132b](#),
H. Evans [ID67](#), L.S. Evans [ID47](#), S. Ezzarqtouni [ID36a](#), F. Fabbri [ID24b,24a](#), L. Fabbri [ID24b,24a](#), G. Facini [ID96](#),
V. Fadeyev [ID138](#), D. Fakoudis [ID100](#), S. Falciano [ID74a](#), L.F. Falda Ulhoa Coelho [ID27](#), F. Fallavollita [ID110](#),

G. Falsetti ^{43b,43a}, J. Faltova ¹³⁵, C. Fan ¹⁶⁵, K.Y. Fan ^{63b}, Y. Fan ¹⁴, Y. Fang ^{14,112c}, M. Fanti ^{70a,70b}, M. Faraj ^{68a,68c}, Z. Farazpay ⁹⁷, A. Farbin ⁸, A. Farilla ^{76a}, K. Farman ¹⁵², J.N. Farr ¹⁷⁵, M.S. Farrington ⁶⁰, S.M. Farrington ^{136,51}, F. Fassi ^{36e}, D. Fassouliotis ⁹, L. Fayard ⁶⁵, G. Fazzino ^{62b}, P. Federic ¹³⁵, P. Federicova ¹³³, M. Feickert ¹⁷³, L. Feligioni ¹⁰², D.E. Fellers ^{18a}, C. Feng ^{113b}, Y. Feng ¹⁴, Z. Feng ⁶⁵, B. Fernandez Barbadillo ⁹¹, P. Fernandez Martinez ⁶⁶, C. Fernandez Ruiz ³³, J. Ferrando ⁹¹, A. Ferrari ¹⁶⁴, P. Ferrari ^{116,115}, R. Ferrari ^{72a}, D. Ferrere ⁵⁵, C. Ferretti ¹⁰⁶, M.P. Fewell ¹, D. Fiacco ^{74a,74b}, F. Fiedler ¹⁰⁰, P. Fiedler ¹³⁴, S. Filimonov ³⁸, M.S. Filip ^{28b,s}, A. Filipčič ⁹³, E.K. Filmer ^{160a}, F. Filthaut ¹¹⁵, M.C.N. Fiolhais ^{132a,132c,c}, L. Fiorini ¹⁶⁶, W.C. Fisher ¹⁰⁷, T. Fitschen ¹⁰¹, I. Fleck ¹⁴⁵, P. Fleischmann ¹⁰⁶, T. Flick ¹⁷⁴, M. Flores ^{34d,ag}, L.R. Flores Castillo ^{63a}, M. Foll ¹²⁷, F.M. Follega ^{77a,77b}, N. Fomin ³³, J.H. Foo ¹⁵⁹, A. Formica ¹³⁷, M. Fornasiero ¹⁵⁰, A.C. Forti ¹⁰¹, N. Forti ^{24b,24a}, E. Fortin ¹⁰², A.W. Fortman ^{18a}, L. Foster ^{18a}, L. Fountas ⁹, H. Fox ⁹¹, P. Francavilla ^{73a,73b}, S. Francescato ⁶⁰, S. Franchellucci ²⁰, M. Franchini ^{24b,24a}, S. Franchino ^{62a}, D. Francis ³⁷, L. Franco ⁴⁷, L. Franconi ⁴⁷, M. Franklin ⁶⁰, G. Frattari ²⁷, Y.Y. Frid ¹⁵⁵, N. Fritzsche ³⁷, A. Froch ⁵⁵, D. Froidevaux ³⁷, J.A. Frost ¹³⁶, Y. Fu ¹⁰⁷, S. Fuenzalida Garrido ^{139g}, Y.C. Fujikake ¹³⁸, M. Fujimoto ¹⁴⁹, K.Y. Fung ^{63a}, E. Furtado De Simas Filho ^{81e}, M. Furukawa ¹⁵⁷, M. Fuste Costa ⁴⁷, J. Fuster ¹⁶⁶, A. Gaa ⁵⁴, A. Gabrielli ^{24b,24a}, A. Gabrielli ¹⁵⁹, G. Gagliardi ^{56b,56a}, L.G. Gagnon ^{18a}, S. Galantzan ¹⁵⁵, J. Gallagher ¹, E.J. Gallas ¹²⁸, A.L. Gallen ¹⁶⁴, B.J. Gallop ¹³⁶, K.K. Gan ¹²¹, Y. Gao ⁵¹, Z. Gao ^{112a}, A. Garabaglu ¹⁴¹, F.M. Garay Walls ^{139a,139b}, C. García ¹⁶⁶, A. Garcia Alonso ¹¹⁶, A.G. Garcia Caffaro ¹⁷⁵, J.E. García Navarro ¹⁶⁶, M.A. Garcia Ruiz ^{23b}, M. Garcia-Sciveres ^{18a}, G.L. Gardner ¹³⁰, R.W. Gardner ³⁹, N. Garelli ¹⁶², R.B. Garg ¹⁴⁷, J.M. Gargan ³³, C.A. Garner ¹⁵⁹, C.M. Garvey ^{34a}, V.K. Gassmann ¹⁶², G. Gaudio ^{72a}, A.J. Gavin ⁹⁴, J. Gavranovic ⁹³, I.L. Gavrilenko ^{132a}, C. Gay ¹⁶⁷, G. Gaycken ¹²⁵, A. Gekow ¹²¹, C. Gemme ^{56b}, M.H. Genest ⁵⁹, A.D. Gentry ¹¹⁴, S. George ⁹⁵, T. Geralis ⁴⁵, A.A. Gerwin ¹²², P. Gessinger-Befurt ³⁷, M. Ghani ¹⁷⁰, K. Ghorbanian ⁹⁴, A. Ghosal ¹⁴⁵, A. Ghosh ¹⁶³, A. Ghosh ⁷, B. Giacobbe ^{24b}, S. Giagu ^{74a,74b}, A. Giannini ⁶¹, S.M. Gibson ⁹⁵, D.T. Gil ^{85b}, A.K. Gilbert ^{85a}, B.J. Gilbert ⁴¹, D. Gillberg ³⁵, G. Gilles ¹¹⁶, D.M. Gingrich ^{2,aj}, M.P. Giordani ^{68a,68c}, P.F. Giraud ¹³⁷, G. Giugliarelli ^{68a,68c}, D. Giugni ^{70a}, F. Giuli ^{75a,75b,al}, I. Gkialas ^{9,i}, C. Glasman ⁹⁹, M. Glazewska ²⁰, R.M. Gleason ¹⁶³, G. Glemža ⁴⁷, I. Gnesi ^{24b,24a,am}, Y. Go ³⁰, M. Goblirsch-Kolb ³⁷, B. Gocke ⁴⁸, D. Godin ¹⁰⁸, B. Gokturk ^{22a}, S. Goldfarb ¹⁰⁵, T. Golling ⁵⁵, M.G.D. Gololo ^{34c}, A. Golub ¹⁴¹, J.P. Gombas ¹⁰⁷, A. Gomes ^{132a,132b}, G. Gomes Da Silva ¹⁴⁵, A.J. Gomez Delegido ³⁷, R. Gonçalves ^{132a}, A. Gongadze ^{153c}, F. Gonnella ²¹, J.L. Gonski ¹⁴⁷, R.Y. González Andana ⁵¹, S. González de la Hoz ¹⁶⁶, M.V. Gonzalez Rodrigues ⁴⁷, R. Gonzalez Suarez ¹⁶⁴, S. Gonzalez-Sevilla ⁵⁵, L. Goossens ³⁷, B. Gorini ³⁷, E. Gorini ^{69a,69b}, A. Gorišek ⁹³, T.C. Gosart ¹³⁰, A.T. Goshaw ⁵⁰, M.I. Gostkin ³⁸, S. Goswami ¹²³, C.A. Gottardo ³⁷, S.A. Gotz ¹⁰⁹, M. Goughri ^{36b}, A.G. Goussiou ¹⁴¹, N. Govender ^{34c}, R.P. Grabarczyk ¹²⁸, I. Grabowska-Bold ^{85a}, K. Graham ³⁵, E. Gramstad ¹²⁷, S. Grancagnolo ^{69a,69b}, C.M. Grant ¹, P.M. Gravila ^{28f}, F.G. Gravili ^{69a,69b}, H.M. Gray ^{18a}, M. Greco ¹¹⁰, M.J. Green ¹, C. Grefe ²⁵, A.S. Grefsrud ¹⁷, I.M. Gregor ⁴⁷, K.T. Greif ¹⁶³, P. Grenier ¹⁴⁷, S.G. Grewe ¹¹⁰, K. Grimm ³², S. Grinstein ^{13,x}, E. Gross ¹⁷², J. Grosse-Knetter ⁵⁴, L.H. Grossman ^{18b}, L. Guan ¹⁰⁶, G. Guerrieri ³⁷, R. Guevara ¹²⁷, R. Gugel ¹⁰⁰, J.A.M. Guhit ¹⁰⁶, A. Guida ¹⁹, E. Guilloton ¹⁷⁰, S. Guindon ³⁷, F. Guo ^{14,112c}, J. Guo ^{142a}, L. Guo ⁴⁷, L. Guo ^{112b,u}, Y. Guo ¹⁰⁶, Y. Guo ⁴¹, A. Gupta ⁴⁸, R. Gupta ¹³¹, S. Gupta ²⁷, S. Gurbuz ²⁵, S.S. Gurdasani ⁴⁷, G. Gustavino ^{74a,74b}, P. Gutierrez ¹²², L.F. Gutierrez Zagazeta ¹³⁰, M. Gutsche ⁴⁹, C. Gutschow ⁹⁶, W. Guérin ⁸⁹, C. Gwenlan ¹²⁸, C.B. Gwilliam ⁹², E.S. Haaland ¹²⁷, A. Haas ¹¹⁹, M. Habedank ⁵⁸, C. Haber ^{18a},

R.J. Haberle ¹⁷², H.K. Hadavand ⁸, A. Haddad ⁴⁰, A. Hadeef ⁴⁹, A.I. Hagan ⁹¹, J.J. Hahn ¹⁴⁵,
 M. Haleem ¹⁶⁹, J. Haley ¹²³, G.D. Hallelwell ¹⁰², J.A. Hallford ⁴⁷, K. Hamano ¹⁶⁸,
 H. Hamdaoui ¹⁶⁴, M. Hamer ²⁵, S.E.D. Hammoud ⁶⁵, E.J. Hampshire ⁹⁵, L. Han ^{112a},
 L. Han ⁶¹, S. Han ¹⁴, K. Hanagaki ⁸², M. Hance ¹³⁸, D.A. Hangal ⁴¹, H. Hanif ¹⁴⁶,
 M.D. Hank ¹³⁰, J.B. Hansen ⁴², P.H. Hansen ⁴², T. Harenberg ¹⁷⁴, S. Harkusha ¹⁷⁶,
 M.L. Harris ¹⁰³, Y.T. Harris ²⁵, J. Harrison ¹³, P.F. Harrison ¹⁷⁰, M.L.E. Hart ⁹⁶,
 N.M. Hartman ¹¹⁰, N.M. Hartmann ¹⁰⁹, R.Z. Hasan ^{95,136}, Y. Hasegawa ¹⁴⁴, D. Hashimoto ¹¹¹,
 F. Haslbeck ³⁷, S. Hassan ¹²⁷, R. Hauser ¹⁰⁷, M. Haviernik ¹³⁵, C.M. Hawkes ²¹,
 R.J. Hawkings ³⁷, Y. Hayashi ¹⁵⁷, D. Hayden ¹⁰⁷, R.L. Hayes ¹¹⁶, C.P. Hays ¹²⁸, J.M. Hays ⁹⁴,
 H.S. Hayward ⁹², M. He ^{14,112c}, Y. He ⁴⁷, Y. He ⁹⁶, N.B. Heatley ⁹⁴, V. Hedberg ⁹⁸,
 J. Heilman ³⁵, S. Heim ⁴⁷, T. Heim ^{18a}, J.J. Heinrich ¹²⁵, L. Heinrich ¹¹⁰, J. Hejbal ¹³³,
 M. Helbig ⁴⁹, A. Held ¹⁷³, S. Hellesund ¹⁷, C.M. Helling ¹⁶⁷, F.N.E. Henry ⁵⁸, H. Herde ⁹⁸,
 Y. Hernández Jiménez ¹⁴⁹, G. Herten ⁵³, R. Hertenberger ¹⁰⁹, L. Hervas ³⁷, M.E. Hespings ¹⁰⁰,
 N.P. Hessey ^{160a}, J. Hessler ¹¹⁰, R. Hicks ¹³⁰, M. Hidaoui ^{36b}, N. Hidic ¹³⁵, E. Hill ¹⁵⁹,
 T.S. Hillersoy ¹⁷, S.J. Hillier ²¹, J.R. Hinds ¹⁰⁷, F. Hinterkeuser ²⁵, M. Hirose ¹²⁶, S. Hirose ¹⁶¹,
 D. Hirschbuehl ¹⁷⁴, B. Hiti ⁹³, J. Hobbs ¹⁴⁹, R. Hobincu ^{28e}, N. Hod ¹⁷², A.M. Hodges ¹⁶⁵,
 M.C. Hodgkinson ¹⁴³, B.H. Hodgkinson ¹²⁸, A. Hoecker ³⁷, D.D. Hofer ¹⁰⁶, J. Hofer ¹⁶⁶,
 J. Hofner ¹⁰⁰, M. Holzbock ³⁷, L.B.A.H. Hommels ³³, V. Homsak ¹²⁸, J.J. Hong ⁶⁷,
 T.M. Hong ¹³¹, B.H. Hooberman ¹⁶⁵, W.H. Hopkins ⁶, M.C. Hoppesch ¹⁶⁵, Y. Horii ¹¹¹,
 M.E. Horstmann ¹¹⁰, M.M. Horzela ⁵⁴, S. Hou ¹⁵², M.R. Housenga ¹⁶⁵, J. Howarth ⁵⁸,
 J. Hoya ⁶, M. Hrabovsky ¹²⁴, T. Hryn'ova ⁴, P.J. Hsu ⁶⁴, S.-C. Hsu ¹⁴¹, T. Hsu ⁶⁵, M. Hu ^{18a},
 P. Hu ^{63b}, Q. Hu ⁶¹, S. Huang ³³, X. Huang ^{14,112c}, Y. Huang ¹³⁵, Y. Huang ^{112b}, Y. Huang ¹⁴,
 Z. Huang ⁶⁵, Z. Hubacek ¹³⁴, F. Huegging ²⁵, T.B. Huffman ¹²⁸,
 M. Hufnagel Maranha De Faria ^{81a}, C.A. Hugli ⁴⁷, M. Huhtinen ³⁷, S.K. Huiberts ¹⁷,
 R. Hulsken ¹⁰⁴, C.E. Hultquist ^{18a}, D.L. Humphreys ¹⁰³, N. Huseynov ¹², J. Huston ¹⁰⁷,
 B. Huth ³⁷, J. Huth ⁶⁰, L. Huth ⁴⁷, R. Hyneman ⁷, G. Iacobucci ⁵⁵, G. Iakovidis ³⁰,
 L. Iconomidou-Fayard ⁶⁵, J.P. Iddon ³⁷, P. Iengo ^{71a,71b}, Y. Iiyama ¹⁵⁷, T. Iizawa ¹⁵⁷,
 Y. Ikegami ⁸², D. Iliadis ¹⁵⁶, N. Ilic ¹⁵⁹, H. Imam ^{36a}, G. Inacio Goncalves ^{81d},
 S.A. Infante Cabanas ^{139c}, T. Ingebretsen Carlson ^{46a,46b}, J.M. Inglis ⁹⁴, G. Introzzi ^{72a,72b},
 M. Iodice ^{76a}, V. Ippolito ^{74a,74b}, R.K. Irwin ⁹², M. Ishino ¹⁵⁷, W. Islam ¹⁷³, C. Issever ¹⁹,
 S. Istin ^{22a,ar}, K. Itabashi ¹²⁶, H. Ito ¹⁷¹, R. Iuppa ^{77a,77b}, A. Ivina ¹⁷², F. Ivone ³⁷,
 S. Izumiyama ¹¹¹, V. Izzo ^{71a}, P. Jacka ¹³⁴, P. Jackson ¹, P.R. Jacobson ⁵⁰, P. Jain ⁴⁷,
 K. Jakobs ⁵³, J. Jamieson ⁵⁸, W. Jang ¹⁵⁷, S. Jankovych ¹¹⁶, B.K. Jashal ¹³⁶, M. Javurkova ¹⁰³,
 P. Jawahar ¹⁰¹, L. Jeanty ¹²⁵, J. Jejelava ^{153a,ae}, P. Jenni ^{53,f}, L. Jerala ⁹³, C.E. Jessiman ³⁵,
 H. Jia ¹⁶⁷, J. Jia ¹⁴⁹, X. Jia ^{110,112c}, C. Jiang ⁵¹, Q. Jiang ^{63b}, S. Jiggins ⁴⁷,
 M. Jimenez Ortega ¹⁶⁶, J. Jimenez Pena ¹³, S. Jin ^{112a}, A. Jinaru ^{28b}, O. Jinnouchi ¹⁴⁰,
 P. Johansson ¹⁴³, K.A. Johns ⁷, J.W. Johnson ¹³⁸, F.A. Jolly ⁴⁷, D.M. Jones ¹⁵⁰, E. Jones ⁴⁷,
 K.S. Jones ⁸, P. Jones ³³, R.W.L. Jones ⁹¹, T.J. Jones ⁹², H.L. Joos ³⁷, R. Joshi ¹²¹,
 J. Jovicevic ¹⁶, X. Ju ^{18a}, J.J. Junggeburth ³⁷, T. Junkermann ^{62a}, A. Juste Rozas ^{13,x},
 M.K. Juzek ⁸⁶, S. Kabana ^{139f}, A. Kaczmarzka ⁸⁶, S.A. Kadir ¹⁴⁷, M. Kado ¹¹⁰, H. Kagan ¹²¹,
 M. Kagan ¹⁴⁷, A. Kahn ¹³⁰, C. Kahra ¹⁰⁰, T. Kaji ¹⁵⁷, E. Kajomovitz ¹⁵⁴, N. Kakati ¹⁷²,
 N. Kakoty ¹³, S. Kandel ⁸, N. Kanellos ¹⁰, D. Kar ^{34,*}, E. Karentzos ²⁵, K. Karki ⁸,
 O. Karkout ¹¹⁶, S.N. Karpov ³⁸, Z.M. Karpova ³⁸, V. Kartvelishvili ^{91,153b}, E. Kasimi ¹⁵⁶,
 J. Katzy ⁴⁷, S. Kaur ³⁵, R. Kavak ¹⁶⁵, K. Kawade ¹⁴⁴, M.P. Kawale ¹²², C. Kawamoto ⁸⁷,
 E.F. Kay ³⁷, S. Kazakos ¹⁰⁷, K. Kazakova ¹⁰², J.M. Keaveney ^{34a}, R. Keeler ¹⁶⁸, G.V. Kehris ⁶⁰,
 J.S. Keller ³⁵, J.M. Kelly ¹⁶⁸, J.J. Kempster ¹⁵⁰, O. Kepka ¹³³, J. Kerr ^{160b}, B.P. Kerridge ¹³⁶,
 B.P. Kerševan ⁹³, L. Keszeghova ^{29a}, R.A. Khan ¹³¹, A. Khanov ¹²³, M. Kholodenko ^{132a},

T.J. Khoo ¹⁹, G. Khoriali ¹⁶⁹, Y. Khoulaki ^{36a}, Y.A.R. Khwaira ¹²⁹, D. Kim ⁶, D.W. Kim ^{18b}, Y.K. Kim ³⁹, N. Kimura ⁹⁶, M.K. Kingston ⁵⁴, F. Kirfel ²⁵, J. Kirk ¹³⁶, A.E. Kiryunin ¹¹⁰, S. Kita ¹⁶¹, O. Kivernyk ²⁵, M. Klassen ¹⁶², C. Klein ³⁵, L. Klein ¹⁶⁹, M.H. Klein ⁴⁴, S.B. Klein ⁵⁵, U. Klein ⁹², A. Klimentov ³⁰, P. Kluit ¹¹⁶, S. Kluth ¹¹⁰, E. Kneringer ⁷⁸, T.M. Knight ¹⁵⁹, A. Knue ⁴⁸, M. Kobel ⁴⁹, D. Kobylianskii ¹⁷², S.F. Koch ³⁷, M. Kocian ¹⁴⁷, P. Kodyš ¹³⁵, D.M. Koeck ¹²⁵, T. Koffas ³⁵, K. Kojima ⁸², O. Kolay ⁴⁹, I. Koletsou ⁴, T. Komarek ⁸⁶, S. Kondo ¹⁵⁷, K. Köneke ⁵⁴, A.X.Y. Kong ¹, T. Kono ¹²⁰, N. Konstantinidis ⁹⁶, P. Kontaxakis ⁵⁵, B. Konya ⁹⁸, R. Kopeliansky ⁴¹, S. Koperny ^{35a}, R. Koppenhofer ⁵³, K. Korcyl ⁸⁶, K. Kordas ^{156,d}, A. Korn ⁹⁶, S. Korn ⁵⁴, I. Korolkov ¹³, B. Kortman ¹¹⁶, O. Kortner ¹¹⁰, S. Kortner ¹¹⁰, W.H. Kostecka ¹¹⁷, M. Kostov ^{29a}, V.V. Kostyukhin ¹⁴⁵, A. Kotsokechagia ³⁷, A. Kotwal ⁵⁰, A. Koulouris ³⁷, A. Kourkoumeli-Charalampidi ^{72a,72b}, O. Kovanda ¹²⁵, R. Kowalewski ¹⁶⁸, W. Kozanecki ¹²⁵, G. Kramberger ⁹³, P. Kramer ²⁵, A. Krasznahorkay ¹⁰³, A.C. Kraus ¹¹⁷, J.W. Kraus ¹⁷⁴, J.A. Kremer ⁴⁷, N.B. Krengel ¹⁴⁵, T. Kresse ¹⁵⁹, L. Kretschmann ¹⁷⁴, J. Kretschmar ⁹², P. Krieger ¹⁵⁹, K. Krizka ²¹, K. Kroeninger ⁴⁸, H. Kroha ¹¹⁰, J. Kroll ¹³³, J. Kroll ¹³⁰, K.S. Krowpman ¹⁰⁷, U. Kruchonak ³⁸, H. Krüger ²⁵, N. Krumnack ⁷⁹, J. Krupa ¹⁴⁷, M.C. Kruse ⁵⁰, O. Kuchinskaia ³⁸, S. Kuday ^{3a}, S. Kuehn ³⁷, R. Kuesters ⁵³, T. Kuhl ⁴⁷, V. Kukhtin ³⁸, Y. Kulchitsky ³⁸, S. Kuleshov ^{139d,139b}, J. Kull ¹, E.V. Kumar ¹⁰⁹, M. Kumar ^{34j}, N. Kumari ⁴⁷, P. Kumari ^{160b}, A. Kupco ¹³³, O. Kuprash ⁵³, H. Kurashige ⁸⁴, L.L. Kurchaninov ^{160a}, O. Kurdysh ⁴, M. Kuze ¹⁴⁰, A.K. Kvam ¹⁰³, J. Kvita ¹²⁴, N.G. Kyriacou ¹⁴¹, M. Laassiri ³⁰, C. Lacasta ¹⁶⁶, H. Lacker ¹⁹, D. Lacour ¹²⁹, E. Ladygin ³⁸, A. Lafarge ⁴⁰, B. Laforge ¹²⁹, T. Lagouri ¹⁷⁵, F.Z. Lahbabi ^{36a}, S. Lai ⁵⁴, W.S. Lai ⁹⁶, I.K. Lakomic ⁵⁴, J.E. Lambert ¹⁶⁸, S. Lammers ⁶⁷, W. Lampl ⁷, C. Lampoudis ¹⁵⁶, G. Lamprinoudis ¹⁶⁹, A.N. Lancaster ¹¹⁷, U. Landgraf ⁵³, M.P.J. Landon ⁹⁴, V.S. Lang ⁵³, A.J. Lankford ¹⁶³, F. Lanni ³⁷, C.S. Lantz ¹⁶⁵, K. Lantzsch ²⁵, A. Lanza ^{72a}, M. Lanzac Berrocal ¹⁶⁶, T. Lari ^{70a}, D. Larsen ¹⁷, L. Larson ¹¹, F. Lasagni Manghi ^{24b}, M. Lassnig ³⁷, H.C. Lau ¹⁶⁸, S.D. Lawlor ¹⁴³, R. Lazaridou ¹⁶³, M. Lazzaroni ^{70a,70b}, E.T.T. Le ¹⁶³, H.D.M. Le ¹⁰⁷, E.M. Le Boulicaut ¹⁷⁵, L.T. Le Pottier ^{18a}, B. Leban ^{24b,24a}, F. Ledroit-Guillon ⁵⁹, T.F. Lee ^{160b}, L.L. Leeuw ^{34h}, M. Lefebvre ¹⁶⁸, C. Leggett ^{18a}, L.M. Lehmann ¹¹⁶, G. Lehmann Miotto ³⁷, M. Leigh ⁵⁵, W.A. Leight ¹⁰³, W. Leinonen ¹¹⁵, A. Leisos ^{156,t}, M.A.L. Leite ^{81c}, C.E. Leitgeb ¹⁹, R. Leitner ¹³⁵, K.J.C. Leney ⁴⁴, T. Lenz ²⁵, S. Leone ^{73a}, C. Leonidopoulos ⁵¹, A. Leopold ¹⁴⁸, J. LePage-Bourbonnais ³⁵, R. Les ¹⁰⁷, C.G. Lester ³³, J. Levêque ⁴, L.J. Levinson ¹⁷², G. Levrini ^{24b,24a}, M.P. Lewicki ⁸⁶, C. Lewis ¹⁴¹, D.J. Lewis ⁴, L. Lewitt ¹⁴³, A. Li ³⁰, B. Li ^{113b}, C. Li ¹⁰⁶, C-Q. Li ¹¹⁰, H. Li ^{113b}, H. Li ¹⁰¹, H. Li ¹⁵, H. Li ⁶¹, H. Li ^{113b}, J. Li ^{142a}, L. Li ^{142a}, R. Li ¹⁷⁵, S. Li ^{142b,142a}, T. Li ⁵, Y. Li ¹⁴, Z. Li ^{14,112c}, Z. Li ⁶¹, S. Liang ^{14,112c}, Z. Liang ¹⁴, M. Liberatore ¹³⁷, B. Liberti ^{75a}, G.B. Libotte ^{81d}, K. Lie ^{63c}, J. Lieber Marin ^{81e}, H. Lien ⁶⁷, H. Lin ¹⁰⁶, S.F. Lin ¹⁴⁹, L. Linden ¹⁰⁹, R.E. Lindley ⁷, J.H. Lindon ³⁷, J. Ling ⁶⁰, E. Lipeles ¹³⁰, A. Lipniacka ¹⁷, A. Lister ¹⁶⁷, J.D. Little ⁶⁷, B. Liu ^{113a}, B.X. Liu ^{112b}, D. Liu ¹⁵⁴, D. Liu ¹³⁸, E.H.L. Liu ²¹, H. Liu ^{112b}, J.K.K. Liu ¹¹⁹, K. Liu ^{142b}, K. Liu ^{142b}, M. Liu ⁶¹, M.Y. Liu ⁶¹, P. Liu ^{113b}, Q. Liu ¹⁴⁷, S. Liu ¹⁴⁹, X. Liu ^{113b}, Y. Liu ^{112b,112c}, Y. Liu ¹⁶⁵, Y.L. Liu ^{113b}, Y.W. Liu ⁶¹, Z. Liu ^{65,j}, S.L. Lloyd ⁹⁴, E.M. Lobodzinska ⁴⁷, P. Loch ⁷, E. Lodhi ¹⁵⁹, K. Lohwasser ¹⁴³, E. Loiacono ¹²³, J.D. Lomas ²¹, I. Longarini ¹⁶³, R. Longo ^{24b,24a,am}, A. Lopez Solis ¹³, N.A. Lopez-canelas ⁷, N. Lorenzo Martinez ⁴, A.M. Lory ¹⁰⁹, M. Losada ^{118a}, G. Lösckce Centeno ⁴, X. Lou ^{14,112c}, P.A. Love ⁹¹, M. Lu ⁶⁵, S. Lu ¹³⁰, Y.J. Lu ¹⁵², H.J. Lubatti ¹⁴¹, C. Luci ^{74a,74b}, F.L. Lucio Alves ^{112a}, F. Luehring ⁶⁷, B.S. Lunday ¹³⁰, O. Lundberg ¹⁴⁸, J. Lunde ³⁷, N.A. Luongo ⁶, M.S. Lutz ¹⁵⁹, A.B. Lux ²⁶, D. Lynn ³⁰, R. Lysak ¹³³, V. Lysenko ¹³⁴, E. Lytken ⁹⁸, V. Lyubushkin ³⁸, T. Lyubushkina ³⁸, M.M. Lyukova ¹⁴⁹, H. Ma ³⁰, K. Ma ⁶¹,

L.L. Ma ^{113b}, W. Ma ⁶¹, Y. Ma ^{113b}, J.C. MacDonald ¹⁰⁰, P.C. Machado De Abreu Farias ^{81e}, D. Macina ³⁷, R. Madar ⁴⁰, T. Madula ⁹⁶, J. Maeda ⁸⁴, T. Maeno ³⁰, P.T. Mafa ^{34f}, H. Maguire ¹⁴³, M. Maheshwari ³³, V. Maiboroda ⁶⁵, A. Maio ^{132a,132b,132d}, K. Maj ^{85a}, O. Majersky ⁴⁷, S. Majewski ¹²⁵, A. Makita ¹⁵⁷, N. Makovec ⁶⁵, V. Maksimovic ¹⁶, B. Malaescu ¹²⁹, J. Malamant ¹²⁷, Pa. Malecki ⁸⁶, F. Malek ^{59,n}, M. Mali ⁹³, D. Malito ⁹⁵, A. Maloizel ⁵, A. Malvezzi Lopes ^{81d}, S. Malyukov ³⁸, J. Mamuzic ⁹³, G. Mancini ⁵², M.N. Mancini ²⁷, G. Manco ^{72a,72b}, S.S. Mandarry ¹⁵⁰, I. Mandić ⁹³, L. Manhaes de Andrade Filho ^{81a}, I.M. Maniatis ¹⁷², J. Manjarres Ramos ⁸⁹, D.C. Mankad ¹⁷², A. Mann ¹⁰⁹, T. Manoussos ³⁷, M.N. Mantinan ³⁹, S. Manzoni ³⁷, L. Mao ^{142a}, X. Mapekula ^{34c}, A. Marantis ¹⁵⁶, R.R. Marcelo Gregorio ¹, G. Marchiori ⁵, C. Marcon ^{70a}, E. Maricic ¹⁶, M. Marinescu ⁴⁷, S. Marium ⁴⁷, M. Marjanovic ¹²², A. Markhoos ⁵³, M. Markovitch ⁶⁵, M.K. Maroun ¹⁰³, M.C. Marr ¹⁴⁶, G.T. Marsden ¹⁰¹, Z. Marshall ^{18a}, S. Marti-Garcia ¹⁶⁶, J. Martin ⁹⁶, T.A. Martin ¹³⁶, V.J. Martin ⁵¹, B. Martin dit Latour ¹⁷, L. Martinelli ^{74a,74b}, V.I. Martinez Outschoorn ¹⁰³, P. Martinez Suarez ³⁷, S. Martin-Haugh ¹³⁶, G. Martinovicova ¹³⁵, V.S. Martoiu ^{28b}, A. Martone ⁸⁹, A.C. Martyniuk ⁹⁶, A. Marzin ³⁷, D. Mascione ^{77a,77b}, L. Masetti ¹⁰⁰, J. Masik ¹⁰¹, A.L. Maslennikov ³⁸, S.L. Mason ⁴¹, P. Massarotti ^{71a,71b}, P. Mastrandrea ^{73a,73b}, A. Mastroberardino ^{43b,43a}, T. Masubuchi ¹²⁶, T.T. Mathew ¹²⁵, J. Matousek ¹³⁵, D.M. Mattern ⁴⁸, K. Mauer ⁴⁷, J. Maurer ^{28b}, T. Maurin ⁵⁸, A.J. Maury ⁶⁵, B. Maček ⁹³, C. Mavungu Tsava ¹⁰², A.E. May ¹⁰¹, E. Mayer ⁴⁰, R. Mazini ^{34j}, S.M. Mazza ¹³⁸, E. Mazzeo ³⁷, J.P. Mc Gowan ¹⁶⁸, S.P. Mc Kee ¹⁰⁶, C.C. McCracken ¹⁶⁷, E.F. McDonald ¹⁰⁵, L.F. Mcelhinney ⁹¹, J.A. Mcfayden ¹⁵⁰, R.P. McGovern ¹³⁰, R.P. Mckenzie ^{34j}, D.J. Mclaughlin ⁹⁶, S.J. McMahan ¹³⁶, C.M. Mcpartland ⁹², R.A. McPherson ^{168,ab}, S. Mehlhase ¹⁰⁹, A. Mehta ⁹², D. Melini ¹⁶⁶, B.R. Mellado Garcia ^{14,ah}, A.H. Melo ⁵⁴, F. Meloni ⁴⁷, A.M. Mendes Jacques Da Costa ¹⁰¹, L. Meng ⁹¹, S. Menke ¹¹⁰, M. Mentink ³⁷, E. Meoni ^{43b,43a}, G. Mercado ¹¹⁷, S. Merianos ¹⁵⁶, C. Merlassino ^{68a,68c}, C. Meroni ^{70a,70b}, J. Metcalfe ⁶, A.S. Mete ⁶, E. Meuser ¹⁰⁰, C. Meyer ⁶⁷, J-P. Meyer ¹³⁷, Y. Miao ^{112a}, R.P. Middleton ¹³⁶, M. Mihovilovic ⁶⁵, L. Mijović ⁵¹, G. Mikenberg ¹⁷², M. Mikestikova ¹³³, M. Mikuž ⁹³, H. Mildner ¹⁰⁰, A. Milic ³⁷, D.W. Miller ³⁹, E.H. Miller ¹⁴⁷, A. Milov ¹⁷², D.A. Milstead ^{46a,46b}, T. Min ^{112a}, I.A. Minashvili ^{153b}, A.I. Mincer ¹¹⁹, B. Mindur ^{85a}, M. Mineev ³⁸, Y. Mino ⁸⁷, L.M. Mir ¹³, M. Miralles Lopez ⁵⁸, M. Mironova ^{18a}, M. Missio ⁴⁰, A. Mitra ¹⁷⁰, V.A. Mitsou ¹⁶⁶, Y. Mitsumori ¹¹¹, P.S. Miyagawa ⁹⁴, R. Mizuhiki ⁸⁴, T. Mkrtchyan ³⁷, M. Mlinarevic ⁹⁶, T. Mlinarevic ⁹⁶, M. Mlynarikova ¹³⁵, L. Mlynarska ^{85a}, C. Mo ^{142a}, S. Mobius ²⁰, M.H. Mohamed Farook ¹¹⁴, S. Mohapatra ⁴¹, M.F. Mohd Soberi ⁵¹, S. Mohiuddin ¹²³, G. Mokgatitswane ^{34j}, R. Mole ²¹, L. Moleri ¹⁷², U. Molinatti ¹²⁸, L.G. Mollier ²⁰, B. Mondal ¹³³, S. Mondal ¹³⁵, K. Mönig ⁴⁷, E. Monnier ¹⁰², L. Monsonis Romero ¹⁶⁶, A. Montella ^{46a,46b}, M. Montella ¹²¹, F. Montereali ^{76a,76b}, F. Monticelli ⁹⁰, S. Monzani ^{68a,68c}, M.E.E. Moors ²⁵, A. Morancho Tarda ⁴², N. Morange ⁶⁵, M. Moreno Llácer ¹⁶⁶, C. Moreno Martinez ⁵⁵, J.M. Moreno Perez ^{23b}, P. Morettini ^{56b}, S. Morgenstern ^{62a}, M. Morii ⁶⁰, M. Morinaga ¹⁵⁷, F. Morodei ^{74a,74b}, P. Moschovakos ³⁷, B. Moser ⁵³, M. Mosidze ^{153b}, T. Moskalets ⁴⁴, P. Moskvitina ¹¹⁵, C.J. Mosomane ^{34b}, J. Moss ³², T. Motta Quirino ^{81d}, A. Moussa ^{36d}, Y. Moyal ^{172,k}, H. Moyano Gomez ¹³, E.J.W. Moyse ¹⁰³, T.G. Mroz ⁸⁶, S. Muanza ¹⁰², M. Mucha ²⁵, J. Mueller ¹³¹, D. Muller ¹⁴⁵, G.A. Mullier ¹⁶⁴, A.J. Mullin ³³, J.J. Mullin ⁵⁰, A.C. Mullins ⁴⁴, A.E. Mulski ⁶⁰, D.P. Mungo ¹⁵⁹, D. Munoz Perez ¹²³, F.J. Munoz Sanchez ¹⁰¹, W.J. Murray ^{170,136}, E. Musajan ⁶¹, M. Muškinja ⁹³, C. Mwewa ⁴⁷, A.J. Myers ⁸, G. Myers ¹⁰⁶, M. Myska ¹³⁴, B.P. Nachman ¹⁴⁷, K. Nagai ¹²⁸, K. Nagano ⁸², R. Nagasaka ¹⁵⁷, J.L. Nagle ^{30,ao}, E. Nagy ¹⁰², A.M. Nairz ³⁷, T. Nakagawa ⁸⁷, Y. Nakahama ⁸², K. Nakamura ⁸², K. Nakkalil ⁵, A. Nandi ^{62b}, H. Nanjo ¹²⁶, E.A. Narayanan ⁴⁴,

Y. Narukawa [ID157](#), L. Nasella [ID70a,70b](#), S. Nasri [ID118b](#), C. Nass [ID25](#), G. Navarro [ID23a](#), A. Nayaz [ID19](#),
 S. Nechaeva [ID24b,24a](#), F. Nechansky [ID133](#), L. Nedic [ID128](#), A. Negri [ID72a,72b](#), M. Negrini [ID24b](#),
 C. Nellist [ID116](#), C. Nelson [ID104](#), K. Nelson [ID106](#), S. Nemecek [ID133](#), M. Nessi [ID37,g](#), M.S. Neubauer [ID165](#),
 J. Newell [ID92](#), P.R. Newman [ID21](#), Y.W.Y. Ng [ID165](#), B. Ngair [ID118a](#), H.D.N. Nguyen [ID108](#),
 J.D. Nichols [ID122](#), R. Nicolaidou [ID137](#), J. Nielsen [ID138](#), M. Niemeyer [ID54](#), J. Niermann [ID37](#),
 N. Nikiforou [ID37](#), I. Nikolic-Audit [ID129](#), P. Nilsson [ID30](#), G. Ninio [ID155](#), A. Nisati [ID74a](#), R. Nisius [ID110](#),
 N. Nitika [ID172](#), E.K. Nkadimeng [ID34b](#), T. Nobe [ID157](#), D. Noll [ID147](#), T. Nommensen [ID151](#),
 M.B. Norfolk [ID143](#), B.J. Norman [ID35](#), L.C. Nosler [ID18a](#), M. Noury [ID36a](#), J. Novak [ID93](#), T. Novak [ID93](#),
 P. Novotny [ID172](#), R. Novotny [ID134](#), L. Nozka [ID124](#), K. Ntekas [ID37](#), D. Ntounis [ID147](#),
 N.M.J. Nunes De Moura Junior [ID81b](#), J. Ocariz [ID129](#), I. Ochoa [ID132a](#), A. Odella Rodriguez [ID13](#),
 S. Oerde [ID47](#), J.T. Offermann [ID39](#), A. Ogrodnik [ID86](#), A. Oh [ID101](#), C.C. Ohm [ID148](#), H. Oide [ID82](#),
 M.L. Ojeda [ID37](#), Y. Okumura [ID157](#), L.F. Oleiro Seabra [ID132a](#), I. Oleksiyuk [ID55](#), G. Oliveira Correa [ID13](#),
 D. Oliveira Damazio [ID30](#), J.L. Oliver [ID1](#), R. Omar [ID67](#), A.P. O'Neill [ID20](#), Y. Onoda [ID140](#),
 A. Onofre [ID132a,132e,e](#), P.U.E. Onyisi [ID11](#), M.J. Oreglia [ID39](#), D. Orestano [ID76a,76b](#), R. Orlandini [ID76a,76b](#),
 R.S. Orr [ID159](#), L.M. Osojnak [ID41](#), Y. Osumi [ID111](#), G. Otero y Garzón [ID31](#), H. Otono [ID88](#),
 M. Ouchrif [ID36d](#), F. Ould-Saada [ID127](#), T. Ovsiannikova [ID141](#), M. Owen [ID58](#), R.E. Owen [ID136](#),
 S.A. Oyeniran [ID114](#), V.E. Ozcan [ID22a](#), F. Ozturk [ID86](#), N. Ozturk [ID8](#), S. Ozturk [ID80](#), H.A. Pacey [ID128](#),
 K. Pachal [ID160a](#), A. Pacheco Pages [ID13](#), C. Padilla Aranda [ID13](#), G. Padovano [ID74a,74b](#),
 S. Pagan Griso [ID18a](#), L. Pagani [ID75a,75b](#), J. Pampel [ID25](#), D.K. Panchal [ID11](#), C.E. Pandini [ID59](#),
 J.G. Panduro Vazquez [ID136](#), H.D. Pandya [ID1](#), H. Pang [ID137](#), P. Pani [ID47](#), G. Panizzo [ID68a,68c](#),
 L. Panwar [ID129,w](#), L. Paolozzi [ID55](#), S. Parajuli [ID165](#), A. Paramonov [ID6](#), C. Paraskevopoulos [ID52](#),
 D. Paredes Hernandez [ID63b](#), S.R. Paredes Saenz [ID51](#), A. Pareti [ID72a,72b](#), K.R. Park [ID41](#), T.H. Park [ID110](#),
 F. Parodi [ID56b,56a](#), J.A. Parsons [ID41](#), U. Parzefall [ID53](#), B.A. Paschen [ID18a](#), B. Pascual Dias [ID40](#),
 L. Pascual Dominguez [ID99](#), E. Pasqualucci [ID74a](#), S. Passaggio [ID56b](#), F. Pastore [ID95](#), P. Patel [ID86](#),
 U.M. Patel [ID50](#), J.R. Pater [ID101](#), T. Pauly [ID37](#), A. Paunovic [ID16](#), F. Pauwels [ID135](#), C.I. Pazos [ID162](#),
 M. Pedersen [ID127](#), R. Pedro [ID132a](#), O. Penc [ID133](#), C.C. Penelaud [ID129](#), S. Peng [ID15](#), G.D. Penn [ID175](#),
 B.S. Peralva [ID81d](#), A.P. Pereira Peixoto [ID141](#), L. Pereira Sanchez [ID147](#), D.V. Perepelitsa [ID30,ao](#),
 G. Perera [ID103](#), E. Perez Codina [ID37](#), M. Perganti [ID10](#), H. Pernegger [ID37](#), S. Perrella [ID74a,74b](#),
 K. Peters [ID47](#), R.F.Y. Peters [ID101](#), B.A. Petersen [ID37](#), T.C. Petersen [ID42](#), E. Petit [ID102](#), V. Petousis [ID134](#),
 A.R. Petri [ID70a,70b](#), T. Petru [ID135](#), M. Pettee [ID18a](#), A. Petukhov [ID80](#), K. Petukhova [ID37](#), R. Pezoa [ID139g](#),
 L. Pezzotti [ID24b,24a](#), G. Pezzullo [ID175](#), L. Pfaffenbichler [ID37](#), A.J. Pflieger [ID78](#), T.M. Pham [ID173](#),
 T. Pham [ID105](#), P.W. Phillips [ID136](#), G. Piacquadio [ID149](#), E. Pianori [ID18a](#), F. Piazza [ID125](#), R. Piegai [ID31](#),
 D. Pietreanu [ID28b](#), A.D. Pilkington [ID101](#), M. Pinamonti [ID68a,68c](#), J.L. Pinfeld [ID2](#), G. Pinheiro Matos [ID41](#),
 B.C. Pinheiro Pereira [ID132a](#), J. Pinol Bel [ID13](#), A.E. Pinto Pinoargote [ID129](#), L. Pintucci [ID68a,68c](#),
 K.M. Piper [ID150](#), A. Pirttikoski [ID55](#), D.A. Pizzi [ID35](#), L. Pizzimento [ID63b](#), A. Plebani [ID33](#),
 M.-A. Pleier [ID30](#), V. Pleskot [ID135](#), E. Plotnikova [ID38](#), G. Poddar [ID94](#), R. Poettgen [ID98](#), L. Poggioli [ID129](#),
 S. Polacek [ID135](#), G. Polesello [ID72a](#), A. Poley [ID146](#), A. Polini [ID24b](#), C.S. Pollard [ID170](#), Z.B. Pollock [ID121](#),
 E. Pompa Pacchi [ID122](#), N.I. Pond [ID96](#), D. Ponomarenko [ID67](#), L. Pontecorvo [ID37](#), S. Popa [ID28a](#),
 G.A. Popeneciu [ID28d](#), A. Poreba [ID62a](#), D.M. Portillo Quintero [ID160a](#), S. Pospisil [ID134](#), M.A. Postill [ID143](#),
 P. Postolache [ID28c](#), K. Potamianos [ID170](#), P.A. Potepa [ID85a](#), I.N. Potrap [ID38](#), C.J. Potter [ID33](#), H. Potti [ID151](#),
 J. Poveda [ID166](#), M.E. Pozo Astigarraga [ID37](#), R. Pozzi [ID37](#), A. Prades Ibanez [ID75a,75b](#), S.R. Pradhan [ID143](#),
 J. Pretel [ID168](#), D. Price [ID101](#), M. Primavera [ID69a](#), L. Primomo [ID68a,68c](#), M.A. Principe Martin [ID99](#),
 R. Privara [ID124](#), T. Procter [ID85b](#), M.L. Proffitt [ID141](#), N. Proklova [ID130](#), K. Prokofiev [ID63c](#), G. Proto [ID110](#),
 J. Proudfoot [ID6](#), M. Przybycien [ID85a](#), W.W. Przygoda [ID85b](#), A. Psallidas [ID45](#), D. Pudzha [ID52](#), P. Puhl [ID57](#),
 H.I. Purnell [ID1](#), D. Pyatiizbyantseva [ID115](#), J. Qian [ID106](#), R. Qian [ID107](#), D. Qichen [ID128](#), Y. Qin [ID13](#),
 T. Qiu [ID51](#), A. Quadt [ID54](#), M. Queitsch-Maitland [ID101](#), G. Quetant [ID55](#), R.P. Quinn [ID167](#),
 D. Rafanoharana [ID110](#), J.L. Rainbolt [ID39](#), S. Rajagopalan [ID30](#), E. Ramakoti [ID38](#), L. Rambelli [ID56b,56a](#),

I.A. Ramirez-Berend ³⁵, K. Ran ^{106,112c}, S.D. Randles ⁹², D.S. Rankin ¹³⁰, N.P. Rapheeha ^{34j},
 H. Rasheed ^{28b}, A. Rastogi ^{18a}, S. Rave ¹⁰⁰, S. Ravera ^{56b,56a}, B. Ravina ³⁷, I. Ravinovich ¹⁷²,
 M. Raymond ³⁷, A.L. Read ¹²⁷, N.P. Readioff ¹⁴³, D.M. Rebuzzi ^{72a,72b}, A.S. Reed ⁵⁸,
 K. Reeves ²⁷, D. Reikher ³⁷, A. Rej ⁴⁸, C. Rembser ³⁷, H. Ren ⁶¹, M. Renda ^{28b}, F. Renner ⁴⁷,
 A.G. Rennie ⁵⁸, M. Repik ⁵⁵, A.L. Rescia ^{56b,56a}, S. Resconi ^{70a}, M. Ressegotti ^{56b},
 S. Rettie ¹¹⁶, W.F. Rettie ³⁵, M.M. Revering ³³, O.L. Rezanova ³⁸, P. Reznicek ¹³⁵, H. Riani ^{36d},
 N. Ribaric ⁵⁰, B. Ricci ^{68a,68c}, E. Ricci ^{77a,77b}, R. Richter ¹¹⁰, E. Richter-Was ^{85b}, M. Ridel ¹²⁹,
 S. Ridouani ^{36d}, P. Riedler ³⁷, E.M. Riefel ^{46a,46b}, J.O. Rieger ¹¹⁶, M. Rimoldi ^{34c},
 L. Rinaldi ^{24b,24a}, P. Rincke ^{164,54}, G. Ripellino ¹⁶⁴, I. Riu ¹³, J.C. Rivera Vergara ¹⁶⁸,
 F. Rizatdinova ¹²³, E. Rizvi ⁹⁴, B.R. Roberts ³⁹, S.S. Roberts ¹³⁸, D. Robinson ³³, A. Robson ⁵⁸,
 A. Rocchi ^{75a,75b}, C. Roda ^{73a,73b}, F.A. Rodriguez ¹¹⁷, S. Rodriguez Bosca ³⁷,
 Y. Rodriguez Garcia ^{23a}, A.M. Rodríguez Vera ¹¹⁷, S. Roe ³⁷, J.T. Roemer ³⁷, O. Røhne ¹²⁷,
 R.A. Rojas ³⁷, Z. Rokavec ⁹³, C.P.A. Roland ¹²⁹, A. Romaniouk ⁷⁸, E. Romano ^{72a,72b},
 M. Romano ^{24b}, N. Rompotis ⁹², L. Roos ¹²⁹, S. Rosati ^{74a}, L. Roscher ⁴⁷, B.J. Rosser ³⁹,
 E. Rossi ¹²⁸, E. Rossi ^{71a,71b}, L.P. Rossi ⁶⁰, L. Rossini ⁵³, R. Rosten ¹²¹, M. Rotaru ^{28b},
 R. Roth ³⁷, D. Rousseau ⁶⁵, D. Rousso ⁴⁷, S. Roy-Garand ¹⁵⁹, A. Rozanov ¹⁰²,
 Z.M.A. Rozario ⁵⁸, Y. Rozen ¹⁵⁴, A. Rubio Jimenez ¹⁶⁶, V.H. Ruelas Rivera ¹⁹, T.A. Ruggeri ¹,
 A. Ruggiero ¹²⁸, A. Ruiz-Martinez ¹⁶⁶, A. Rummler ³⁷, G.B. Rupnik Boero ³⁷,
 N.A. Rusakovich ³⁸, S. Ruscelli ⁴⁸, H.L. Russell ¹⁶⁸, G. Russo ¹³⁸, J.P. Rutherford ⁷,
 S. Rutherford Colmenares ¹¹⁹, M. Rybar ¹³⁵, P. Rybczynski ^{85a}, A. Ryzhov ⁴⁴,
 F. Safai Tehrani ^{74a}, S. Saha ¹, B. Sahoo ¹⁷², A. Saibel ¹⁶⁶, B.T. Saifuddin ¹²², M. Saimpert ¹³⁷,
 I. Sainz Saenz Diez ^{62a}, G.T. Saito ^{81c}, M. Saito ¹⁵⁷, T. Saito ¹⁵⁷, A. Sala ^{70a,70b}, O.T. Salin ⁶⁵,
 A. Salnikov ¹⁴⁷, J. Salt ¹⁶⁶, A. Salvador Salas ¹⁵⁵, F. Salvatore ¹⁵⁰, A. Salzburger ³⁷,
 D. Sammel ⁵³, E. Sampson ⁹¹, D. Sampsonidis ^{156,d}, D. Sampsonidou ¹²⁵, M.A.A. Samy ⁵⁸,
 J. Sánchez ¹⁶⁶, V. Sanchez Sebastian ¹⁶⁶, H. Sandaker ¹²⁷, C.O. Sander ⁴⁷, J.A. Sandesara ¹⁷³,
 M. Sandhoff ¹⁷⁴, C. Sandoval ^{23b}, L. Sanfilippo ^{62a}, D.P.C. Sankey ¹³⁶, T. Sano ⁸⁷,
 A. Sansar ^{22c}, A. Sansoni ⁵², M. Santana Queiroz ^{18b}, L. Santi ³⁷, C. Santoni ⁴⁰,
 H. Santos ^{132a,132b}, L. Santos Pereira Trigo ⁴⁷, E. Sanzani ^{24b,24a}, K.A. Saoucha ^{83b},
 J.G. Saraiva ^{132a,132d}, J. Sardain ⁷, S. Sarkar ⁵⁰, O. Sasaki ⁸², K. Sato ¹⁶¹, C. Sauer ³⁷,
 E. Sauvan ⁴, P. Savard ^{159,aj}, R. Sawada ¹⁵⁷, C. Sawyer ¹³⁶, L. Sawyer ⁹⁷, A.M. Sayed ²⁷,
 C. Sbarra ^{24b}, A. Sbrizzi ^{24b,24a}, R. Scaglioni ^{72a,72b}, T. Scanlon ⁹⁶, J. Schaarschmidt ¹⁴¹,
 U. Schäfer ¹⁰⁰, A.C. Schaffer ^{65,44}, D. Schaile ¹⁰⁹, R.D. Schamberger ¹⁴⁹, C. Scharf ¹⁹,
 M.M. Schefer ²⁰, D. Scheirich ¹³⁵, M. Schernau ^{139f}, C. Scheulen ⁵⁵, C. Schiavi ^{56b,56a},
 M. Schioppa ^{43b,43a}, S. Schlenker ³⁷, T. Schlomer ⁵⁴, J. Schmeing ¹⁷⁴, C.R. Schmidt ⁴⁹,
 E. Schmidt ¹¹⁰, M.A. Schmidt ¹⁷⁴, K. Schmieden ²⁵, C. Schmitt ¹⁰⁰, N. Schmitt ¹⁰⁰,
 S. Schmitt ⁴⁷, N.A. Schneider ¹⁰⁹, L. Schoeffel ¹³⁷, A. Schoening ^{62b}, P.G. Scholer ³⁵,
 E. Schopf ¹⁴⁵, M. Schott ²⁵, S. Schramm ⁵⁵, T. Schroer ⁵⁵, H-C. Schultz-Coulon ^{62a},
 M. Schumacher ⁵³, B.A. Schumm ¹³⁸, Ph. Schune ¹³⁷, H.R. Schwartz ⁷, A. Schwartzman ¹⁴⁷,
 T.A. Schwarz ¹⁰⁶, Ph. Schwemling ¹³⁷, R. Schwienhorst ¹⁰⁷, F.G. Sciacca ²⁰, A. Sciandra ³⁰,
 G. Sciolla ²⁷, S.A. Scoville ¹³¹, F. Scuri ^{73a}, C.D. Sebastiani ³⁷, K. Sedlaczek ¹¹⁷,
 A. Sehrawat ^{139b}, S.C. Seidel ¹¹⁴, B.D. Seidlitz ⁴¹, C. Seitz ⁴⁷, J.M. Seixas ^{81b},
 G. Sekhniadze ^{71a}, L. Selem ¹²⁹, N. Semprini-Cesari ^{24b,24a}, A. Semushin ¹⁷⁶,
 V. Senthilkumar ¹¹⁶, L. Serin ⁶⁵, M. Sessa ^{71a,71b}, H. Severini ¹²², F. Sforza ^{56b,56a}, A. Sfyrla ⁵⁵,
 Q. Sha ¹⁴, H. Shaddix ¹¹⁷, A.H. Shah ³³, R. Shaheen ¹⁴⁸, J.D. Shahinian ¹³⁰, M. Shamim ³⁷,
 L.Y. Shan ¹⁴, M. Shapiro ^{18a}, A. Sharma ³⁷, A.S. Sharma ¹⁶⁷, P. Sharma ³⁰, K. Shaw ¹⁵⁰,
 S.M. Shaw ¹⁰¹, D. Shemyakin ¹⁷², Q. Shen ¹⁴, D.J. Sheppard ¹⁴⁶, P. Sherwood ⁹⁶, L. Shi ^{112b},
 X. Shi ¹⁴, S. Shimizu ⁸², S. Shirabe ⁸⁸, M. Shiyakova ^{38,z}, M.J. Shochet ³⁹, D.R. Shope ¹²⁷,

B. Shrestha ¹²², S. Shrestha ^{121,aq}, I. Shreyber ³⁸, M.J. Shroff ¹⁰⁴, P. Sicho ¹³³, A.M. Sickles ¹⁶⁵,
 E. Sideras Haddad ^{34j}, A.C. Sidley ¹¹⁶, A. Sidoti ^{24b}, F. Siegert ⁴⁹, Dj. Sijacki ¹⁶, F. Sili ⁶¹,
 J.M. Silva ⁵¹, I. Silva Ferreira ^{81b}, M.V. Silva Oliveira ³⁰, S.B. Silverstein ^{46a}, S. Simion ⁶⁵,
 R. Simoniello ³⁷, E.L. Simpson ¹⁰¹, H. Simpson ¹⁵⁰, L.R. Simpson ⁶, S. Simsek ⁸⁰,
 S. Sindhu ⁵⁴, S.N. Singh ²⁷, S. Singh ³⁰, S. Sinha ⁴⁷, S. Sinha ¹⁰¹, M. Sioli ^{24b,24a},
 K. Sioulas ⁹, I. Siral ³⁷, E. Sitnikova ⁴⁷, J. Sjölin ^{46a,46b}, A. Skaf ⁵⁴, E. Skorda ²¹,
 P. Skubic ¹²², M. Slawinska ⁸⁶, I. Slazyk ¹⁷, I. Sliusar ¹²⁷, V. Smakhtin ¹⁷², B.H. Smart ¹³⁶,
 S.Yu. Smirnov ^{139b}, Y. Smirnov ^{34c}, O. Smirnova ⁹⁸, A.C. Smith ⁴¹, J.L. Smith ¹⁰¹,
 M.B. Smith ³⁵, R. Smith ¹⁴⁷, H. Smitmanns ¹⁰⁰, M. Smizanska ⁹¹, K. Smolek ¹³⁴,
 P. Smolyanskiy ¹³⁴, A.A. Snesarev ³⁸, H.L. Snoek ¹¹⁶, R.M. Snyder ⁵⁰, S. Snyder ³⁰,
 R. Sobie ^{168,ab}, A. Soffer ¹⁵⁵, C.A. Solans Sanchez ³⁷, E.Yu. Soldatov ³⁸, U. Soldevila ¹⁶⁶,
 A.A. Solodkov ^{34j}, S. Solomon ²⁷, A. Soloshenko ³⁸, O.V. Solovyanov ⁴⁰, P. Sommer ⁴⁹,
 A. Sopczak ¹³⁴, A.L. Soppio ⁵¹, F. Sopkova ^{29b}, J.D. Sorenson ¹¹⁴, I.R. Sotarriva Alvarez ¹⁴⁰,
 V. Sothilingam ^{62a}, O.J. Soto Sandoval ^{139c,139b}, S. Sottocornola ⁶⁷, R. Soualah ^{83a}, D. South ⁴⁷,
 N. Soybelman ¹⁷², S. Spagnolo ^{69a,69b}, A.S. Spellman ¹²⁵, D. Sperlich ⁵³, B. Spisso ^{71a,71b},
 L. Splendori ¹⁰², M. Spousta ¹³⁵, E.J. Staats ³⁵, R. Stamen ^{62a}, E. Stanecka ⁸⁶,
 W. Stanek-Maslouska ⁴⁷, M.V. Stange ⁴⁹, B. Stanislaus ^{18a}, M.M. Stanitzki ⁴⁷, G.H. Stark ¹³⁸,
 J. Stark ⁸⁹, P. Staroba ¹³³, P. Starovoitov ^{83b}, R. Staszewski ⁸⁶, C. Stauch ¹⁰⁹,
 G. Stavropoulos ⁴⁵, A. Stefl ³⁷, A. Stein ¹⁰⁰, P. Steinberg ³⁰, B. Stelzer ^{146,160a}, H.J. Stelzer ¹³¹,
 O. Stelzer ^{160a}, H. Stenzel ⁵⁷, T.J. Stevenson ¹⁵⁰, G.A. Stewart ⁴⁷, G. Stoicea ^{28b},
 M. Stolarski ^{132a}, S. Stonjek ¹¹⁰, A. Straessner ⁴⁹, J. Strandberg ¹⁴⁸, S. Strandberg ^{46a,46b},
 M. Stratmann ¹⁷⁴, M. Strauss ¹²², T. Strebler ¹⁰², P. Strizenec ^{29b}, R. Ströhmer ¹⁶⁹,
 D.M. Strom ¹²⁵, R. Stroynowski ⁴⁴, A. Strubig ^{46a,46b}, S.A. Stucci ³⁰, B. Stugu ¹⁷, J. Stupak ¹²²,
 N.A. Styles ⁴⁷, D. Su ¹⁴⁷, S. Su ⁶¹, X. Su ⁶¹, D. Suchy ^{29a}, A.D. Sudhakar Ponnuru ⁵⁴,
 L. Sudit ¹⁷², Y. Sue ⁸², K. Sugizaki ¹³⁰, D.M.S. Sultan ¹²⁸, L. Sultanaliyeva ²⁵, S. Sultansoy ^{3b},
 S. Sun ¹⁷³, W. Sun ¹⁴, S. Sundar Raman ¹⁶⁷, N. Sur ⁹⁸, J.P. Surdutovich ¹²¹, N. Suri Jr ¹⁷⁵,
 M.R. Sutton ¹⁵⁰, M. Svatos ¹³³, P.N. Swallow ³³, S.N. Swatman ³⁷, M. Swiatlowski ^{160a},
 A. Swoboda ³⁷, I. Sykora ^{29a}, M. Sykora ¹³⁵, T. Sykora ¹³⁵, D. Ta ¹⁰⁰, K. Tackmann ^{47,y},
 A. Taffard ¹⁶³, R. Tafirout ^{160a}, Y. Takubo ⁸², M. Talby ¹⁰², N.M. Tamir ¹⁵⁵, A. Tanaka ¹⁵⁷,
 J. Tanaka ¹⁵⁷, R. Tanaka ⁶⁵, M. Tanasini ¹⁴⁹, Z. Tao ¹⁶⁷, S. Tapia Araya ^{139g}, S. Tapprogge ¹⁰⁰,
 A. Tarek Abouelfadl Mohamed ³⁷, S. Tarem ¹⁵⁴, K. Tariq ¹⁴, G. Tarna ³⁷, G.F. Tartarelli ^{70a},
 M.J. Tartarin ^{142b}, P. Tas ¹³⁵, M. Tasevsky ¹³³, E. Tassi ^{43b,43a}, A.C. Tate ¹⁶⁵, Y. Tayalati ^{36e,aa},
 G.N. Taylor ¹⁰⁵, W. Taylor ^{160b}, R.J. Taylor Vara ¹⁶⁶, A.S. Tegetmeier ⁸⁹, P. Teixeira-Dias ⁹⁵,
 J.J. Teoh ¹⁵⁹, K. Terashi ¹⁵⁷, J. Terron ⁹⁹, S. Terzo ¹³, M. Testa ⁵², R.J. Teuscher ^{159,ab},
 A. Thaler ⁷⁸, T. Theveneaux-Pelzer ¹⁰², J.P. Thomas ²¹, E.A. Thompson ^{18a}, P.D. Thompson ²¹,
 E. Thomson ¹³⁰, R.E. Thornberry ³⁰, T.M. Thory-Rao ²¹, C. Tian ⁶¹, Y. Tian ⁵⁵,
 V. Tikhomirov ⁸⁰, Yu.A. Tikhonov ³⁸, D. Timoshyn ¹³⁵, E.X.L. Ting ¹, P. Tipton ¹⁷⁵,
 A. Tishelman-Charny ³⁰, K. Todome ¹⁴⁰, S. Todorova-Nova ¹³⁵, L. Toffolin ^{68a,68c}, M. Togawa ⁸²,
 J. Tojo ⁸⁸, S. Tokár ^{29a}, O. Toldaiev ⁶⁷, G. Tolkachev ¹⁰², M. Tomoto ⁸², L. Tompkins ¹⁴⁷,
 E. Torrence ¹²⁵, H. Torres ⁸⁹, D.I. Torres Arza ^{139g}, E. Torres Reoyo ¹⁶⁶, E. Torró Pastor ¹⁶⁶,
 M. Toscani ³¹, C. Toscirci ³⁹, M. Tost ¹¹, D.R. Tovey ¹⁴³, T. Trefzger ¹⁶⁹, P.M. Tricarico ¹³,
 A. Tricoli ³⁰, I.M. Trigger ^{160a}, S. Trincaz-Duvoid ¹²⁹, D.A. Trischuk ¹⁶⁸, A. Tropina ³⁸,
 D. Truncali ^{75a,75b}, L. Truong ^{34c}, M. Trzebinski ⁸⁶, A. Trzupek ⁸⁶, F. Tsai ¹⁴⁹, A. Tsiamis ¹⁵⁶,
 P.V. Tsiarehsha ³⁸, S. Tsigaridas ^{160a}, A. Tsirigotis ^{156,t}, V. Tsiskaridze ^{153a}, E.G. Tskhadadze ^{153a},
 H.F. Tsoi ¹³⁰, Y. Tsujikawa ⁸⁷, V. Tsulaia ^{18a}, K. Tsuru ¹²⁰, D. Tsybychev ¹⁴⁹, Y. Tu ^{63b},
 A. Tudorache ^{28b}, V. Tudorache ^{28b}, S.B. Tuncay ¹²⁸, S. Turchikhin ^{56b,56a}, I. Turk Cakir ^{3a},
 R. Turra ^{70a}, T. Turtuvshin ^{38,ac}, P.M. Tuts ⁴¹, Y. Uematsu ⁸², F. Ukegawa ¹⁶¹,

P.A. Ulloa Poblete [ID139c,139b](#), G. Unal [ID37](#), A. Undrus [ID30](#), J. Urban [ID29b](#), P. Urrejola [ID139e](#), G. Usai [ID8](#),
 R. Ushioda [ID158](#), M. Usman [ID108](#), F. Ustuner [ID51](#), Z. Uysal [ID80](#), V. Vacek [ID134](#), B. Vachon [ID104](#),
 T. Vafeiadis [ID37](#), A. Vaitkus [ID96](#), C. Valderanis [ID109](#), E. Valdes Santurio [ID46a,46b](#), M. Valente [ID37](#),
 S. Valentinetti [ID24b,24a](#), A. Valero [ID166](#), E. Valiente Moreno [ID166](#), A. Vallier [ID89](#), J.A. Valls Ferrer [ID166](#),
 D.R. Van Arneman [ID116](#), R. Van Den Broucke [ID129](#), A. Van Der Graaf [ID48](#), H.Z. Van Der Schyf [ID34j](#),
 P. Van Gemmeren [ID6](#), M. Van Rijnbach [ID37](#), S. Van Stroud [ID96](#), I. Van Vulpen [ID116](#), P. Vana [ID135](#),
 M. Vanadia [ID75a,75b](#), U.M. Vande Voorde [ID148](#), W. Vandelli [ID37](#), E.R. Vandewall [ID147](#), D. Vannicola [ID155](#),
 R. Vari [ID74a](#), M. Varma [ID175](#), E.W. Varnes [ID7](#), C. Varni [ID85a](#), D. Varouchas [ID65](#), L. Varriale [ID166](#),
 K.E. Varvell [ID151](#), M.E. Vasile [ID28b](#), A. Vasileiadou⁹, L. Vaslin⁸², M.D. Vassilev [ID147](#), A. Vasyukov [ID38](#),
 L.M. Vaughan [ID123](#), R. Vavricka¹³⁵, T. Vazquez Schroeder [ID13](#), J. Veatch [ID32](#), V. Vecchio [ID101](#),
 M.J. Veen [ID103](#), I. Veliscek [ID30](#), I. Velkovska [ID93](#), L.M. Veloce [ID159](#), F. Veloso [ID132a,132c](#),
 A.G. Veltman [ID51](#), S.H. Venetianer [ID162](#), S. Veneziano [ID74a](#), A. Ventura [ID69a,69b](#), A. Verbitskiy [ID110](#),
 M. Verducci [ID73a,73b](#), C. Vergis [ID94](#), M. Verissimo De Araujo [ID81b](#), W. Verkerke [ID116](#),
 J.C. Vermeulen [ID116](#), C. Vernieri [ID147](#), M. Vessella [ID163](#), M.C. Vetterli [ID146,aj](#), A. Vgenopoulos [ID100](#),
 N. Viaux Maira [ID139g,af](#), L. Vicenik [ID134](#), T. Vickey [ID143](#), O.E. Vickey Boeriu [ID143](#),
 G.H.A. Viehhauser [ID128](#), L. Vigani [ID62b](#), M. Vigl [ID110](#), M. Villa [ID24b,24a](#), M. Villaplana Perez [ID166](#),
 E.M. Villhauer³⁹, E. Vilucchi [ID52](#), M. Vincent [ID166](#), M.G. Vincter [ID35](#), A. Visibile [ID116](#), A. Visive [ID116](#),
 C. Vittori [ID162](#), I. Vivarelli [ID24b,24a](#), M.I. Vivas Albornoz [ID47](#), E. Voevodina [ID110](#), F. Vogel [ID109](#),
 J.C. Voigt [ID49](#), P. Vokac [ID134](#), Yu. Volkotrub [ID85b](#), L. Vomberg [ID25](#), E. Von Toerne [ID25](#),
 B. Vormwald [ID37](#), K. Vorobev [ID50](#), M. Vos [ID166](#), K. Voss [ID145](#), M. Vozak [ID37](#), L. Vozdecky [ID122](#),
 N. Vranjes [ID16](#), M. Vranjes Milosavljevic [ID16](#), M. Vreeswijk [ID116](#), N.K. Vu [ID112a](#), R. Vuillermet [ID37](#),
 O. Vujinovic [ID100](#), I. Vukotic [ID39](#), I.K. Vyas [ID35](#), J.F. Wack [ID33](#), A. Wada [ID111](#), S. Wada [ID161](#),
 C. Wagner¹⁴⁷, J.M. Wagner [ID18a](#), W. Wagner [ID174](#), S. Wahdan [ID174](#), H. Wahlberg [ID90](#), C.H. Waits [ID122](#),
 J. Walder [ID136](#), R. Walker [ID109](#), K. Walkingshaw Pass [ID58](#), W. Walkowiak [ID145](#), A. Wall [ID130](#),
 E.J. Wallin [ID98](#), T. Wamorkar [ID147](#), K. Wandall-Christensen [ID166](#), A. Wang [ID61](#), A.Z. Wang [ID138](#),
 C. Wang [ID47](#), C. Wang [ID11](#), H. Wang [ID18a](#), J. Wang [ID63c](#), P. Wang [ID101](#), P. Wang [ID96](#), R. Wang [ID60](#),
 R. Wang [ID106](#), R. Wang [ID6](#), S.M. Wang [ID152](#), S. Wang [ID14](#), T. Wang [ID115](#), T. Wang [ID61](#), W.T. Wang [ID128](#),
 X. Wang [ID165](#), X. Wang [ID142a](#), X. Wang [ID47](#), Y. Wang [ID149](#), Y. Wang [ID114](#), Z. Wang [ID106](#), Z. Wang [ID14](#),
 Z. Wang^{63b}, C. Wanotayaroj [ID82](#), A. Warburton [ID104](#), A.L. Warnerbring [ID145](#), S. Waterhouse [ID96](#),
 A.T. Watson [ID21](#), H. Watson [ID51](#), M.F. Watson [ID21](#), E. Watton [ID37](#), G. Watts [ID141](#), B.M. Waugh [ID96](#),
 J.M. Webb [ID53](#), C. Weber [ID30](#), M.S. Weber [ID20](#), C. Wei [ID61](#), Y. Wei [ID53](#), A.R. Weidberg [ID128](#),
 E.J. Weik [ID119](#), J. Weingarten [ID48](#), C. Weiser [ID53](#), C.J. Wells [ID47](#), T. Wenaus [ID30](#), T. Wengler [ID37](#),
 N.S. Wenke¹¹⁰, N. Wermes [ID25](#), M. Wessels [ID62a](#), A.M. Wharton [ID91](#), A.S. White [ID37](#), A. White [ID8](#),
 M.J. White [ID1](#), D. Whiteson [ID163](#), L. Wickremasinghe [ID126](#), W. Wiedenmann [ID173](#), M. Wielers [ID136](#),
 R. Wierda [ID148](#), C. Wiglesworth [ID42](#), H.G. Wilkens [ID37](#), J.J.H. Wilkinson [ID33](#), S. Williams [ID33](#),
 S. Willocq [ID103](#), D.J. Wilson [ID101](#), P.J. Windischhofer [ID39](#), F.I. Winkel [ID31](#), F. Winklmeier [ID125](#),
 B.T. Winter [ID53](#), M. Wittgen¹⁴⁷, M. Wobisch [ID97](#), T. Wojtkowski⁵⁹, Z. Wolffs [ID116](#), J. Wollrath³⁷,
 M.W. Wolter [ID86](#), H. Wolters [ID132a,132c](#), M.C. Wong¹³⁸, E.L. Woodward [ID41](#), S.D. Worm [ID47](#),
 B.K. Wosiek [ID86](#), K.A. Wozniak [ID55](#), K.W. Woźniak [ID86](#), S. Wozniowski [ID54](#), K. Wraight [ID58](#),
 C. Wu [ID159](#), C. Wu [ID21](#), J. Wu [ID157](#), M. Wu [ID112b](#), M. Wu [ID115](#), S.L. Wu [ID173](#), S. Wu [ID14,an](#), X. Wu [ID61](#),
 Y.Q. Wu [ID159](#), Y. Wu [ID61](#), Z. Wu [ID102](#), Z. Wu [ID112a](#), J. Wuerzinger [ID110](#), T.R. Wyatt [ID101](#),
 B.M. Wynne [ID51](#), S. Xella [ID42](#), L. Xia [ID112a](#), M. Xie [ID61](#), A. Xiong [ID125](#), I. Xiotidis [ID37](#), D. Xu [ID14](#),
 H. Xu [ID61](#), L. Xu [ID61](#), R. Xu [ID130](#), T. Xu [ID106](#), W. Xu^{112a}, Y. Xu [ID141](#), Z. Xu [ID51](#), R. Xue [ID131](#),
 B. Yabsley [ID151](#), S. Yacoob [ID11](#), Y. Yamaguchi [ID82](#), E. Yamashita [ID157](#), H. Yamauchi [ID161](#),
 T. Yamazaki [ID18a](#), Y. Yamazaki [ID84](#), S. Yan [ID58](#), Z. Yan [ID103](#), C. Yang [ID18a](#), H.J. Yang [ID142a](#),
 H.T. Yang [ID61](#), S. Yang [ID61](#), X. Yang [ID37](#), X. Yang [ID14](#), Y. Yang [ID157](#), Y. Yang⁶¹, W-M. Yao [ID18a](#),
 C.L. Yardley [ID150](#), J. Ye [ID14](#), S. Ye [ID30](#), X. Ye [ID61](#), I. Yeletsikh [ID38](#), B. Yeo [ID18b](#), M.R. Yexley [ID96](#),

T.P. Yildirim , K. Yorita , C.J.S. Young , C. Young , I.N.L. Young , N.D. Young , Y. Yu , J. Yuan , M. Yuan , R. Yuan , L. Yue , M. Zaazoua , B. Zabinski , I. Zahir , Q.U.A. Zahoor , A. Zaio , Z.K. Zak , T. Zakareishvili , S. Zambito , J. Zang , R. Zanzottera , O. Zaplatilek , E. Zaya , C. Zeitnitz , H. Zeng , D.T. Zenger Jr , T. Ženiš , S. Zenz , D. Zerwas , B. Zhang , D.F. Zhang , G. Zhang , J. Zhang , J. Zhang , L. Zhang , L. Zhang , P. Zhang , R. Zhang , S. Zhang , Y. Zhang , Y. Zhang , Y. Zhang , Y. Zhang , Z. Zhang , Z. Zhang , Z. Zhang , H. Zhao , T. Zhao , Y. Zhao , Z. Zhao , Z. Zhao , A. Zhemchugov , J. Zheng , K. Zheng , L. Zheng , X. Zheng , Z. Zheng , D. Zhong , B. Zhou , B. Zhou , N. Zhou , Y. Zhou , Y. Zhou , Y. Zhou , Z. Zhou , J. Zhu , X. Zhu , Y. Zhu , X. Zhuang , K. Zhukov , P. Ziakas , N.I. Zimine , J. Zinsser , M. Ziolkowski , L. Živković , A. Zoccoli , K. Zoch , A. Zografos , T.G. Zorbas , L. Zwalinski .

¹Department of Physics, University of Adelaide, Adelaide; Australia.

²Department of Physics, University of Alberta, Edmonton AB; Canada.

^{3(a)}Department of Physics, Ankara University, Ankara; ^(b)Division of Physics, TOBB University of Economics and Technology, Ankara; Türkiye.

⁴LAPP, Université Savoie Mont Blanc, CNRS/IN2P3, Annecy; France.

⁵APC, Université Paris Cité, CNRS/IN2P3, Paris; France.

⁶High Energy Physics Division, Argonne National Laboratory, Argonne IL; United States of America.

⁷Department of Physics, University of Arizona, Tucson AZ; United States of America.

⁸Department of Physics, University of Texas at Arlington, Arlington TX; United States of America.

⁹Physics Department, National and Kapodistrian University of Athens, Athens; Greece.

¹⁰Physics Department, National Technical University of Athens, Zografou; Greece.

¹¹Department of Physics, University of Texas at Austin, Austin TX; United States of America.

¹²Institute of Physics, Azerbaijan Academy of Sciences, Baku; Azerbaijan.

¹³Institut de Física d'Altes Energies (IFAE), Barcelona Institute of Science and Technology, Barcelona; Spain.

¹⁴Institute of High Energy Physics, Chinese Academy of Sciences, Beijing; China.

¹⁵Physics Department, Tsinghua University, Beijing; China.

¹⁶Institute of Physics, University of Belgrade, Belgrade; Serbia.

¹⁷Department for Physics and Technology, University of Bergen, Bergen; Norway.

^{18(a)}Physics Division, Lawrence Berkeley National Laboratory, Berkeley CA; ^(b)University of California, Berkeley CA; United States of America.

¹⁹Institut für Physik, Humboldt Universität zu Berlin, Berlin; Germany.

²⁰Albert Einstein Center for Fundamental Physics and Laboratory for High Energy Physics, University of Bern, Bern; Switzerland.

²¹School of Physics and Astronomy, University of Birmingham, Birmingham; United Kingdom.

^{22(a)}Department of Physics, Bogazici University, Istanbul; ^(b)Department of Physics Engineering, Gaziantep University, Gaziantep; ^(c)Department of Physics, Istanbul University, Istanbul; Türkiye.

^{23(a)}Facultad de Ciencias y Centro de Investigaciones, Universidad Antonio Nariño,

Bogotá; ^(b)Departamento de Física, Universidad Nacional de Colombia, Bogotá; Colombia.

^{24(a)}Dipartimento di Fisica e Astronomia A. Righi, Università di Bologna, Bologna; ^(b)INFN Sezione di Bologna; Italy.

²⁵Physikalisches Institut, Universität Bonn, Bonn; Germany.

²⁶Department of Physics, Boston University, Boston MA; United States of America.

- ²⁷Department of Physics, Brandeis University, Waltham MA; United States of America.
- ²⁸(^a) Transilvania University of Brasov, Brasov; (^b) Horia Hulubei National Institute of Physics and Nuclear Engineering, Bucharest; (^c) Department of Physics, Alexandru Ioan Cuza University of Iasi, Iasi; (^d) National Institute for Research and Development of Isotopic and Molecular Technologies, Physics Department, Cluj-Napoca; (^e) National University of Science and Technology Politehnica, Bucharest; (^f) West University in Timisoara, Timisoara; (^g) Faculty of Physics, University of Bucharest, Bucharest; Romania.
- ²⁹(^a) Faculty of Mathematics, Physics and Informatics, Comenius University, Bratislava; (^b) Department of Subnuclear Physics, Institute of Experimental Physics of the Slovak Academy of Sciences, Kosice; Slovak Republic.
- ³⁰Physics Department, Brookhaven National Laboratory, Upton NY; United States of America.
- ³¹Universidad de Buenos Aires, Facultad de Ciencias Exactas y Naturales, Departamento de Física, y CONICET, Instituto de Física de Buenos Aires (IFIBA), Buenos Aires; Argentina.
- ³²California State University, CA; United States of America.
- ³³Cavendish Laboratory, University of Cambridge, Cambridge; United Kingdom.
- ³⁴(^a) Department of Physics, University of Cape Town, Cape Town; (^b) iThemba Labs, Western Cape; (^c) Department of Mechanical Engineering Science, University of Johannesburg, Johannesburg; (^d) National Institute of Physics, University of the Philippines Diliman (Philippines); (^e) Department of Physics, Stellenbosch University, Matieland; (^f) University of KwaZulu-Natal, School of Agriculture and Science, Mathematics, Westville; (^g) University of South Africa, Department of Physics, Pretoria; (^h) University of Pretoria, Department of Mechanical and Aeronautical Engineering, Pretoria; (ⁱ) University of Zululand, KwaDlangezwa; (^j) School of Physics, University of the Witwatersrand, Johannesburg; South Africa.
- ³⁵Department of Physics, Carleton University, Ottawa ON; Canada.
- ³⁶(^a) Faculté des Sciences Ain Chock, Université Hassan II de Casablanca; (^b) Faculté des Sciences, Université Ibn-Tofail, Kénitra; (^c) Faculté des Sciences Semailia, Université Cadi Ayyad, LPHEA-Marrakech; (^d) LPMR, Faculté des Sciences, Université Mohamed Premier, Oujda; (^e) Faculté des sciences, Université Mohammed V, Rabat; (^f) Institute of Applied Physics, Mohammed VI Polytechnic University, Ben Guerir; Morocco.
- ³⁷CERN, Geneva; Switzerland.
- ³⁸Affiliated with an international laboratory covered by a cooperation agreement with CERN.
- ³⁹Enrico Fermi Institute, University of Chicago, Chicago IL; United States of America.
- ⁴⁰LPC, Université Clermont Auvergne, CNRS/IN2P3, Clermont-Ferrand; France.
- ⁴¹Nevis Laboratory, Columbia University, Irvington NY; United States of America.
- ⁴²Niels Bohr Institute, University of Copenhagen, Copenhagen; Denmark.
- ⁴³(^a) Dipartimento di Fisica, Università della Calabria, Rende; (^b) INFN Gruppo Collegato di Cosenza, Laboratori Nazionali di Frascati; Italy.
- ⁴⁴Physics Department, Southern Methodist University, Dallas TX; United States of America.
- ⁴⁵National Centre for Scientific Research "Demokritos", Agia Paraskevi; Greece.
- ⁴⁶(^a) Department of Physics, Stockholm University; (^b) Oskar Klein Centre, Stockholm; Sweden.
- ⁴⁷Deutsches Elektronen-Synchrotron DESY, Hamburg and Zeuthen; Germany.
- ⁴⁸Fakultät Physik, Technische Universität Dortmund, Dortmund; Germany.
- ⁴⁹Institut für Kern- und Teilchenphysik, Technische Universität Dresden, Dresden; Germany.
- ⁵⁰Department of Physics, Duke University, Durham NC; United States of America.
- ⁵¹SUPA - School of Physics and Astronomy, University of Edinburgh, Edinburgh; United Kingdom.
- ⁵²INFN e Laboratori Nazionali di Frascati, Frascati; Italy.
- ⁵³Physikalisches Institut, Albert-Ludwigs-Universität Freiburg, Freiburg; Germany.
- ⁵⁴II. Physikalisches Institut, Georg-August-Universität Göttingen, Göttingen; Germany.

- ⁵⁵Département de Physique Nucléaire et Corpusculaire, Université de Genève, Genève; Switzerland.
- ⁵⁶(^a) Dipartimento di Fisica, Università di Genova, Genova; (^b) INFN Sezione di Genova; Italy.
- ⁵⁷II. Physikalisches Institut, Justus-Liebig-Universität Giessen, Giessen; Germany.
- ⁵⁸SUPA - School of Physics and Astronomy, University of Glasgow, Glasgow; United Kingdom.
- ⁵⁹LPSC, Université Grenoble Alpes, CNRS/IN2P3, Grenoble INP, Grenoble; France.
- ⁶⁰Laboratory for Particle Physics and Cosmology, Harvard University, Cambridge MA; United States of America.
- ⁶¹Department of Modern Physics and State Key Laboratory of Particle Detection and Electronics, University of Science and Technology of China, Hefei; China.
- ⁶²(^a) Kirchoff-Institut für Physik, Ruprecht-Karls-Universität Heidelberg, Heidelberg; (^b) Physikalisches Institut, Ruprecht-Karls-Universität Heidelberg, Heidelberg; Germany.
- ⁶³(^a) Department of Physics, Chinese University of Hong Kong, Shatin, N.T., Hong Kong; (^b) Department of Physics, University of Hong Kong, Hong Kong; (^c) Department of Physics and Institute for Advanced Study, Hong Kong University of Science and Technology, Clear Water Bay, Kowloon, Hong Kong; China.
- ⁶⁴Department of Physics, National Tsing Hua University, Hsinchu; Taiwan.
- ⁶⁵IJCLab, Université Paris-Saclay, CNRS/IN2P3, 91405, Orsay; France.
- ⁶⁶Centro Nacional de Microelectrónica (IMB-CNM-CSIC), Barcelona; Spain.
- ⁶⁷Department of Physics, Indiana University, Bloomington IN; United States of America.
- ⁶⁸(^a) INFN Gruppo Collegato di Udine, Sezione di Trieste, Udine; (^b) ICTP, Trieste; (^c) Dipartimento Politecnico di Ingegneria e Architettura, Università di Udine, Udine; Italy.
- ⁶⁹(^a) INFN Sezione di Lecce; (^b) Dipartimento di Matematica e Fisica, Università del Salento, Lecce; Italy.
- ⁷⁰(^a) INFN Sezione di Milano; (^b) Dipartimento di Fisica, Università di Milano, Milano; Italy.
- ⁷¹(^a) INFN Sezione di Napoli; (^b) Dipartimento di Fisica, Università di Napoli, Napoli; Italy.
- ⁷²(^a) INFN Sezione di Pavia; (^b) Dipartimento di Fisica, Università di Pavia, Pavia; Italy.
- ⁷³(^a) INFN Sezione di Pisa; (^b) Dipartimento di Fisica E. Fermi, Università di Pisa, Pisa; Italy.
- ⁷⁴(^a) INFN Sezione di Roma; (^b) Dipartimento di Fisica, Sapienza Università di Roma, Roma; Italy.
- ⁷⁵(^a) INFN Sezione di Roma Tor Vergata; (^b) Dipartimento di Fisica, Università di Roma Tor Vergata, Roma; Italy.
- ⁷⁶(^a) INFN Sezione di Roma Tre; (^b) Dipartimento di Matematica e Fisica, Università Roma Tre, Roma; Italy.
- ⁷⁷(^a) INFN-TIFPA; (^b) Università degli Studi di Trento, Trento; Italy.
- ⁷⁸Universität Innsbruck, Department of Astro and Particle Physics, Innsbruck; Austria.
- ⁷⁹Department of Physics and Astronomy, Iowa State University, Ames IA; United States of America.
- ⁸⁰Istinye University, Sariyer, Istanbul; Türkiye.
- ⁸¹(^a) Departamento de Engenharia Elétrica, Universidade Federal de Juiz de Fora (UFJF), Juiz de Fora; (^b) Universidade Federal do Rio De Janeiro COPPE/EE/IF, Rio de Janeiro; (^c) Instituto de Física, Universidade de São Paulo, São Paulo; (^d) Rio de Janeiro State University, Rio de Janeiro; (^e) Federal University of Bahia, Bahia; Brazil.
- ⁸²KEK, High Energy Accelerator Research Organization, Tsukuba; Japan.
- ⁸³(^a) Khalifa University of Science and Technology, Abu Dhabi; (^b) University of Sharjah, Sharjah; United Arab Emirates.
- ⁸⁴Graduate School of Science, Kobe University, Kobe; Japan.
- ⁸⁵(^a) AGH University of Krakow, Faculty of Physics and Applied Computer Science, Krakow; (^b) Marian Smoluchowski Institute of Physics, Jagiellonian University, Krakow; Poland.
- ⁸⁶Institute of Nuclear Physics Polish Academy of Sciences, Krakow; Poland.
- ⁸⁷Faculty of Science, Kyoto University, Kyoto; Japan.
- ⁸⁸Research Center for Advanced Particle Physics and Department of Physics, Kyushu University, Fukuoka ;

Japan.

⁸⁹L2IT, Université de Toulouse, CNRS/IN2P3, UPS, Toulouse; France.

⁹⁰Instituto de Física La Plata, Universidad Nacional de La Plata and CONICET, La Plata; Argentina.

⁹¹Physics Department, Lancaster University, Lancaster; United Kingdom.

⁹²Oliver Lodge Laboratory, University of Liverpool, Liverpool; United Kingdom.

⁹³Department of Experimental Particle Physics, Jožef Stefan Institute and Department of Physics, University of Ljubljana, Ljubljana; Slovenia.

⁹⁴Department of Physics and Astronomy, Queen Mary University of London, London; United Kingdom.

⁹⁵Department of Physics, Royal Holloway University of London, Egham; United Kingdom.

⁹⁶Department of Physics and Astronomy, University College London, London; United Kingdom.

⁹⁷Louisiana Tech University, Ruston LA; United States of America.

⁹⁸Fysiska institutionen, Lunds universitet, Lund; Sweden.

⁹⁹Departamento de Física Teórica C-15 and CIAFF, Universidad Autónoma de Madrid, Madrid; Spain.

¹⁰⁰Institut für Physik, Universität Mainz, Mainz; Germany.

¹⁰¹School of Physics and Astronomy, University of Manchester, Manchester; United Kingdom.

¹⁰²CPPM, Aix-Marseille Université, CNRS/IN2P3, Marseille; France.

¹⁰³Department of Physics, University of Massachusetts, Amherst MA; United States of America.

¹⁰⁴Department of Physics, McGill University, Montreal QC; Canada.

¹⁰⁵School of Physics, University of Melbourne, Victoria; Australia.

¹⁰⁶Department of Physics, University of Michigan, Ann Arbor MI; United States of America.

¹⁰⁷Department of Physics and Astronomy, Michigan State University, East Lansing MI; United States of America.

¹⁰⁸Group of Particle Physics, University of Montreal, Montreal QC; Canada.

¹⁰⁹Fakultät für Physik, Ludwig-Maximilians-Universität München, München; Germany.

¹¹⁰Max-Planck-Institut für Physik (Werner-Heisenberg-Institut), München; Germany.

¹¹¹Graduate School of Science and Kobayashi-Maskawa Institute, Nagoya University, Nagoya; Japan.

¹¹²(^a) Department of Physics, Nanjing University, Nanjing; (^b) School of Science, Shenzhen Campus of Sun Yat-sen University; (^c) University of Chinese Academy of Science (UCAS), Beijing; China.

¹¹³(^a) School of Physics, Nankai University, Tianjin; (^b) Institute of Frontier and Interdisciplinary Science and Key Laboratory of Particle Physics and Particle Irradiation (MOE), Shandong University, Qingdao; (^c) School of Physics, Zhengzhou University; China.

¹¹⁴Department of Physics and Astronomy, University of New Mexico, Albuquerque NM; United States of America.

¹¹⁵Institute for Mathematics, Astrophysics and Particle Physics, Radboud University/Nikhef, Nijmegen; Netherlands.

¹¹⁶Nikhef National Institute for Subatomic Physics and University of Amsterdam, Amsterdam; Netherlands.

¹¹⁷Department of Physics, Northern Illinois University, DeKalb IL; United States of America.

¹¹⁸(^a) New York University Abu Dhabi, Abu Dhabi; (^b) United Arab Emirates University, Al Ain; United Arab Emirates.

¹¹⁹Department of Physics, New York University, New York NY; United States of America.

¹²⁰Ochanomizu University, Otsuka, Bunkyo-ku, Tokyo; Japan.

¹²¹Ohio State University, Columbus OH; United States of America.

¹²²Homer L. Dodge Department of Physics and Astronomy, University of Oklahoma, Norman OK; United States of America.

¹²³Department of Physics, Oklahoma State University, Stillwater OK; United States of America.

¹²⁴Palacký University, Joint Laboratory of Optics, Olomouc; Czech Republic.

- ¹²⁵Institute for Fundamental Science, University of Oregon, Eugene, OR; United States of America.
- ¹²⁶Graduate School of Science, University of Osaka, Osaka; Japan.
- ¹²⁷Department of Physics, University of Oslo, Oslo; Norway.
- ¹²⁸Department of Physics, Oxford University, Oxford; United Kingdom.
- ¹²⁹LPNHE, Sorbonne Université, Université Paris Cité, CNRS/IN2P3, Paris; France.
- ¹³⁰Department of Physics, University of Pennsylvania, Philadelphia PA; United States of America.
- ¹³¹Department of Physics and Astronomy, University of Pittsburgh, Pittsburgh PA; United States of America.
- ¹³²(^a)Laboratório de Instrumentação e Física Experimental de Partículas - LIP, Lisboa; (^b)Departamento de Física, Faculdade de Ciências, Universidade de Lisboa, Lisboa; (^c)Departamento de Física, Universidade de Coimbra, Coimbra; (^d)Centro de Física Nuclear da Universidade de Lisboa, Lisboa; (^e)Departamento de Física, Escola de Ciências, Universidade do Minho, Braga; (^f)Departamento de Física Teórica y del Cosmos, Universidad de Granada, Granada (Spain); (^g)Departamento de Física, Instituto Superior Técnico, Universidade de Lisboa, Lisboa; Portugal.
- ¹³³Institute of Physics of the Czech Academy of Sciences, Prague; Czech Republic.
- ¹³⁴Czech Technical University in Prague, Prague; Czech Republic.
- ¹³⁵Charles University, Faculty of Mathematics and Physics, Prague; Czech Republic.
- ¹³⁶Particle Physics Department, Rutherford Appleton Laboratory, Didcot; United Kingdom.
- ¹³⁷IRFU, CEA, Université Paris-Saclay, Gif-sur-Yvette; France.
- ¹³⁸Santa Cruz Institute for Particle Physics, University of California Santa Cruz, Santa Cruz CA; United States of America.
- ¹³⁹(^a)Departamento de Física, Pontificia Universidad Católica de Chile, Santiago; (^b)Millennium Institute for Subatomic physics at high energy frontier (SAPHIR), Santiago; (^c)Instituto de Investigación Multidisciplinario en Ciencia y Tecnología, y Departamento de Física, Universidad de La Serena; (^d)Universidad Andres Bello, Department of Physics, Santiago; (^e)Universidad San Sebastian, Recoleta; (^f)Instituto de Alta Investigación, Universidad de Tarapacá, Arica; (^g)Departamento de Física, Universidad Técnica Federico Santa María, Valparaíso; Chile.
- ¹⁴⁰Department of Physics, Institute of Science, Tokyo; Japan.
- ¹⁴¹Department of Physics, University of Washington, Seattle WA; United States of America.
- ¹⁴²(^a)State Key Laboratory of Dark Matter Physics, School of Physics and Astronomy, Shanghai Jiao Tong University, Key Laboratory for Particle Astrophysics and Cosmology (MOE), SKLPPC, Shanghai; (^b)State Key Laboratory of Dark Matter Physics, Tsung-Dao Lee Institute, Shanghai Jiao Tong University, Shanghai; China.
- ¹⁴³Department of Physics and Astronomy, University of Sheffield, Sheffield; United Kingdom.
- ¹⁴⁴Department of Physics, Shinshu University, Nagano; Japan.
- ¹⁴⁵Department Physik, Universität Siegen, Siegen; Germany.
- ¹⁴⁶Department of Physics, Simon Fraser University, Burnaby BC; Canada.
- ¹⁴⁷SLAC National Accelerator Laboratory, Stanford CA; United States of America.
- ¹⁴⁸Department of Physics, Royal Institute of Technology, Stockholm; Sweden.
- ¹⁴⁹Departments of Physics and Astronomy, Stony Brook University, Stony Brook NY; United States of America.
- ¹⁵⁰Department of Physics and Astronomy, University of Sussex, Brighton; United Kingdom.
- ¹⁵¹School of Physics, University of Sydney, Sydney; Australia.
- ¹⁵²Institute of Physics, Academia Sinica, Taipei; Taiwan.
- ¹⁵³(^a)E. Andronikashvili Institute of Physics, Iv. Javakhishvili Tbilisi State University, Tbilisi; (^b)High Energy Physics Institute, Tbilisi State University, Tbilisi; (^c)University of Georgia, Tbilisi; Georgia.
- ¹⁵⁴Department of Physics, Technion, Israel Institute of Technology, Haifa; Israel.

- ¹⁵⁵Raymond and Beverly Sackler School of Physics and Astronomy, Tel Aviv University, Tel Aviv; Israel.
- ¹⁵⁶Department of Physics, Aristotle University of Thessaloniki, Thessaloniki; Greece.
- ¹⁵⁷International Center for Elementary Particle Physics and Department of Physics, University of Tokyo, Tokyo; Japan.
- ¹⁵⁸Graduate School of Science and Technology, Tokyo Metropolitan University, Tokyo; Japan.
- ¹⁵⁹Department of Physics, University of Toronto, Toronto ON; Canada.
- ¹⁶⁰^(a)TRIUMF, Vancouver BC; ^(b)Department of Physics and Astronomy, York University, Toronto ON; Canada.
- ¹⁶¹Division of Physics and Tomonaga Center for the History of the Universe, Faculty of Pure and Applied Sciences, University of Tsukuba, Tsukuba; Japan.
- ¹⁶²Department of Physics and Astronomy, Tufts University, Medford MA; United States of America.
- ¹⁶³Department of Physics and Astronomy, University of California Irvine, Irvine CA; United States of America.
- ¹⁶⁴Department of Physics and Astronomy, University of Uppsala, Uppsala; Sweden.
- ¹⁶⁵Department of Physics, University of Illinois, Urbana IL; United States of America.
- ¹⁶⁶Instituto de Física Corpuscular (IFIC), Centro Mixto Universidad de Valencia - CSIC, Valencia; Spain.
- ¹⁶⁷Department of Physics, University of British Columbia, Vancouver BC; Canada.
- ¹⁶⁸Department of Physics and Astronomy, University of Victoria, Victoria BC; Canada.
- ¹⁶⁹Fakultät für Physik und Astronomie, Julius-Maximilians-Universität Würzburg, Würzburg; Germany.
- ¹⁷⁰Department of Physics, University of Warwick, Coventry; United Kingdom.
- ¹⁷¹Waseda University, Tokyo; Japan.
- ¹⁷²Department of Particle Physics and Astrophysics, Weizmann Institute of Science, Rehovot; Israel.
- ¹⁷³Department of Physics, University of Wisconsin, Madison WI; United States of America.
- ¹⁷⁴Fakultät für Mathematik und Naturwissenschaften, Fachgruppe Physik, Bergische Universität Wuppertal, Wuppertal; Germany.
- ¹⁷⁵Department of Physics, Yale University, New Haven CT; United States of America.
- ¹⁷⁶Yerevan Physics Institute, Yerevan; Armenia.
- ^a Also at Affiliated with an institute formerly covered by a cooperation agreement with CERN.
- ^b Also at An-Najah National University, Nablus; Palestine.
- ^c Also at Borough of Manhattan Community College, City University of New York, New York NY; United States of America.
- ^d Also at Center for Interdisciplinary Research and Innovation (CIRI-AUTH), Thessaloniki; Greece.
- ^e Also at Centre of Physics of the Universities of Minho and Porto (CF-UM-UP); Portugal.
- ^f Also at CERN, Geneva; Switzerland.
- ^g Also at Département de Physique Nucléaire et Corpusculaire, Université de Genève, Genève; Switzerland.
- ^h Also at Departament de Física de la Universitat Autònoma de Barcelona, Barcelona; Spain.
- ⁱ Also at Department of Financial and Management Engineering, University of the Aegean, Chios; Greece.
- ^j Also at Department of Modern Physics and State Key Laboratory of Particle Detection and Electronics, University of Science and Technology of China, Hefei; China.
- ^k Also at Department of Physics, Ben Gurion University of the Negev, Beer Sheva; Israel.
- ^l Also at Department of Physics, Bolu Abant İzzet Baysal University, Bolu; Türkiye.
- ^m Also at Department of Physics, King's College London, London; United Kingdom.
- ⁿ Also at Department of Physics, Stellenbosch University; South Africa.
- ^o Also at Department of Physics, University of Fribourg, Fribourg; Switzerland.
- ^p Also at Department of Physics, University of Thessaly; Greece.
- ^q Also at Department of Physics, Westmont College, Santa Barbara; United States of America.

- r* Also at Faculty of Physics, Sofia University, 'St. Kliment Ohridski', Sofia; Bulgaria.
- s* Also at Faculty of Physics, University of Bucharest; Romania.
- t* Also at Hellenic Open University, Patras; Greece.
- u* Also at Henan University; China.
- v* Also at Imam Mohammad Ibn Saud Islamic University; Saudi Arabia.
- w* Also at Indian Institute of Technology (IIT), Jodhpur; India.
- x* Also at Institutio Catalana de Recerca i Estudis Avancats, ICREA, Barcelona; Spain.
- y* Also at Institut für Experimentalphysik, Universität Hamburg, Hamburg; Germany.
- z* Also at Institute for Nuclear Research and Nuclear Energy (INRNE) of the Bulgarian Academy of Sciences, Sofia; Bulgaria.
- aa* Also at Institute of Applied Physics, Mohammed VI Polytechnic University, Ben Guerir; Morocco.
- ab* Also at Institute of Particle Physics (IPP); Canada.
- ac* Also at Institute of Physics and Technology, Mongolian Academy of Sciences, Ulaanbaatar; Mongolia.
- ad* Also at Institute of Physics, Azerbaijan Academy of Sciences, Baku; Azerbaijan.
- ae* Also at Institute of Theoretical Physics, Iliia State University, Tbilisi; Georgia.
- af* Also at Millennium Institute for Subatomic physics at high energy frontier (SAPHIR), Santiago; Chile.
- ag* Also at National Institute of Physics, University of the Philippines Diliman (Philippines); Philippines.
- ah* Also at School of Physics, University of the Witwatersrand, Johannesburg; South Africa.
- ai* Also at The Collaborative Innovation Center of Quantum Matter (CICQM), Beijing; China.
- aj* Also at TRIUMF, Vancouver BC; Canada.
- ak* Also at Università di Napoli Parthenope, Napoli; Italy.
- al* Also at Università degli Studi Link; Italy.
- am* Also at University and INFN Torino, Torino; Italy.
- an* Also at University of Chinese Academy of Sciences (UCAS), Beijing; China.
- ao* Also at University of Colorado Boulder, Department of Physics, Colorado; United States of America.
- ap* Also at University of Siena; Italy.
- aq* Also at Washington College, Chestertown, MD; United States of America.
- ar* Also at Yeditepe University, Physics Department, Istanbul; Türkiye.
- * Deceased